Lattice gauge theory with non-perturbative gauge-fixing

By

Mugdha Sarkar

Enrolment No.: PHYS05201304002

Saha Institute of Nuclear Physics
Kolkata

A thesis submitted to the
Board of Studies in Physical Science Discipline
In partial fulfillment of requirements
For the Degree of

DOCTOR OF PHILOSOPHY
of
HOMI BHABHA NATIONAL INSTITUTE

November, 2018

Homi Bhabha National Institute

Recommendations of the Viva Voce Committee

As members of the Viva Voce Committee, we certify that we have read the dissertation prepared by Mugdha Sarkar entitled "Lattice gauge theory with non-perturbative gauge-fixing" and recommend that it may be accepted as fulfilling the thesis requirement for the award of Degree of Doctor of Philosophy.

Chairman - Prof. Munshi Golam Mustafa	Munshi	**Date:** 18/04/19
Guide / Convener - Prof. Asit Kumar De	Asitkrde	**Date:** 18/4/2019
Examiner - Prof. Saumen Datta	Saumen Datta	**Date:** 22.4.2019
Member 1- Prof. Amit Ghosh	AGhosh	**Date:** 18/4/2019
Member 2- Prof. Arnab Kundu	AKundu	**Date:** 18/4/2019

Final approval and acceptance of this thesis is contingent upon the candidate's submission of the final copies of the thesis to HBNI.

I hereby certify that I have read this thesis prepared under my direction and recommend that it may be accepted as fulfilling the thesis requirement.

Date: 18/4/2019

Place: Kolkata

Asitkrde

Guide

Version approved during the meeting of Standing Committee of Deans held during 29-30 Nov 2013

STATEMENT BY AUTHOR

MUGDHA SARKAR

DECLARATION

I, hereby declare that the investigation presented in the thesis has been carried out by me. The work is original and has not been submitted earlier as a whole or in part for a degree / diploma at this or any other Institution / University.

MUGDHA SARKAR

List of Publications Arising from the Thesis

Peer reviewed journals:

1. "Tricritical points in a compact $U(1)$ lattice gauge theory at strong coupling"

   Asit K. De and Mugdha Sarkar

   Phys. Rev. D **93** (2016) 114504

2. "Non-perturbatively gauge-fixed compact $U(1)$ lattice gauge theory"

   Asit K. De and Mugdha Sarkar

   JHEP **10** (2017) 125

OTHER PUBLICATIONS

a. Book/Book Chapters: NIL

b. Conference/Symposium:

1. **Perspectives and Challenges in Lattice Gauge Theory, Indo-German Workshop**
   Organised by Tata Institute of Fundamental Research, Mumbai, and Universität Regensburg. Held at TIFR, Mumbai, India. **(February 16-20, 2015)**.

   ✓ *Talk presented on* **"Compact U(1) lattice gauge theory with non-perturbative gauge fixing"**.

2. **School on numerical analysis and algorithms towards exascale**
   Organized By HPC-LEAP. Held at Bergische Universität Wuppertal, Germany. **(September 23 - October 13, 2015)**.

3. **Lattice Practices 2015**
   Organized By & Held at Forschungszentrum Jülich, Jülich Supercomputing Centre, Germany. **(October 14-16, 2015)**.

4. **SERC Main School in Theoretical High Energy Physics**

   Organized By & Held at University of Kalyani, Kalyani, India.

   (January 9-28, 2017).

5. **Helmholtz International Summer School "Hadron Structure, Hadronic Matter, Lattice QCD"**

   Organized By & Held at the Bogoliubov Laboratory of Theoretical Physics, JINR, Dubna, Russia. **(August 20 - September 2, 2017)**.

   ✓ *Talk presented on* **"Non-perturbative gauge-fixing of compact gauge fields on the lattice"**.

6. **The 36th Annual International Symposium on Lattice Field Theory (LATTICE 2018)**

   Organized By & Held at Michigan State University, East Lansing, Michigan, USA. **(July 2228, 2018)**.

   ✓ *Talk presented on* **"eBRST SU(2) Gauge Theory on Lattice"**.

MUGDHA SARKAR

To My Loving Family.......

ACKNOWLEDGEMENTS

These five years of PhD has been a great learning experience for me, both for my academic and personal life. I have profoundly benefited from my interactions with my advisor, Prof. Asit Kumar De. I am deeply indebted to him for providing me unstinting support throughout the tenure of my PhD and I hope he would continue to do so in the future. Thank you, Sir, for painstakingly going through this thesis and providing me with valuable feedback. I wish you and your family all the very best for your future endeavors.

I would like to thank my teachers from my childhood to the present for believing in me and helping me grow to be the person who I am today. I am grateful to Prof. M. G. Mustafa, Prof. P. B. Pal, Prof. A. Harindranath, Prof. A. Ghosh, Prof. G. Bhattacharya, Prof. P. K. Mohanty and other faculty of Saha Institute of Nuclear Physics (SINP), Kolkata for useful discussions. Our work has greatly benefited through invaluable discussions with Maarten and Yigal, that we had at various stages of the work. The support from the Department of Atomic Energy (DAE), Government of India (GOI) and the administration of SINP is acknowledged. The work would not have been possible without the Cray XE6 computational cluster at SINP, acquired and maintained during the 11th plan and the 12th plan periods through projects under the DAE, GOI. A big thanks to you, Richard, for helping me with everything in regard to the supercomputer.

My friends in and out of SINP played an integral role in my life during my PhD. My batch-mates, seniors and juniors have made my stay in SINP a memorable one.

My loving family (Mum, Baba and Dada) has been the anchor of my life and have always supported and encouraged me to carry on with my academic journey, even though it meant a lot of sacrifices. I have been staying away from my family since a long time and it was very difficult for all of us. I hope this hardship did not go in vain. My love to the new members, Boudi and tiny Mithi, who came in to our family during my PhD. In the course of my PhD, I slowly became a part of another family and I now have another set of parents (Ma and Baba), who are equally loving and supportive. I had a new home to go, whenever I wanted, where I can be myself, apart from my home which is far away. Thank you Didi and Bivas da for making me a part of your life. Love you, Kuhu, for adding colour to my life. I am fortunate to be your one and only, Kaku.

Finally and very importantly, I met Amrita, my wife, the love of my life, during my PhD. You were literally there with me through all the ups and downs. You are the one with whom I can discuss everything that matters to me, from physics to life. Thank you for going through the entire thesis and suggesting several corrections. Thank you for everything.

Mugdha Sarkar

CONTENTS

SYNOPSIS

In quantum field theories with gauge symmetry, one encounters the problem of gauge redundancy due to the unphysical longitudinal modes of gauge fields. To overcome this, the most popular method is to fix the gauge using the Fadeev-Popov scheme. With a covariant gauge-fixing condition, one can define a renormalizable quantum field theory (QFT) with BRST (Becchi-Rouet-Stora-Tyutin) symmetry and calculate physical observables. However, this scheme is applicable only in the perturbative regime or in other words, for small gauge coupling. In the non-perturbative sector, we find numerous solutions to the gauge-fixing condition and thus the usual approach fails. The question of non-perturbative gauge-fixing (NPGF) is a vast field of ongoing research.

The lattice is a well-known regulator for QFTs. In the usual Wilson approach in Euclidean spacetime, gauge invariance is manifest at all stages of the calculation and gauge-fixing is not required in principle. The theory is rigorously defined through a functional integral with a gauge-invariant (Haar) measure and group-valued gauge links, something that makes the algebra-valued gauge fields compact. The algebra-valued gauge fields become noncompact, smooth and dimensionful only in the continuum limit. However, gauge-fixing is sometimes done on the lattice, in retrospect, on a given gauge-field configuration

to match results with a particular perturbative renormalization scheme. One can now ask what happens when one tries to fix the gauge as in continuum *a la* Fadeev-Popov. We will see that this leads to an impasse since there is a no-go theorem by Neuberger [1] that does not allow BRST symmetric theories to be formulated on a lattice.

Let us now turn our attention to fermions on the lattice. Naive discretization of fermions on the lattice leads to the infamous fermion doubling problem. The Nielsen-Ninomiya theorem points to a possible way out to avoid the doubling by explicitly breaking the chiral symmetry [2–4]. This leads us to the important issue of achieving chiral gauge symmetry on the lattice. In a manifestly local formalism of lattice chiral gauge theories, the standard Wilson method with a gauge-invariant measure leads to various problems. The problems arise due to the undesired presence, in such theories, of the longitudinal gauge degrees of freedom (*lgdof*) which become manifest as physical degrees of freedom (as scalar fields) in a gauge-noninvariant theory such as manifestly local proposals of lattice chiral gauge theory [5,6]. The *lgdof* couple to the physical degrees of freedom in the terms of the action that explicitly break gauge invariance. The interactions of the *lgdof* with the physical sector can generally be strong since any point on the gauge orbit is as likely as any other in a gauge-invariant formalism. This is because the functional integration takes place also along the longitudinal direction or the gauge orbit.

The usual method to tackle such situations is to give the *lgdof* a dynamics through a particular gauge-fixing mechanism that is expected to control or tame the *lgdof*. (In a different approach to lattice chiral gauge theory that modifies chiral symmetry on lattice according to the Ginsparg-Wilson relation [7], one arrives at a link field dependent fermion measure and an exact solution to the integrability condition on the space of the lattice link fields was obtained in the Abelian case [8]. This method is fundamentally different from the gauge-fixing approach and if successful, would not require gauge-fixing.)

In the usual Fadeev-Popov gauge-fixing procedure, one inserts a constant gauge-fixing functional integral in the partition function such that gauge-invariant correlation functions of the gauge-fixed theory are identical to the manifestly gauge-invariant unfixed theory. However, for a BRST-invariant theory with compact gauge fields on the lattice, one finds that the gauge-fixing integral is identically zero due to exact cancellation among the lattice Gribov copies [1]. This leads to indeterminate $0/0$ form for the expectation values of gauge-invariant operators. One needs to find a way out to fix the gauge non-perturbatively, such that manifestly local lattice chiral gauge theories can be constructed. In this thesis, we discuss the possible ways of gauge-fixing and their implications in both the Abelian ($U(1)$) and non-Abelian ($SU(2)$) cases.

In our first problem, we address the issue of gauge-fixing in the Abelian case. Naive discretization of the covariant gauge-fixing condition on the lattice allow multiple solutions leading to degenerate minima of the action. A suitable higher derivative (HD) gauge-fixing term, proposed by Golterman and Shamir [9], avoids multiple solutions, thereby providing a unique minimum around which a weak coupling perturbation theory can be done. The theory also explicitly breaks the BRST symmetry, thus evading the no-go theorem. The pure gauge theory with the HD gauge-fixing term was studied extensively in the past, in the weak gauge coupling (g) region [10]. For a sufficiently large value of the bare coupling of the HD term ($\tilde{\kappa}$), one obtains a novel continuous phase transition (FM-FMD) where gauge symmetry is restored and *lgdof* are decoupled, and the usual continuum results are obtained. It was also shown that a chiral gauge theory could be constructed successfully [11–14] for weak gauge couplings, by decoupling the *lgdof*s with this propsal. The success of the HD gauge-fixing proposal in the weak coupling region raises the important question about the nature of the theory at strong gauge couplings. We have tried to address this question in our work [15, 16], by exploring the strong gauge coupling region of the gauge-fixed theory.

The main result of our work is that the Lorentz covariant physics emerging in the strong gauge coupling region, by approaching the FM-FMD transition from the FM-side, is actually governed by that at the phase transition at $g = 0$, $\tilde{\kappa} \to \infty$ and $\kappa \sim 0$, κ being the coefficient of a dimension-2 mass counter-term required to recover gauge symmetry (In the weak gauge coupling limit g = 0, the action has a unique global minimum). At the continuous transition, we find the expected physics with free massless photons and decoupled *lgdof*. We used Hybrid Monte Carlo (HMC), a global algorithm, to develop the code, which was used to numerically obtain all the results. Our work also establishes the inadequacy of a local algorithm like Multihit Metropolis (which was used in earlier works) for larger $\tilde{\kappa}$ and bigger volumes, by comparing results with the HMC algorithm at different regions of the coupling parameter space. A novel tricritical line emerges for $g > 1$ in the 3-dimensional phase diagram $(g, \tilde{\kappa}, \kappa)$ separating the first order and the continuous FM-FMD transition surfaces, which indicates a new universality class with non-trivial physics. However, proper investigation of the properties of the tricritical line is presently beyond the scope of our work.

Our second problem of investigation is about the non-perturbative gauge-fixing in non-Abelian theories with the equivariant BRST (eBRST) scheme. It was first devised by Schaden [17] for $SU(2)$ and later generalized for general $SU(N)$ theories by Golterman anad Shamir [18]. The basic idea is to gauge-fix in the coset space G/H, where G is $SU(N)$, leaving the action invariant under the subgroup $H \subset G$, which contains the maximal Abelian subgroup of G. The action is now eBRST symmetric with a 4-ghost term, which was previously absent in a BRST symmetric theory. This 4-ghost term helps to evade the Neuberger's no-go theorem while maintaining an overall eBRST symmetry. The nilpotency condition of BRST is now modified and the double variation of an eBRST transformation is now a transformation in the H subgroup. The remaining unfixed Abelian invariance of the theory may now be gauge-fixed to potentially construct a manifestly local chiral lattice gauge theory. It is also interesting to study the eBRST gauge-fixed theory as an alternate formulation of lattice gauge theories.

It has been shown that the coupling of the eBRST gauge-fixing term for general $SU(N)$ is asymptotically free, suggesting that the gauge-fixing coupling grows strong at some scale $\tilde{\Lambda}$ [19]. This raises the unusual question which is generally not thought of, that whether the dynamics of the longitudinal sector can affect the physical sector. Approximate analytical calculations have shown that such a theory may have non-trivial phase structure in the sector of *lgdof* [20, 21]. It has been speculated that the gauge-fixing coupling may become strong while the gauge coupling still remains weak and a new phase may emerge. A very convenient way to study the dynamics of the longitudinal sector would be to take the gauge coupling to the extreme weak limit i.e. zero, effectively decoupling the transverse gauge degrees, resulting in the so-called reduced model. A non-perturbative study of the reduced model would reveal any non-trivial phenomenon in the *lgdof* sector. One can then weakly turn on the gauge coupling to study the implications of the strong *lgdof* sector on the physical transverse sector.

However, an invariance theorem [18] establishes that on a finite lattice, the expectation value of any gauge-invariant observable is the same in both the eBRST gauge-fixed theory and the unfixed theory, or in other words, the transverse degrees of freedom are unaffected by the dynamics of the *lgdof*. This is what one would expect from perturbative physics where the results are independent of the gauge-fixing coefficient. A corollary of the invariance theorem is that the gauge-fixing partition function does not depend on the gauge link and the coupling of the gauge-fixing term, thus defining a topological field theory (TFT). Hence, the reduced model of theory, which is just the theory of the longitudinal degrees of freedom and ghost fields, is a TFT. However, it was speculated in [20], that a topological field theory with a BRST-like symmetry can have a spontaneous symmetric breaking (SSB). The idea is to add a explicit symmetry breaking term which when turned off leads to a vacuum with broken symmetry. The same idea can be applied to the eBRST gauge-fixed theory. It needs to be seen then that what is the implication of a SSB in the full theory with both transverse and longitudinal gauge degrees of freedom.

We have studied the pure $SU(2)$ gauge theory, where the only possible way to maintain eBRST symmetry is by gauge-fixing in the coset $SU(2)/U(1)$, leaving a $U(1)$ subgroup invariant. We have numerically studied both the full theory and the reduced model using HMC algorithm. An important part of the numerical problem is the tracking of zero crossing of the small eigenvalues of the real-valued eBRST ghost matrix, which has been studied using the stochastic tunneling HMC algorithm (sTHMC) [22]. The reduced model of the theory has a global $SU(2)$ symmetry, which was shown to undergo a SSB from $SU(2)$ to $U(1)$ [20]. We have strong evidence of such a broken phase in the reduced model. We have also found the validity of the invariance theorem in the full theory. This is a hard system to simulate numerically and the canonical algorithms used in our study suffer from various issues due to the complexity of the problem. As a result, the physics conclusions cannot be established beyond doubt. We have studied these drawbacks and we hope these would help us to devise more efficient ways to study the theory in the future. Our work has shed light on the dynamics of the *lgdof* in a non-perturbatively gauge-fixed non-Abelian gauge theory and we hope that it would be very useful in the gauge-fixing formulation of lattice chiral gauge theories in the future and in our understanding of quantum field theory, in general.

The development of the codes for the numerical simulations was an integral part of the research work. This is the first-time lattice calculation of the eBRST theory and also the first-time implementation of sTHMC [22]. Working out the involved analytical calculations required for the algorithm, the three codes, viz. the full theory with HMC, the reduced model with HMC and the full theory with sTHMC, were built from scratch. The codes were parallelized using MPI (Message Passing Interface), partly based on the MILC collaborations public lattice gauge theory code [23], making it possible to obtain results from the path integral, with enormous number of degrees of freedom involving gauge fields and Grassmannian ghost fields, using Monte Carlo calculations in a reasonable time using a supercomputer.

LIST OF FIGURES

List of Tables

CHAPTER 1

INTRODUCTION

Through a strong coupling expansion of a Wilson loop in a space-time (Euclidean) lattice, Wilson [24] showed evidence for confinement in a pure *compact* $SU(3)$ gauge theory, marking the beginning of a new method for non-perturbative investigation of quantum field theories. A salient feature of the Wilson's approach is that gauge invariance is manifest at all stages of the calculation and gauge-fixing is not required. The theory is rigorously defined through a functional integral with a gauge-invariant Haar measure with group-valued gauge links. The algebra-valued gauge fields become non-compact, smooth and dimensionful only in the quantum continuum limit.

However, situations arise where it is necessary to control the unphysical longitudinal modes of the lattice gauge fields. The formulations of manifestly local chiral gauge theories on the lattice in the Wilson framework face several issues due to the unavoidable presence of these unphysical gauge degrees of freedom. It is therefore desirable to control these modes through gauge-fixing in a non-perturbative set-up.

The Fadeev-Popov gauge-fixing scheme and the resulting the Becchi-Rouet-Stora-Tyutin

(BRST) formalism is of vital importance in perturbative definitions of gauge theories. However, this scheme is not directly applicable for non-perturbatively defined gauge theories on the lattice due to a no-go theorem. The proposal for a remedy evading the above no-go situation, in case of non-Abelian gauge theory, is the so-called equivariant BRST (eBRST) scheme that gauge-fixes only the coset space, leaving minimally a Cartan subgroup invariant [17, 18]. For the Abelian case, a non-perturbative gauge-fixing scheme as proposed by [9, 25] includes a specially engineered higher derivative (HD) gauge-fixing term in the lattice action breaking BRST invariance. Recovery of gauge symmetry in the physical sector in the continuum limit is expected to be achieved by tuning appropriate counter-terms. Apart from their role in constructing lattice chiral gauge theories, these proposals offer an alternative way of defining gauge theories on the lattice.

This thesis is based on our study of the above-mentioned non-perturbative gauge-fixing schemes for compact gauge fields on the lattice for both Abelian and non-Abelian cases. Before the research work is described in the later chapters, we first discuss the basic underlying concepts of our research work in this introduction.

We start our discussion by introducing the lattice as a laboratory to study quantum field theories (QFTs) non-perturbatively using computers. This is followed by the construction of theories on the lattice with special emphasis on gauge fields. The fermion doubling problem and Wilson fermions are discussed, followed by the Nielsen-Ninomiya theorem to motivate the issues of chiral gauge theories on the lattice. After introducing the basic aspects of the lattice QFTs, we then discuss the necessity of gauge-fixing in the continuum QFT in the purview of perturbation theory. The basics of BRST gauge-fixing framework is described in some detail.

After this introduction of the lattice field theories and gauge-fixing in continuum, we will go into the aspects of gauge-fixing on the lattice. This will then be followed by the motivation for non-perturbative gauge-fixing from the viewpoint of chiral gauge theories on the lattice. Finally, we discuss problems of naive gauge fixing on the lattice.

1.1 Quantum Field Theory on the Lattice

In perturbative QFTs in physical dimensions, calculations are done with an ultraviolet regulator due to the divergences encountered. Physical results, after the renormalization process, are then obtained as finite without a cutoff dependence. Dimensional regularization and Pauli-Villars regularization are two examples of perturbative regularizations. Lattice is a general regulator at the action level for QFTs where, by restricting the spacetime in a box (infrared regularization) with discrete co-ordinates (ultraviolet regularization), the degrees of freedom become finite. The lattice theory is then quantized by the functional integral method and infinities are not encountered in calculations. This makes it a very powerful tool for doing various non-perturbative calculations, using Monte Carlo importance sampling on computers, which otherwise may not be possible. The lattice regularization for QFTs was developed by Kenneth G. Wilson in his seminal work [24] in 1974, where he presented the lattice as a tool to understand confinement in non-Abelian gauge theories. The idea to construct QFTs on lattice was also independently proposed by Jan Smit around 1972 and briefly mentioned in his thesis in 1974.

In lattice QFT, one generally works with 4 dimensional Euclidean spacetime, where all the coordinates are equivalent. The cutoff is the lattice spacing a which is the same in all 4 directions for a hypercubic lattice. The analytic continuation of Euclidean correlation functions to the Minkowski spacetime requires the Euclidean theory to satisfy the conditions of the Osterwalder-Schrader theorem [26]. The matter fields are put on the lattice points and as we shall see, the gauge fields on the links between the lattice points. The renormalized physics is obtained in the vicinity of a continuous quantum phase transition in the parameter space of the theory. The general prescription is as follows:

- Write the action $S[\phi]$ on an Euclidean lattice where $S[\phi]$ is a functional of the fields ϕ defined on all spacetime points.
- Quantize the theory using path integral approach where the partition function is given as $Z = \int \mathcal{D}\phi \; e^{-S[\phi]}$.
- Find out expectation value of an operator as

$$\langle \hat{\mathcal{O}} \rangle = \frac{1}{Z} \int \mathcal{D}\phi \; e^{-S[\phi]} \mathcal{O}. \tag{1.1}$$

Lattice gauge theory has also been formulated in Hamiltonian approach where time is continuous and the fields are canonically quantized. We do not discuss Hamiltonian lattice gauge theory in this thesis.

Since this thesis deals primarily with gauge fields on the lattice, we shall now proceed with how to define gauge theories on the lattice.

1.1.1 Gauge Fields on the Lattice

One way of introducing gauge fields on the lattice, or in the continuum as well, is to start with a theory of free matter fields and elevate an internal global symmetry to a local symmetry. Accordingly, action for free Dirac fermions in Euclidean continuum is given by,

$$S = \int \mathrm{d}^4x \; \bar{\psi}(\partial\!\!\!/ + m)\psi \; , \tag{1.2}$$

where $\partial\!\!\!/ = \gamma_\mu \partial_\mu$ is anti-Hermitian with all Dirac matrices γ_μ taken as Hermitian, as is common in Euclidean space-time.

In the lattice regularized theory, the action is discretized on a simple hypercubic lattice as $S = \int \mathrm{d}^4x \mathcal{L}_E \to a^4 \sum_x \mathcal{L}_E$ where $\mathcal{L}_E = \bar{\psi}(\partial\!\!\!/ + m)\psi$ is the Euclidean Lagrangian density and a is the uniform lattice spacing in all directions. The fermionic matter fields are defined at each lattice point and the continuous spacetime dependence is now replaced by a discrete spacetime index, $\psi(x) \to \psi_x$ where in the latter, $x = \{x_0, x_1, x_2, x_3; x_i \in \mathbf{Z}\}$. For the discrete spacetime, the derivatives will now be replaced by finite differences. Therefore, we have forward and backward differences in place of derivatives as follows

$$\begin{aligned} (\Delta^f_\mu \psi)(x) &= \frac{1}{a}(\psi_{x+\mu} - \psi_x) = \frac{1}{a}(\delta_{y,x+\mu} - \delta_{y,x})\psi_y \ , \\ (\Delta^b_\mu \psi)(x) &= \frac{1}{a}(\psi_x - \psi_{x-\mu}) = \frac{1}{a}(\delta_{y,x} - \delta_{y,x-\mu})\psi_y \ . \end{aligned} \tag{1.3}$$

where μ is a unit vector pointing along any of the four directions. Considering Hermitian conjugates, we obtain the useful relations

$$(\Delta^f_\mu)^\dagger = -\Delta^b_\mu \quad , \quad (\Delta^b_\mu)^\dagger = -\Delta^f_\mu \ . \tag{1.4}$$

Constructing the new operator

$$\Delta^s_\mu = \frac{1}{2}(\Delta^f_\mu + \Delta^b_\mu) \ , \tag{1.5}$$

and using Eq. 1.4, we find,

$$(\Delta_\mu^s)^\dagger = -\Delta_\mu^s \,, \tag{1.6}$$

$$(\gamma_\mu \Delta_\mu^s)^\dagger = -\gamma_\mu \Delta_\mu^s \,. \tag{1.7}$$

Δ_μ^s, being anti-Hermitian appears to be a good choice for the lattice action. Note that, we could have considered different discretizations of the derivatives but they all are expected to lead to the same physics in the continuum limit, albeit with different discretization effects.

Incorporating all of the above, the lattice regularized action for free fermions can finally be written as

$$\begin{aligned} S &= a^4 \sum_{x\,\mu} \frac{1}{2a} \bar{\psi}_x \gamma_\mu \Delta_\mu^s \psi_x + a^4 \sum_x m \bar{\psi}_x \psi_x \\ &= a^4 \sum_{x\,\mu} \frac{1}{2a} \bar{\psi}_x \gamma_\mu (\psi_{x+\mu} - \psi_{x-\mu}) + a^4 \sum_x m \bar{\psi}_x \psi_x \,. \end{aligned} \tag{1.8}$$

A very important point to note here is that the above action is actually inadequate, as it gives rise to the infamous *species doubling* problem. We will discuss more about this in a later section and mention ways to avoid it.

Under a global vector transformation in its internal degrees of freedom in the representation of a unitary group, the fermionic fields ψ_x transform the same way as in continuum,

$$\psi_x \to e^{i\theta} \psi_x \,, \quad \bar{\psi}_x \to \bar{\psi}_x e^{-i\theta} \,. \tag{1.9}$$

When the transformation parameter θ is independent of x, the fermionic Lagrangian in Eq. 1.8 is invariant under the above transformation. However, the terms of following type below are no longer invariant when θ is a function of spacetime,

$$\bar{\psi}_x \psi_{x+\mu} \to \bar{\psi}_x e^{-i\,(\theta_x - \theta_{x+\mu})} \psi_{x+\mu} \; . \tag{1.10}$$

Requirement of local gauge invariance necessitates introduction of a field which has a vector index μ and should transform covariantly. Hence, this field should transform under local gauge transformation as

$$U_{x\mu} \to e^{i\theta_x} U_{x\,\mu} e^{-i\theta_{x+\mu}} \; , \tag{1.11}$$

such that the quantity $\bar{\psi}_x U_{x\mu} \psi_{x+\mu}$ is gauge invariant. $U_{x\mu}$ is taken as an element of the special unitary gauge group as a minimal requirement. Hence, $U_{x\mu}$ can be written in general as $e^{iA_{x\mu}}$ where $A_{x\mu}$ is Hermitian. We will see in a short while that the field $A_{x\mu}$ is essentially related to the usual gauge fields in the continuum, thus explaining the notation.

We can now rewrite the action as a locally gauge invariant one. Inserting the $U_{x\mu}$ fields, to be called from now onwards as gauge "link" variables, the kinetic part of the fermionic lattice action becomes

$$a^4 \sum_{x\,\mu} \bar{\psi}_x \frac{1}{2a} \gamma_\mu (U_{x\mu} \psi_{x+\mu} - U^\dagger_{x-\mu,\mu} \psi_{x-\mu}) \; , \tag{1.12}$$

where

$$U^\dagger_{x-\mu,\mu} = U_{x,-\mu}. \tag{1.13}$$

The action is now invariant under the local gauge transformations. We will see now how the gauge link fields are related to the continuum field.

Writing $U_{x\mu} = e^{iA_{x\mu}} = e^{iag\mathcal{A}_{x\mu}}$, where $\mathcal{A}_{x\mu}$ has a mass dimension, g is the dimension-

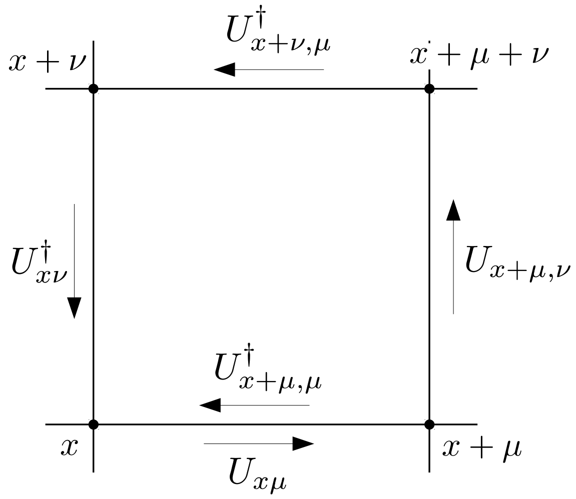

Figure 1.1: The smallest square on a lattice in (μ, ν)-plane indicating the sites and the directional gauge links between them.

less gauge coupling, we have, for small lattice spacing a,

$$a^4 \sum_{x\,\mu} \bar{\psi}_x \frac{1}{2a} \gamma_\mu ((1 + iag\mathcal{A}_{x\mu})\psi_{x+\mu} - (1 - iag\mathcal{A}_{x-\mu,\mu})\psi_{x-\mu}) \tag{1.14}$$

$$= a^4 \sum_{x\,\mu} \bar{\psi}_x \gamma_\mu \left(\frac{\psi_{x+\mu} - \psi_{x-\mu}}{2a} + ig\frac{\mathcal{A}_{x\mu}\psi_{x+\mu} + \mathcal{A}_{x-\mu,\mu}\psi_{x-\mu}}{2} \right) \tag{1.15}$$

$$\xrightarrow{a\to 0} \int \mathrm{d}^4x \, \left(\bar{\psi}(x)\gamma_\mu \partial_\mu \psi(x) + ig\bar{\psi}(x)\gamma_\mu \mathcal{A}_\mu(x)\psi(x) \right) \ , \tag{1.16}$$

where $\mathcal{A}_\mu(x)$ and $\psi(x)$ are the gauge and fermion fields in the continuum respectively. This shows the relation between the dimensionful algebra-valued gauge fields in the continuum with the group-valued gauge links on the lattice. The field $U_{x\mu}$ lies on the line joining two lattice points/sites as shown in Fig. 1.1.

The next step is to construct a gauge-invariant kinetic term for the gauge fields. Writing

$e^{i\theta} \equiv \mathrm{g}_x$ as an element of the gauge group G, we notice the following transformations

$$U_{x\mu} \to \mathrm{g}_x U_{x\mu} \mathrm{g}^\dagger_{x+\mu} \ , \tag{1.17}$$

$$U_{x+\mu,\nu} \to \mathrm{g}_{x+\mu} U_{x+\mu,\nu} \mathrm{g}^\dagger_{x+\mu+\nu} \ . \tag{1.18}$$

It is to be noted that, gauge transformations would be denoted by g and the gauge coupling by g, throughout this thesis. Now taking a directed product in the counterclockwise direction for an elementary square in the $\mu\nu$ plane of the lattice as shown in Fig. 1.1, we see that, under a gauge transformation g,

$$U_{x\mu} U_{x+\mu,\nu} U_{x+\mu+\nu,-\mu} U_{x+\nu,-\nu} \to \mathrm{g}_x U_{x\mu} U_{x+\mu,\nu} U_{x+\mu+\nu,-\mu} U_{x+\nu,-\nu} \mathrm{g}^\dagger_x \ . \tag{1.19}$$

Denoting the above quantity as $P_{x\mu\nu}$, we find that $\mathrm{Tr} P_{x\mu\nu}$ is gauge invariant due to the cyclic property of trace. When the gauge group G is Abelian, $P_{x\mu\nu}$ itself is invariant. The object $P_{x\mu\nu}$ is called a $plaquette$, which is the smallest Wilson loop. Wilson loops are gauge-invariant traces of directed product of U fields on a closed loop, with arbitrary shapes and not necessarily in the same plane.

The necessity of the plaquette will soon be evident. Let us work in the Abelian theory for simplicity. Using Eq. 1.13 and 1.3, we have

$$\begin{aligned} P_{x\mu\nu} &= U_{x\mu} U_{x+\mu,\nu} U^\dagger_{x+\nu,\mu} U^\dagger_{x,\nu} \\ &= \exp(iag\left(\mathcal{A}_{x\mu} + \mathcal{A}_{x+\mu,\nu} - \mathcal{A}_{x+\nu,\mu} - \mathcal{A}_{x,\nu}\right)) \\ &= \exp(ia^2 g\left(\Delta_\mu \mathcal{A}_{x\nu} - \Delta_\nu \mathcal{A}_{x\mu}\right)) \equiv \exp(ia^2 g \mathcal{F}_{x\mu\nu}) \ . \end{aligned} \tag{1.20}$$

Taking the real part of the plaquette which is also equivalent to taking sum of the plaquettes in both directions,

$$\begin{aligned}\mathrm{Re}P_{x\mu\nu} &= P_{x\mu\nu} + P^{\dagger}_{x\mu\nu} \\ &= e^{ia^2 g\mathcal{F}_{x\mu\nu}} + e^{-ia^2 g\mathcal{F}_{x\mu\nu}} \xrightarrow[\mathcal{F}\to F,\ \Delta\to\partial]{\text{for small a}} 2 - a^4 g^2 F^2_{\mu\nu}(x) + \mathcal{O}(a^6)\ .\end{aligned} \tag{1.21}$$

Therefore, in the continuum limit, we have

$$S_W = \frac{1}{g^2}\sum_{x,\,\mu<\nu}\left(1 - \mathrm{Re}\,P_{x\mu\nu}\right) \xrightarrow{a\to 0} \frac{1}{4}\int \mathrm{d}^4x F_{\mu\nu}F_{\mu\nu}\ . \tag{1.22}$$

This clearly shows that the left hand side (LHS) in Eq. 1.22, the so-called Wilson gauge action for Abelian case, acts as the kinetic energy term of the gauge fields in the limit of vanishing lattice spacing.

For non-Abelian gauge theories, the Wilson gauge action is similar to the action in Eq. 1.22, except for the introduction of trace for matrix-valued gauge links, and is given as

$$S_W = \frac{2}{g^2}\sum_{x,\,\mu<\nu}\mathrm{Re}\,\mathrm{tr}\left(1 - P_{x\mu\nu}\right)\ . \tag{1.23}$$

1.1.2 Haar measure

As mentioned in Sec. 1.1, the quantum field theory is studied on the lattice regulator in the path integral approach in Euclidean spacetime (see Eq. 1.1). The partition function Z contains all the information about the QFT. The integrand of Z, $\exp(-S)$, consists of the lattice action S of the matter and gauge fields, the construction of which has been discussed in the previous Sec. 1.1.1. In this section, we discuss the measure of the path integral for gauge fields.

In the continuum, the path integral integrates over the gauge fields $A_\mu(x)$ from $-\infty$ to ∞. We encounter issues with gauge redundancy which needs to be taken care of by gauge-fixing. This will be discussed in detail in the next section. On the other hand, we have link variables $U_{x\mu}$ on the lattice which are gauge group elements. Therefore, integrating over the gauge link amounts to integrating over the gauge transformation parameters which are bounded. For example, in $U(1)$ gauge theory, the transformation parameter θ is bounded between 0 and 2π.

An important requirement for the integration measure for gauge fields is gauge invariance. The partition function should be invariant under a gauge transformation,

$$Z = \int \mathcal{D}U \; e^{-S[U]} = \int \mathcal{D}U' \; e^{-S[U']} \; , \tag{1.24}$$

where a gauge transformation has been shown by $U \to U'$. The other fields have been suppressed in the above equation for simplicity. We have already seen in the previous section that the action is invariant under a gauge transformation, i.e. $S[U] = S[U']$. This means that the measure should also be gauge invariant. Since $\mathcal{D}U$ is a product of the measures over all links, each measure $\mathrm{d}U$ should be individually gauge invariant.

With appropriate normalization factors and gauge invariant structure, we now introduce the mathematically well-known $Haar$ measure for $SU(N)$ gauge groups, given by,

$$\mathrm{d}U = c\sqrt{\det(g(\theta))} \prod_{a=0}^{N^2-1} \mathrm{d}\theta_a \; , \tag{1.25}$$

where θ_a are the $N^2 - 1$ gauge group parameters of the $SU(N)$ group. $g(\theta)$ is the group metric defined by the group invariant distance $\mathrm{d}s$ as

$$\mathrm{d}s^2 = g(\theta)_{ab}\,\mathrm{d}\theta_a\,\mathrm{d}\theta_b\ . \tag{1.26}$$

The metric dependent factor in Eq. 1.25 ensures the gauge invariance of the measure. Explicit expressions are available in [27]. The factor c sets the appropriate normalization, usually,

$$\int \mathrm{d}U\ 1 = 1. \tag{1.27}$$

This ends our discussion of the measure of the path integral, and also the discussion regarding the construction of the lattice QFT.

1.1.3 Fermion doubling problem

We now take a detour to discuss about a very important issue of fermions on the lattice - the infamous fermion doubling problem. This has remarkable consequences for the construction of chiral gauge theories on the lattice. It was previously mentioned in Sec. 1.1.1, that the action for a single free fermion in Eq. 1.8 is not correct, as it gives rise to several species of fermions or doublers. Let us see how this happens.

We repeat the Euclidean lattice action for a single free fermion again for convenience,

$$S = a^4 \sum_{x\,\mu} \frac{1}{2a}\bar{\psi}_x\gamma_\mu(\psi_{x+\mu} - \psi_{x-\mu}) + a^4 \sum_x m\bar{\psi}_x\psi_x\ . \tag{1.28}$$

We now take the Fourier transform of the action using $\psi_x = \int \mathrm{d}^4k\, e^{ik\cdot x}\psi_k$, $\bar{\psi}_x = \int \mathrm{d}^4k\, e^{-ik\cdot x}\bar{\psi}_k$

and obtain

$$S = a^4 \int \mathrm{d}^4k \; \bar{\psi}_k \left(\sum_\mu \frac{i\gamma_\mu \sin k_\mu a}{a} + m \right) \psi_k \; , \tag{1.29}$$

where we have used $k\cdot\mu \equiv k\cdot a\hat{\mu} = k_\mu a$, $\hat{\mu}$ being the unit vector along the μ direction. The propagator in momentum space now reads as

$$G(k) = \frac{1}{\frac{i\gamma_\mu \sin k_\mu a}{a} + m} \; . \tag{1.30}$$

There is a summation over the repeated indices. Taking $m = 0$, we find 16 poles for the fermion propagator at

$$k_\mu = P_\mu^D = \begin{cases} (0,0,0,0) & D = 0 \\ (\frac{\pi}{a},0,0,0) \ \text{and 3 other combinations} & D = 1,2,3,4 \\ (\frac{\pi}{a},\frac{\pi}{a},0,0) \ \text{and 5 other combinations} & D = 5,\ldots,10 \\ (\frac{\pi}{a},\frac{\pi}{a},\frac{\pi}{a},0) \ \text{and 3 other combinations} & D = 11,\ldots,14 \\ (\frac{\pi}{a},\frac{\pi}{a},\frac{\pi}{a},\frac{\pi}{a}) & D = 15 \end{cases} \; .$$

As a result, we get 16 fermions on a hypercubic lattice at the vertices of the Brillouin zone in momentum space.

Near the poles P_μ^D shown above, let us define $k_\mu \equiv p_\mu + P_\mu^D$. Now,

$$\begin{aligned} \sin ak_\mu &= \sin ap_\mu \cos aP_\mu^D + \cos ap_\mu \sin aP_\mu^D \\ &= \sin ap_\mu \cos aP_\mu^D \qquad (\because \sin aP_\mu^D = 0) \\ &= \pm \sin ap_\mu \qquad (\because \cos aP_\mu^D = \pm 1) \; . \end{aligned} \tag{1.31}$$

Further, define $\gamma_\mu^D \equiv \cos aP_\mu^D \gamma_\mu$ which is a unitarily equivalent representation i.e. $\gamma_\mu^D = (R^D)^\dagger \gamma_\mu R^D$ where R^D are unitary matrices. Now, for each D, at finite p_μ and $a \to 0$, we have

$$\lim_{a\to 0} G^{-1}(k) = i\gamma_\mu^D p_\mu + m \ , \tag{1.32}$$

which is similar to the inverse fermion propagator in continuum, except the fact that we have 16 of them now, in the $a \to 0$ limit!

Ken Wilson proposed an elegant procedure to tackle the problem of multiple fermions by adding an extra term to the action. He added a näively irrelevant term of mass dimension 5 (relevant terms have mass dimension < 4) to the action in Eq. 1.28,

$$S_{WM} \sim -a \int \mathrm{d}^4x \ \bar{\psi}(x)\partial_\mu\partial_\mu\psi(x) \ , \tag{1.33}$$

which reads on the lattice as (with a coupling strength $\frac{r}{2}$)

$$\begin{aligned} S_{WM} &= -a^5 \frac{r}{2} \sum_{x\,\mu} \bar{\psi}_x \Delta_\mu^b \Delta_\mu^f \psi_x \\ &= a^4 \frac{r}{2a} \sum_{x\,\mu} \bar{\psi}_x (2\psi_x - \psi_{x+\mu} - \psi_{x-\mu}) \ . \end{aligned} \tag{1.34}$$

This is a momentum dependent mass term called the Wilson mass term. It breaks chiral symmetry (as mass terms always do). Rewriting the full action along with the Wilson term, we have

$$S_{WF} = a^4 \sum_{x\,\mu} \frac{1}{2a} \bar{\psi}_x \gamma_\mu (\psi_{x+\mu} - \psi_{x-\mu}) + a^4 \sum_x m\bar{\psi}_x\psi_x + a^4 \frac{r}{2a} \sum_{x\,\mu} \bar{\psi}_x (2\psi_x - \psi_{x+\mu} - \psi_{x-\mu}) \ . \tag{1.35}$$

Taking the Fourier transform, we find the inverse propagator to be

$$G^{-1}(k) = \sum_{\mu} i\gamma_{\mu} \frac{\sin k_{\mu} a}{a} + m + \frac{r}{a} \sum_{\mu} (1 - \cos k_{\mu} a) \ . \tag{1.36}$$

Now, repeating the previous analysis by setting $k_{\mu} = p_{\mu} + P_{\mu}^{D}$ and so on, we find at $a \to 0$ limit,

$$G(k) = \frac{1}{i\gamma_{\mu}^{D} p_{\mu} + M}, \quad \text{where} \quad M = m + \frac{2nr}{a}, \tag{1.37}$$

with

$$\begin{aligned}
n = 0 \quad &\text{for} \quad D = 0 \\
n = 1 \quad &\text{for} \quad D = 1, 2, 3, 4 \\
n = 2 \quad &\text{for} \quad D = 5, \ldots, 10 \\
n = 3 \quad &\text{for} \quad D = 11, \ldots, 14 \\
n = 4 \quad &\text{for} \quad D = 15 \quad .
\end{aligned}$$

As $a \to 0$, except for $D = 0$, the fifteen other fermions become infinitely heavy, as a result they do not propagate and get decoupled. Thus, this method does away with the excess fermions in a very elegant manner just by adding an irrelevant term to the action. However, the price one pays is the total loss of chiral symmetry which we discuss later.

1.1.4 Nielsen-Ninomiya theorem

This is a general theorem [2, 3] which considers the symmetries of the lattice fermion action and investigates the cause for the appearance of the fermion doublers. Under general assumptions of locality, Hermiticity and translation invariance, the theorem states that the lattice fermion propagator contains an equal number of left-handed and right-handed particles and the proof is done in the Hamiltonian approach, based on homotopy theory. Following Ref. [28], we present a simple way to only show how fermion doubling occurs with the lattice Euclidean action. There is a more general proof in Euclidean by Karsten [29]. A general lattice fermion action in the Euclidean momentum space is

$$S = \sum_{k} \bar{\psi}_k F(k) \psi_k \ , \tag{1.38}$$

where $F(k)$ is the inverse propagator. We now consider the following properties of the action:

- **Reflection positivity**: This is required for the existence of a self-adjoint Hamiltonian. Under this the ψ fields and $F(k)$ transform as

$$\Theta \psi_{k_0,\mathbf{k}} = \bar{\psi}_{-k_0,\mathbf{k}} \gamma_0 \ , \tag{1.39}$$

$$\Theta \bar{\psi}_{k_0,\mathbf{k}} = \gamma_0 \psi_{-k_0,\mathbf{k}} \ , \tag{1.40}$$

$$\Theta \left(\bar{\psi}_{k_0,\mathbf{k}} F(k) \psi_{k_0,\mathbf{k}} \right) = \bar{\psi}_{-k_0,\mathbf{k}} \gamma_0 F(k) \gamma_0 \psi_{-k_0,\mathbf{k}} \ . \tag{1.41}$$

  Thus, we must have

$$F(k) = \gamma_0 F^{\dagger}(-k_0, \mathbf{k}) \gamma_0 \ . \tag{1.42}$$

- **Invariance under the cubic group**: This comes from the hypercubic symmetry of the lattice. This is basically the previous condition for the rest of the three directions.

So, we have

$$F(k) = \gamma_1 F^\dagger(k_0, -k_1, k_2, k_3)\gamma_1 \tag{1.43}$$

$$= \gamma_2 F^\dagger(k_0, k_1, -k_2, k_3)\gamma_2 \tag{1.44}$$

$$= \gamma_3 F^\dagger(k_0, k_1, k_2, -k_3)\gamma_3 \ . \tag{1.45}$$

- **Chiral invariance**: For the action to be chirally invariant, we must have

$$F(k) = e^{i\theta\gamma_5} F(k) e^{i\theta\gamma_5} \ . \tag{1.46}$$

For an infinitesimal transformation, this becomes

$$F(k) = (1 + i\theta\gamma_5)\, F(k)\, (1 + i\theta\gamma_5) + \mathcal{O}\left(\theta^2\right), \tag{1.47}$$

which further leads to

$$F(k) = -\gamma_5 F(k)\gamma_5 \ . \tag{1.48}$$

Now we start from (1.48) and use the relations (1.45),(1.44),(1.43) and (1.42) progressively to arrive at the following relation :

$$\begin{aligned} F(k) &= -\gamma_0\gamma_1\gamma_2\gamma_3 F(k)\gamma_0\gamma_1\gamma_2\gamma_3 \\ &= \gamma_0\gamma_1\gamma_2 F^\dagger(k_0, k_1, k_2, -k_3)\gamma_0\gamma_1\gamma_2 \\ &= \gamma_0\gamma_1 F(k_0, k_1, -k_2, -k_3)\gamma_0\gamma_1 \\ &= -\gamma_0 F^\dagger(k_0, -k_1, -k_2, -k_3)\gamma_0 = -F(-k) \ . \end{aligned} \tag{1.49}$$

- **Locality**: For a theory with local interactions, we obtain the inverse propagator $F(k)$ to be continuous.

$F(k)$ is a periodic function and all momentum components are obtained modulo $2\pi/a$. From Eq.(1.49), we see that $F(k)$ has to vanish for every $ak_\mu = 0, \pm\pi$, leading to the 16 poles for the propagator. Both reflection positivity and invariance under cubic group are desirable conditions for a Euclidean lattice Lagrangian. The former leads to a real action and the latter to a Lorentz covariant theory in Minkowski spacetime. The only option thus left is to break the chiral symmetry at least partially to get rid of the excess fermions. Wilson achieved it by introducing the extra term that destroys chiral symmetry completely.

The issue of chiral symmetry is also related to the chiral anomaly on the lattice. The lattice regulator creates the extra species of fermions so that individual contributions get cancelled and the total anomaly is zero. Hence chiral symmetry is to be explicitly broken in the action to avoid doubling and generate the anomaly. It was shown by Karsten & Smit in [4] how the fermion doubling problem is deeply related to the chiral anomaly.

This concludes our discussion of some of the basics of lattice gauge theory, tailored for our needs to be used later in this thesis. These concepts will be important when we motivate the necessity of gauge-fixing for the construction of lattice chiral gauge theories.

1.2 Gauge-fixing in the continuum

The Euclidean Lagrangian density of $U(1)$ gauge theory or the free part of $SU(N)$ gauge theory (suppressing group indices) in the continuum is given by

$$\mathcal{L}_E = \frac{1}{4}F_{\mu\nu}F_{\mu\nu} = \frac{1}{4}\left(\partial_\mu A_\nu - \partial_\nu A_\mu\right)^2 . \tag{1.50}$$

One could näively construct a generating functional for the free theory in the following manner,

$$Z[J] = \frac{\int \mathcal{D}A_\mu \, e^{-\int d^4x(\mathcal{L}_E - J_l G_l)}}{\int \mathcal{D}A_\mu \, e^{-\int d^4x \, \mathcal{L}_E}}, \tag{1.51}$$

where the measure is formally gauge invariant and $J_l G_l$ is a gauge invariant source term constructed out of A_μ. But, Eq. 1.51 will not work as we shall see now.

The gauge action can be written, after an integration by parts and dropping the surface term, as

$$S_E = \int d^4x \, \frac{1}{2} A_\mu \underbrace{\left(-\Box \, \delta_{\mu\nu} + \partial_\mu \partial_\nu\right)}_{M_{\mu\nu}} A_\nu. \tag{1.52}$$

We shall see that the quadratic operator $M_{\mu\nu}$ is not invertible. After taking a Fourier transform, we obtain

$$M_{\mu\nu} \longrightarrow k^2 \delta_{\mu\nu} - k_\mu k_\nu. \tag{1.53}$$

Now, let us define two projection operators, P_L and P_T, which satisfy the usual properties of projection operators ($P_L^2 = P_L$, $P_T^2 = P_T$, $P_L P_T = 0$, $P_L + P_T = 1$),

$$(P_L)_{\mu\nu} \equiv \frac{k_\mu k_\nu}{k^2} \quad \text{and} \quad (P_T)_{\mu\nu} \equiv \delta_{\mu\nu} - \frac{k_\mu k_\nu}{k^2}. \tag{1.54}$$

The inverse of a linear combination $H = aP_T + bP_L$ of the above operators is simply $H^{-1} = a^{-1} P_T + b^{-1} P_L$ since $P_L P_T = 0$. In our case,

$$M_{\mu\nu}(k) = k^2 \delta_{\mu\nu} - k_\mu k_\nu = k^2 P_T + 0 \cdot P_L. \tag{1.55}$$

Hence, it is clearly seen that the quadratic operator $M_{\mu\nu}$ is not invertible and thus the free propagator is undefined.

Another way to understand the non-invertibility of $M_{\mu\nu}$ is that it has zero eigenmodes.

It can be easily seen in Eq. 1.55 that k_μ is an eigenvector with zero eigenvalue. Hence, the determinant of $M_{\mu\nu}$ is zero and it is non-invertible.

Let us look at it from another perspective. In momentum space, the gauge field A can be broken into longitudinal and transverse modes as $A = (P_L + P_T)A = A_L + A_T$. The Lagrangian density is essentially

$$\mathcal{L} \sim AMA = (A_L + A_T)k^2 P_T (A_L + A_T) = A_T k^2 A_T, \tag{1.56}$$

clearly showing that $\mathcal{L}$ does not depend on the longitudinal part of A.

Moreover, from the gauge transformation of A_μ in the momentum space i.e. $A_\mu \to A'_\mu = A_\mu + k_\mu\theta$, it is seen that the transformation only affects the longitudinal part of A since $P_T k_\mu = 0$. In path integral formalism, we integrate over both the components of A, but since $\mathcal{L}$ does not depend on A_L, integration over the longitudinal direction gives infinity.

A possible remedy to this problem is to fix the gauge and then quantize. Let us address the method formally. We want to integrate perpendicular to the gauge orbit. Let w be a n-dimensional vector, y a m-dimensional vector and $z = (w, y)$ a $(n+m)$-dimensional vector. Let $S(z) = S(w)$ i.e., the action depends only on w. The partition function is given as

$$\begin{aligned} Z &= \int dw \; \mathrm{e}^{-S[w]} \\ &= \int dw \; dy \; \delta^{[m]}(y) \; \mathrm{e}^{-S[w]}, \end{aligned}$$

where we have chosen to integrate along $y = 0$. But any y will do since S does not depend on y. Accordingly, we have

$$Z = \int \underbrace{dw\ dy}_{dz}\ \delta^{[m]}(y - \hat{y}(w))\ \mathrm{e}^{-S[w]}. \tag{1.57}$$

The integral can be done along any path in z-plane. This can be achieved through an implicit condition,

$$F_k(z) = F_k(w, y) = 0\ , \quad \text{where} \quad k = 1, \ldots, m. \tag{1.58}$$

We need m such conditions to fix all y. The function F has to be chosen carefully such that each value of w gives only one y. Let us assume a unique solution : $y = \hat{y}(w)$. Expanding $F_k(w, y)$ about $y = \hat{y}$ we have

$$F_k(w, y) = \cancelto{0}{F_k(w, \hat{y}(w))} + \sum_j \frac{\partial F_k}{\partial y_j}|_{y=\hat{y}}(y_j - \hat{y}_j(w)) + \cdots\ . \tag{1.59}$$

Define $R_{kj} \equiv \frac{\partial F_k}{\partial y_j}|_{y=\hat{y}}$. Near $y = \hat{y}$, we have

$$F(w, y) = R(y - \hat{y}(w)), \tag{1.60}$$

where we have suppressed the vector indices. The delta function $\delta^{(m)}(y - \hat{y}(w))$ is equal to $\delta^{(m)}(F(w, y))$ upto a factor, as seen below

$$\begin{aligned} \delta^{(m)}(F(w, y)) \underset{\text{near } y=\hat{y}}{=} \delta^{(m)}(R(y - \hat{y})) &= \frac{1}{|\det R|}\delta^{(m)}(y - \hat{y}), \\ \Rightarrow \delta^{(m)}(y - \hat{y}) &= |\det R|\, \delta^{(m)}(F(w, y)). \end{aligned} \tag{1.61}$$

This comes from the relation, $\delta^{(m)}(MX) = \frac{1}{|\det M|}\delta^{(m)}(X)$, where M is a $m \times m$ matrix

M and X is a m-vector.

Hence, the partition function becomes

$$Z = \int dz \left|\det \frac{\partial F}{\partial y}\right| \delta^{(m)}(F(z))\, \mathrm{e}^{-S[w]}. \tag{1.62}$$

This is an important result which we will use now in the case of gauge theory to do gauge-fixing.

Returning to the gauge theory, we have the following correspondence : $z = A_\mu(x)$ and $F(z) = F(A_\mu(x))$ is the gauge-fixing function. Some examples of $F(A_\mu(x))$ are given below :

- $F(A_\mu(x)) = \partial_\mu A_\mu(x)$ Landau or Lorentz gauge
- $F(A_\mu(x)) = \partial_i A_i(x)$ Coulomb gauge
- $F(A_\mu(x)) = A_3(x),$ Axial gauge
- $F(A_\mu(x)) = A_0(x),$ Temporal gauge

The Lorentz gauge is invariant under Euclidean symmetry and is used to prove the renormalizability of the gauge theory. In the Abelian case, all the gauge choices are unique, whereas in non-Abelian case, we find unique solutions only in perturbation theory, where the gauge fields are small. For large gauge transformations, it was shown by Gribov [30] that there are multiple solutions (called Gribov copies) to the gauge-fixing condition in non-Abelian gauge theories. The gauge-fixing procedure described below does not apply in that case straightforwardly. It does work if the gauge fields are restricted to the fundamental domain but it is highly non-trivial to achieve that.

We now have to calculate the determinant of $\partial F/\partial y$. Let us consider a non-Abelian gauge transformation $\mathrm{g} = \mathrm{e}^{-i\theta}$, where $\theta = \theta^a T^a$. The T^a are the gauge group generators, which satisfy the Lie algebra, $[T^a, T^b] = i f_{abc} T^c$, where the structure constants f_{abc} are totally antisymmetric in the indices. The generators are normalized as $\mathrm{tr}(T^a T^b) = \frac{1}{2}\delta_{ab}$. Under such transformations of the gauge field $A_\mu = A_\mu^a T^a$, we have, $A_\mu \to A'_\mu = \mathrm{g} A_\mu \mathrm{g}^\dagger + i(\partial_\mu \mathrm{g})\mathrm{g}^\dagger$. For infinitesimal gauge transformation (small θ), we have

$$\delta A_\mu = \partial_\mu \theta + i[A_\mu, \theta] = D_\mu \theta, \tag{1.63}$$

$$\Rightarrow \frac{\delta A_\mu}{\delta \theta} = D_\mu, \tag{1.64}$$

where $D_\mu^{ab} = \delta_{ab}\partial_\mu + f_{abc} A_\mu^c$, is the covariant derivative in the adjoint representation. Now, we choose the gauge-fixing function to be, $F(x) = \partial_\mu A_\mu(x) - h(x)$, where, $h(x)$ is any given function independent of A_μ. It then follows that

$$\frac{\delta F}{\delta \theta} = \frac{\delta F}{\delta A_\mu}\frac{\delta A_\mu}{\delta \theta} = \partial_\mu D_\mu. \tag{1.65}$$

Following Eq. 1.62, the generating functional for the free gauge theory in Eq. 1.51, then becomes

$$Z[J] = \frac{\int \mathcal{D}A_\mu \; |\det \partial_\mu D_\mu| \;\; \delta(\partial_\mu A_\mu - h) \; \mathrm{e}^{-\int d^4x \, (\mathcal{L}_E - J_l G_l)}}{\int \mathcal{D}A_\mu \; |\det \partial_\mu D_\mu| \;\; \delta(\partial_\mu A_\mu - h') \; \mathrm{e}^{-\int d^4x \, \mathcal{L}_E}}, \tag{1.66}$$

where $\delta(\partial_\mu A_\mu - h)$ is a functional δ-function which contributes only when $\partial_\mu A_\mu(x) - h(x) = 0 \;\; \forall \; x$. Since the function h is arbitrary, we can integrate over all such functions with a Gaussian measure, which amounts to multiplying a constant factor to both the numerator and denominator of the generating functional :

$$Z[J] = \frac{\int \mathcal{D}h \; \mathrm{e}^{-\frac{1}{2\alpha}\int d^4x \; h^2(x)} \int \mathcal{D}A_\mu(x) \;\; |\det \partial_\mu D_\mu| \;\; \delta(\partial_\mu A_\mu - h) \; \mathrm{e}^{-\int d^4x \; (\mathcal{L}_E - J_l G_l)}}{\int \mathcal{D}h' \; \mathrm{e}^{-\frac{1}{2\alpha}\int d^4x \; h'^2(x)} \int \mathcal{D}A_\mu(x) \;\; |\det \partial_\mu D_\mu| \;\; \delta(\partial_\mu A_\mu - h') \; \mathrm{e}^{-\int d^4x \; \mathcal{L}_E}}, \tag{1.67}$$

where α is an arbitrary real parameter. The h, h' integration can be done now to obtain,

$$Z[J] = \frac{\int \mathcal{D}A_\mu(x) \;\; |\det \partial_\mu D_\mu| \;\; \mathrm{e}^{-\int d^4x \; (\mathcal{L}'_E - J_l G_l)}}{\int \mathcal{D}A_\mu(x) \;\; |\det \partial_\mu D_\mu| \;\; , \mathrm{e}^{-\int d^4x \; \mathcal{L}'_E}}, \tag{1.68}$$

where $\mathcal{L}'_E = \mathcal{L}_E + \frac{1}{2\alpha}(\partial_\mu A_\mu)^2$. At this stage, the effective action is non-local due to the presence of the determinant factor. Hence, we must find a way to express the generating functional with a local action.

Since the derivatives ∂_μ and D_μ are anti-Hermitian, the determinant of $\partial_\mu D_\mu$ is real. Moreover in perturbation theory, where the gauge fields are small, the above determinant (which depends only on gauge fields) does not change sign. The overall sign of the determinant is immaterial as it gets canceled among the numerator and denominator of Eq. 1.68. Therefore, we can replace the modulus of determinant by just the determinant, in Eq. 1.68, to obtain

$$Z[J] = \frac{\int \mathcal{D}A_\mu \; \det(\partial_\mu D_\mu) \; \mathrm{e}^{-\int d^4x \; (\mathcal{L}'_E - J_l G_l)}}{\int \mathcal{D}A_\mu \; \det(\partial_\mu D_\mu) \; \mathrm{e}^{-\int d^4x \; \mathcal{L}'_E}}. \tag{1.69}$$

We now introduce two new fields $\bar{\eta}, \eta$ in the adjoint representation of the gauge group. They satisfy the following relations :

$$\{\eta(x), \bar{\eta}(y)\} = 0 \; , \qquad \{\eta(x), \eta(y)\} = 0. \tag{1.70}$$

These are called Grassmann variables. From Berezin rules for integration of Grassmann variables, we know that

$$\det\,(\partial_\mu D_\mu) = \int \mathcal{D}\eta\;\mathcal{D}\bar{\eta}\;\mathrm{e}^{-\int d^4x\;\bar{\eta}\,\partial_\mu D_\mu\,\eta}. \tag{1.71}$$

Plugging the above in Eq. 1.69, we obtain the generating functional with an effective local action,

$$Z[J] = \frac{\int \mathcal{D}A_\mu\;\mathcal{D}\eta\;\mathcal{D}\bar{\eta}\;\mathrm{e}^{-\int d^4x\;(\mathcal{L}''_E - J_l G_l)}}{\int \mathcal{D}A_\mu\;\mathcal{D}\eta\;\mathcal{D}\bar{\eta}\;\mathrm{e}^{-\int d^4x\;\mathcal{L}''_E}}, \tag{1.72}$$

where $\mathcal{L}''_E = \mathcal{L}'_E + \bar{\eta}(\partial_\mu D_\mu)\eta$. The Grassmann fields $\bar{\eta}$ and η are called the Fadeev-Popov ghosts. They do not have spin indices and they are not physical. The ghosts never appear as asymptotic states. The effective action together with fermions is now given as

$$\mathcal{L}_{\text{eff}} = \frac{1}{4}F^a_{\mu\nu}\;F^{\mu\nu a} + \frac{1}{2\alpha}(\partial_\mu A^a_\mu)^2 + \bar{\eta}^a(\partial_\mu D_\mu)^{ab}\eta^b + \bar{\psi}(\partial\!\!\!/ + ig A\!\!\!/^a T^a)\psi. \tag{1.73}$$

It should be stressed that the Fadeev-Popov gauge-fixing procedure explained above is only valid in weak coupling perturbation theory because of the reasons stated above.

We shall now consider the $U(1)$ case. Here, the transformation parameter θ is just a number and not a matrix. From Eqs. 1.63 and 1.65, we have $\delta F/\delta\theta = \Box$, where $\Box$ is the Laplacian in 4-dimensional Euclidean spacetime. The ghost term now becomes $\bar{\eta}(\partial_\mu\partial_\mu)\eta = \bar{\eta}\;\Box\;\eta$, which does not involve gauge fields. As a result, the ghosts are free and get decoupled from rest of the theory. Thus, ghosts play no role in Abelian theory.

Let us now consider the gauge-fixed Lagrangian density for pure $U(1)$ gauge theory,

$$\begin{aligned}\mathcal{L}'_E &= \frac{1}{4}F_{\mu\nu}F^{\mu\nu} + \frac{1}{2\alpha}(\partial_\mu A^a_\mu)^2 \\ &= \frac{1}{2}\partial_\mu A_\nu(\partial_\mu A_\nu - \partial_\nu A_\mu) + \frac{1}{2\alpha}\partial_\mu A_\mu \partial_\nu A_\nu. \end{aligned} \tag{1.74}$$

After integrating by parts, we have for the action

$$\begin{aligned}S'_E &= \int d^4x\ \mathcal{L}'_E \\ &= \frac{1}{2}\int d^4x\ A_\mu(-\Box\delta_{\mu\nu} + \partial_\mu\partial_\nu - \frac{1}{\alpha}\partial_\mu\partial_\nu)A_\mu. \end{aligned} \tag{1.75}$$

In contrast to Eq. 1.53, we now have, in momentum space, $M_{\mu\nu} = k^2\delta_{\mu\nu} - k_\mu k_\nu + \frac{1}{\alpha}k_\mu k_\nu$. The Lagrangian now depends also on the longitudinal components of the gauge field, which stops the path integral from diverging. It also follows that there are no zero eigenmodes of the quadratic operator M. Rewriting using P_L and P_T as defined earlier, we obtain

$$\begin{aligned} M_{\mu\nu} &= k^2 P_T + \frac{k^2}{\alpha}P_L, \\ \Rightarrow M^{-1} &= \frac{1}{k^2}P_T + \frac{\alpha}{k^2}P_L, \\ \Rightarrow M^{-1}_{\mu\nu} &= \frac{1}{k^2}\left(\delta_{\mu\nu} - \frac{k_\mu k_\nu}{k^2}\right) + \frac{\alpha}{k^2}\frac{k_\mu k_\nu}{k^2}, \\ &= \frac{\delta_{\mu\nu} - (1-\alpha)\frac{k_\mu k_\nu}{k^2}}{k^2}. \end{aligned} \tag{1.76}$$

Hence, we now have a well-defined free propagator after gauge-fixing. The gauge propagator in non-Abelian gauge theories can also be obtained in the above manner, after gauge-fixing. Thus, we see that gauge-fixing is essential in perturbation theory to obtain a well-defined gauge theory. The gauge symmetry is now explicitly broken but the Lagrangian still remains unchanged under a symmetry, the BRST symmetry.

Introducing an auxiliary field B^a, the gauge-fixed Lagrangian density $\mathcal{L}_{\text{eff}}$ can now be written as

$$\mathcal{L}_{\text{eff}} = \frac{1}{4} F^a_{\mu\nu}\, F^{\mu\nu a} + \bar{\psi}(\partial\!\!\!/ + ig A\!\!\!/^a T^a)\psi + \bar{\eta}^a(\partial_\mu D_\mu)^{ab}\eta^b + \frac{\alpha}{2} B^a B^a - iB^a \partial_\mu A^a_\mu, \quad (1.77)$$

which gives back (1.73) after a functional integration of B with the measure $\mathcal{D}B$. This form, known as the off-shell version, is suitable for demonstrating the BRST symmetry of the above.

1.2.1 BRST symmetry

In this section, we now discuss the BRST symmetry, introduced by Becchi, Rouet, Stora [31] and independently by Tyutin [32]. The BRST symmetry arises after gauge-fixing both the Abelian and non-Abelian gauge theories. However, in case of non-Abelian theories, it is crucial for proving renormalizability and unitarity. It is important to note that the above modifications to the theory do not change the physics. Using the generalized Ward identities for the BRST symmetry, it can be shown that the propagator for the longitudinal component of the gauge field is free to all orders, i.e. the longitudinal components do not couple to the physical degrees of fredom. The BRST transformations of the various fields are shown below, in some detail.

Let us now consider the non-Abelian gauge variations of the gauge and fermion fields, with a parameter $\theta = \theta^a T^a$. As previously mentioned in Eq. 1.63, infinitesimal variation of the gauge field, denoted by δ_θ, is given by

$$\delta_\theta A_\mu = \partial_\mu \theta + i[A_\mu, \theta] = D_\mu \theta. \tag{1.78}$$

For the fermion fields, the infintesimal gauge variations are as follows

$$\delta\psi = -i\theta\psi, \qquad \delta\bar{\psi} = i\bar{\psi}\theta. \tag{1.79}$$

After gauge-fixing by the Fadeev-Popov procedure and introduction of ghost and auxiliary fields, the gauge symmetry is explicitly broken. However, the action is now exactly invariant under the BRST symmetry transformations. The Fadeev-Popov gauge-fixed Lagrangian density, along with the auxiliary field B, obtained in Eq. 1.77, is once again given below,

$$\mathcal{L}_{\text{eff}} = \frac{1}{4} F^a_{\mu\nu} F^{\mu\nu a} + \bar{\psi}(\partial\!\!\!/ + ig A\!\!\!/^a T^a)\psi + \bar{\eta}^a (\partial_\mu D_\mu)^{ab} \eta^b + \frac{\alpha}{2} B^a B^a - iB^a \partial_\mu A^a_\mu. \tag{1.80}$$

It is to be noted that the ghost fields η and $\bar{\eta}$ are not related to each other.

The *Becchi-Rouet-Stora-Tyutin* or BRST transformation is now defined as follows:

- the BRST variation δ_B is Grassmann-valued and hence anti-commutes with other Grassmann fields (fermions and ghosts).
- the BRST variations of the fermion and the gauge fields remain the same as the infinitesimal gauge variations, in Eqs. (1.78) and (1.79), with parameter $\theta^a(x)$ replaced by $\eta^a(x)$, a real Grassmann field, which is the Fadeev-Popov ghost field.
- the BRST variation satisfies $\delta_B^2 = 0$ for all fields, i.e., the transformation is nilpotent (the nilpotency condition plays a vital role in proving the unitarity of the BRST

symmetric theory).

Hence, the BRST variations for $\psi, \bar{\psi}$ and A are given as follows

$$\delta_B \psi_i = -i\eta^a T^a_{ij} \psi_j \ , \quad \delta_B \bar{\psi}_i = i\eta^a \bar{\psi}_j T^a_{ji} \ , \tag{1.81}$$

$$\delta_B A^a_\mu = (\delta_{ab}\partial_\mu + f_{abc} A^c_\mu)\eta^b = D^{ab}_\mu \eta^b. \tag{1.82}$$

Under the above transformations, the gauge-invariant part of the Lagrangian density,

$$\mathcal{L}_{GI} = \frac{1}{4} F^a_{\mu\nu} \ F^{\mu\nu a} + \bar{\psi}(\partial\!\!\!/ + igA\!\!\!/^a T^a)\psi, \tag{1.83}$$

is still invariant under BRST, or in other words,

$$\delta_B \mathcal{L}_{GI} = 0. \tag{1.84}$$

Taking double BRST variation of the fermion field ψ, we find

$$\begin{aligned}
\delta_B(\delta_B \psi_i) &= \delta_B(-i\eta^a T^a_{ij} \psi_j) \\
&= -i(\delta_B \eta^a) T^a_{ij} \psi_j + i\eta^a T^a_{ij}(-i\eta^b T^b_{jk} \psi_k) \\
&= -i\left(\delta_B \eta^c - \frac{1}{2} f_{abc} \eta^a \eta^b\right) T^c_{ij} \psi_j.
\end{aligned} \tag{1.85}$$

where we have used Eq. 1.81, the anti-commutation of Grassmann-valued δ_B with η, and the antisymmetry of the indices in the second term. Using the nilpotency condition ($\delta_B^2 = 0$), one can now obtain the BRST variation for the ghost field η, from the above as,

$$\delta_B \eta^c = \frac{1}{2} f_{abc} \eta^a \eta^b, \quad \text{or,} \quad \delta_B \eta = -i\eta^2. \tag{1.86}$$

As a consistency check, we can now verify the nilpotency condition for gauge fields :

$$\begin{aligned}\delta_B\left(\delta_B A_\mu^a\right) &= \delta_B\left[\left(\delta_{ab}\partial_\mu + f_{abc}A_\mu^c\right)\eta^b\right] \\ &= \left(\delta_{ab}\partial_\mu + f_{abc}A_\mu^c\right)\delta_B\eta^b + f_{abc}\left(\delta_B A_\mu^c\right)\eta^b \\ &= D_\mu^{ab}\left(\delta_B\eta^b\right) + f_{abc}\left(\partial_\mu\eta^c\right)\eta^b + f_{abc}f_{cde}A_\mu^e\eta^d\eta^b. \end{aligned} \tag{1.87}$$

For the 2^{nd} term in the last line above, we should take only the antisymmetric part of $\left(\partial_\mu\eta^c\right)\eta^b$, since f^{abc} is completely antisymmetric :

$$\begin{aligned}\left(\partial_\mu\eta^{[c}\right)\eta^{b]} &= \frac{1}{2}\left[\left(\partial_\mu\eta^c\right)\eta^b - \left(\partial_\mu\eta^b\right)\eta^c\right] \\ &= \frac{1}{2}\partial_\mu\left(\eta^c\eta^b\right), \end{aligned} \tag{1.88}$$

where we have used the anti-commuting nature of Grassmann variables. Similarly in the 3^{rd} term, the antisymmetry of $\eta^d\eta^b$ is used to replace $f_{abc}f_{cde}$ by its antisymmetric part, which is

$$\frac{1}{2}\left(f_{abc}f_{cde} - f_{adc}f_{cbe}\right) = \frac{1}{2}\left(f_{abc}f_{cde} + f_{dac}f_{cbe}\right) = -\frac{1}{2}f_{bdc}f_{cae}, \tag{1.89}$$

where the Jacobi identity for the structure constants has been used,

$$f_{abc}f_{cde} + f_{dac}f_{cbe} + f_{bdc}f_{cae} = 0. \tag{1.90}$$

Plugging the above results in Eq. 1.87, we find

$$
\begin{aligned}
\delta_B\left(\delta_B A_\mu^a\right) &= D_\mu^{ab}\left(\delta_B \eta^b\right)+\frac{1}{2} f_{abc} \partial_\mu\left(\eta^c \eta^b\right)-\frac{1}{2} f_{bdc} f_{cae} A_\mu^e \eta^d \eta^b \\
&= D_\mu^{ah}\left(\delta_B \eta^h\right)-\left(\delta_{ah} \partial_\mu+f^{ahe} A_\mu^e\right) \frac{1}{2} g f^{cbh} \eta^c \eta^b \\
&= D_\mu^{ah}\left(\delta_B \eta^h-\frac{1}{2} f^{cbh} \eta^c \eta^b\right)=0,
\end{aligned} \tag{1.91}
$$

where we have used the BRST variation of ghost field η, given in Eq. 1.86. The above exercise shows that the η variation is consistent with the nilpotency condition. The BRST transformations for the remaining fields are given as

$$
\delta_B \bar{\eta}^a = -iB^a, \tag{1.92}
$$

$$
\delta_B B^a = 0. \tag{1.93}
$$

All the ghost sector fields, η, $\bar{\eta}$ and B, also satisfy the nilpotency condition. For the auxiliary field B, the nilpotency condition is satisfied trivially and for the $\bar{\eta}$ field, it can be seen easily from Eq. 1.93. The nilpotency condition for the ghost field η can be checked as,

$$
\begin{aligned}
\delta_B\left(\delta_B \eta^c\right) &= \delta_B\left(\frac{1}{2} f_{abc} \eta^a \eta^b\right) \\
&= \frac{1}{2} f_{abc}\left[\left(\delta_B \eta^a\right) \eta^b-\eta^a\left(\delta_B \eta^b\right)\right] \\
&= \frac{1}{2} f_{abc}\left[\frac{1}{2} f_{dea} \eta^d \eta^e \eta^b-\eta^a\left(\frac{1}{2} f_{deb} \eta^d \eta^e\right)\right] \\
&= \frac{1}{4} f_{abc} \eta^d \eta^e\left[f_{dea} \eta^b-f_{deb} \eta^a\right]=0,
\end{aligned} \tag{1.94}
$$

from the antisymmetry of the indices of the structure constants and ghost fields. This completes the discussion of the BRST transformation of the fields of the theory. It can now be finally shown that the gauge-fixed Lagrangian is invariant under the BRST symmetry.

Using Eqs. 1.92,1.82 and 1.93, we see that the Lagrangian density in Eq. 1.80 can be rewritten as,

$$\begin{aligned}\mathcal{L} &= \mathcal{L}_{GI} + \frac{\alpha}{2}B^a B^a - \delta_B\left(\bar{\eta}^a \partial_\mu A^a_\mu\right) \\ &= \mathcal{L}_{GI} + \delta_B\left(i\frac{\alpha}{2}\bar{\eta}^a B^a - \bar{\eta}^a \partial_\mu A^a_\mu\right) ,\end{aligned} \tag{1.95}$$

which is clearly invariant under BRST transformation using Eqs. 1.84 and the nilpotency condition.

1.3 Gauge-fixing on the lattice

So far, we have discussed the necessity of gauge fixing in the continuum. For non-perturbative calculations on a lattice, there is no need for gauge-fixing due to the compact nature of the gauge fields. The functional integral on a finite lattice is well-defined. Gauge-invariant observables can be calculated on the lattice without resorting to any particular gauge. However, gauge-fixing is sometimes done in Lattice Quantum Chromodynamics (LQCD) investigations to match continuum results, obtained in a particular renormalization scheme, for e.g. $\overline{MS}$. The gauge-fixing in this case is usually done on lattice gauge field configurations by numerically extremizing a functional and not at the level of the action. Hence, we may refer to such gauge-fixings as non-perturbative retrospective gauge-fixing (NPRGF). NPRGF is also employed to study gauge non-invariant observables and match results with continuum done in a particular gauge. For a review of NPRGF and problems therein, the reader is referred to Ref. [33].

We shall now discuss the non-perturbative gauge-fixing (NPGF) on the lattice, which is different from NPRGF in the sense that the gauge-fixing now is done at the level of the action. Since the Wilsonian lattice formulation is manifestly gauge-invariant and does not require gauge-fixing, it is an interesting question to ask if NPGF offers a valid alternative formulation of gauge theories on the lattice. The quest to answer this question is one of the aims of this thesis. There are some important motivations to study NPGF on the lattice, for example, the formulation of manifestly local lattice chiral gauge theories (ChLGT).

Before going on to a discussion of ChLGT, it is imperative to point out the role of the longitudinal gauge degrees of freedom (*lgdof* s), in lattice gauge theories containing gauge non-invariant terms. Let us consider a pure gauge action $S[U]$ with gauge invariant $S_{GI}[U]$ and non-invariant $S_{NI}[U]$ terms. Due to the Haar measure, the functional integral is over all gauge configurations, including the ones related to each other by gauge transformations. After a gauge transformation $\mathrm{g} \in G$, the partition function $Z = \int \mathcal{D}U\, \exp(-S[U])$ becomes

$$
\begin{aligned}
Z' &= \int \mathcal{D}U\, \exp(-S_{GI}[U] - S_{NI}[\mathrm{g}_x U_{x\mu} \mathrm{g}^\dagger_{x+\mu}]) \\
&= \int \mathcal{D}U \mathcal{D}\phi\, \exp(-S_{GI}[U] - S_{NI}[\phi^\dagger_x U_{x\mu} \phi_{x+\mu}]), \qquad (1.96)
\end{aligned}
$$

where we have substituted $\mathrm{g}_x = \phi^\dagger_x$ and multiplied $\int \mathcal{D}\phi = 1$.

Thus, we see that the *lgdof*s become explicitly present in the gauge non-invariant terms of the action, involving physical degrees of freedom, and thereby, interact with the physical degrees of freedom. Without gauge-fixing, this interaction is strong irrespective of the strength of the usual gauge coupling. The reason is that the *lgdof* s are random fields in the absence of any gauge-fixing term and any point on the gauge orbit is as likely as any other. This essentially makes the gauge fields very rough. The *lgdof* s now act as gauge-group valued scalar ϕ fields which are radially frozen. Depending on the target renormalized theory, we may want to decouple them in the continuum limit.

1.3.1 Chiral lattice gauge theory

The construction of chiral gauge theories on the lattice (ChLGT) is a long-standing problem with several difficulties. As discussed in Sec. 1.1.4, the Nielsen-Ninomiya theorem and the chiral anomaly pose severe constraints for realizing chiral symmetry on the lattice. In order to avoid the doublers, one has to introduce terms in the action which explicitly break the chiral symmetry. For a vector-like theory, therefore, the global chiral symmetry is explicitly broken on the lattice. However, it does not pose much of a problem as it is expected to be restored in the continuum limit. On the other hand, if we try to gauge the chiral symmetry, we no longer have gauge invariance.

When we construct chiral gauge theory using manifestly local lattice fermions like the Wilson fermions, there are gauge non-invariant terms in the lattice action (see Sec. 1.1.3). As we have seen just in the section above, the *lgdof*s appear in the gauge non-invariant terms which thereby, couple to the fermions. This interaction is generally strong leading to fermion-scalar bound states and the chiral nature of the fermion spectrum is spoiled. Since the coupling of the *lgdof*s and fermions is non-perturbative, the *lgdof*s and their interactions survive even at small gauge couplings towards the continuum limit. This has led to the failure of a wide class of manifestly local ChLGT proposals [5, 6, 34–39]. It should be noted that changing the lattice fermion prescription cannot solve the problem.

A way to address the above problem is to control the dynamics of the unphysical degrees of freedom. This amounts to adding a kinetic term for the *lgdof*s or in other words, gauge-fixing. Addition of a gauge-fixing term enlarges the parameter space of the theory, something that may give rise to a critical point, the continuum limit around which gives us the desired ChLGT, with the unphysical ϕ modes (defined in Eq. 1.96) hopefully decoupling from the physical spectrum. A renormalizable gauge is required to obtain counter terms, if necessary, through usual power-counting and Slavnov-Taylor identities can be used to tune parameters to restore BRST invariance. This approach was first tried in the context of lattice perturbation theory in [40]. For reviews on the gauge-fixing approach to ChLGT, the reader is referred to [41, 42].

A different approach of constructing ChLGT is by going around the Nielsen-Ninomiya theorem, by modifying the definition of chiral symmetry on the lattice. Using fermions which satisfy the Ginsparg-Wilson relation [7], the modified chiral symmetry is then an exact symmetry of the action. However, the fermion measure is gauge link-dependent and leads to an integrability condition on the space of lattice gauge fields. An exact solution to the integrability condition was obtained in the Abelian case [8]. However, for the non-Abelian case, no non-perturbative solution is known. A solution was obtained only in perturbation theory which requires infinite number of irrelevant counter-terms [43]. For a review, see [44].

We end this part with the comment that it appears to be crucial to control the *lgdofs* through gauge-fixing in order to construct manifestly local formulations of ChLGT. However, one faces some difficulties while trying to do NPGF on the lattice, which we discuss in the following sections.

1.3.2 Neuberger's No-Go Theorem

Let us proceed to gauge-fix the lattice gauge action in the BRST scheme, as discussed in Sec. 1.2. The first step is to multiply the path integral by the gauge-fixing partition function

Z_{gf}. After gauge fixing, the partition function becomes

$$Z = \int \mathcal{D}\Xi \; \mathrm{e}^{-S_{GI}} \mathrm{e}^{-S_{GF}}, \tag{1.97}$$

where S_{GI} is the gauge-invariant and S_{GF} is the non-invariant gauge fixing part of the Fadeev-Popov gauge-fixed action. The new integration measure $\mathcal{D}\Xi = \mathcal{D}U \; \mathcal{D}B \; \mathcal{D}\eta \; \mathcal{D}\bar{\eta}$ is a BRST invariant one. The expectation value of a gauge invariant operator now becomes

$$< \mathcal{O} >= \frac{1}{Z} \int \mathcal{D}\Xi \; \mathrm{e}^{-S_{GI}} \mathrm{e}^{-S_{GF}} \; \mathcal{O}. \tag{1.98}$$

Being gauge invariant, the operator which contains only physical fields is also BRST invariant. Therefore the full integrand is BRST invariant. The above expectation value should be equal to the one obtained in the theory without gauge-fixing.

Let us now investigate the new expectation value carefully. From the Fadeev-Popov gauge-fixed action in Eq. 1.95, the gauge-fixing part S_{GF} can be written as

$$S_{GF} = \sum_x \left[\frac{\alpha}{2} B_x^a B_x^a - \delta_B \left(\bar{\eta}_x^a F^a(U_x) \right) \right], \tag{1.99}$$

where $F(U)$ is any gauge-fixing function. Let us define the following

$$S_{GF}(t) \equiv \sum_x \left[\frac{\alpha}{2} B^a B^a - t\delta_B \left(\bar{\eta}^a F^a \right) \right], \tag{1.100}$$

$$F_{\mathcal{O}}(t) \equiv \int \mathcal{D}\Xi \; \mathrm{e}^{-S_{GI}} \mathrm{e}^{-S_{GF}(t)} \mathcal{O}, \tag{1.101}$$

the latter being equal to the numerator of (1.98) when $t = 1$. Now,

$$\begin{aligned}
\frac{dF_{\mathcal{O}}}{dt} &= \int \mathcal{D}\Xi \left[\sum_x \delta_B(\bar{\eta}F)\right] \mathrm{e}^{-S_{GI}} \mathrm{e}^{-S_{GF}} \mathcal{O} \\
&= \int \mathcal{D}\Xi \, \delta_B \left[(\sum_x \bar{\eta}F)\mathrm{e}^{-S_{GI}} \mathrm{e}^{-S_{GF}} \mathcal{O}\right] \\
&= 0,
\end{aligned} \tag{1.102}$$

because the integration of a total BRST variation is zero. It is remarked here that, if the B^2 term were multiplied by t, the above proof would not have gone through, as the $t = 0$ limit is ill-defined due to the divergent B integral in that case.

On the other hand, $F_{\mathcal{O}}(0) = 0$ since $\int \mathcal{D}\Xi \, \mathrm{e}^{-S_{GF}} = 0$ by rules of Grassmann integration, as the integrand is devoid of Grassmann variables for $t = 0$ ($\int d\eta \; \alpha = 0$, where α is a real number and $\int d\eta \; \eta = 1$). By (1.102), we then have $F_{\mathcal{O}}(1) = 0$. Similarly we can show that $Z(1) = 0$. To our dismay, $< \mathcal{O} >$ takes the indeterminate $\frac{0}{0}$ form. This is the Neuberger's no-go theorem [1].

The existence of Gribov copies is connected to the no-go theorem. It has been shown in Ref. [1], that the Gribov copies are always present in even numbers resulting in alternating signs for the contributions of the functional integrals. Thus, BRST symmetry then ensures that the contribution to the functional integration with alternating signs cancel with each other, giving rise to the indeterminate $\frac{0}{0}$ form.

1.3.3 Lattice Gribov copies

For $U(1)$ gauge theory in the continuum, the gauge fixing term is $S_{GF} = \frac{1}{2\alpha}(\partial_\mu A_\mu)^2$. We aim to construct a lattice gauge-fixing term S^L_{GF} which in the continuum limit should go to

S_{GF}. Following the discussion in Ref. [25], let us construct a simple gauge-fixing term as

$$S_{GF}^{\text{näive}} = \frac{1}{2\alpha}\sum_x \left(\sum_\mu (\mathbb{A}_{x\mu} - \mathbb{A}_{x-\mu,\mu})\right)^2 = \frac{1}{2\alpha}\sum_x \left(\sum_\mu \Delta_\mu^b \mathbb{A}_{x\mu}\right)^2, \tag{1.103}$$

where $\mathbb{A}_{x\mu} = \frac{1}{2i}\left(U_{x\mu} - U_{x\mu}^\dagger\right) = \mathrm{Im}(U_{x\mu})$. So, the gauge fixing condition is

$$\sum_\mu (\mathbb{A}_{x\mu} - \mathbb{A}_{x-\mu,\mu}) = 0. \tag{1.104}$$

The above condition is satisfied by $U_{x\mu} = 1$ but this not the only solution. For example, let us make a gauge transformation

$$\begin{aligned} \mathrm{g}_x &= -1 \text{ for } x = x_0, \\ &= \quad 1 \text{ for } x \neq x_0. \end{aligned}$$

This keeps all the gauge fields intact except taking the links touching x_0 i.e. $U_{x_0\mu} \to -U_{x_0\mu}$ and $U_{x_0-\mu,\mu} \to -U_{x_0-\mu,\mu}$. This is clearly another solution to the gauge-fixing condition. These dense set of solutions are called lattice Gribov copies. These have no counterpart in the continuum and leads to deviations from the expected results. Thinking in terms of perturbative expansion, no unique expansion is possible due to the presence of multiple minima. So the näive discretization leads to trouble. One should, therefore, devise a non-perturbative gauge-fixing mechanism on the lattice in such a manner, that it evades both the no-go theorem and the occurrence of lattice Gribov copies.

The main goal of this thesis is to study different non-perturbative gauge-fixing schemes for both Abelian and non-Abelian gauge theories on the lattice.

CHAPTER 2

NUMERICAL TECHNIQUES

Lattice gauge theory highly makes use of computers to obtain results that are otherwise impossible to obtain analytically. This requires the development and use of efficient algorithms to calculate observables on the computer. The use of numerical methods and computational facilities have reached such a level that there is now a devoted lattice gauge community working together with applied mathematicians and computer scientists in order to develop cutting-edge algorithms and state-of-the-art machines. For a review of the latest developments, the reader is referred to Lattice 2018 plenary talk by Meifeng Lin.

In lattice gauge theory, one usually calculates an observable by calculating the path integral as shown in Eq. 1.1. As discussed in the previous chapter, the path integral on the lattice is a large integral over all the possible configurations of the finite number of degrees of freedom on a finite volume. The path integral can be approximately calculated to a high precision using Monte Carlo importance sampling methods. The Monte Carlo method basically generates ensembles of the degrees of freedom with a probability distribution. The measurement of an observable is now done over N number of ensembles and the statistical error associated with the mean value is $O(1/\sqrt{N})$. For a detailed introduction to numerical techniques on the lattice, the reader is referred to the book [27]. Our work was done using the following Monte Carlo updation algorithms - Multihit Metropolis, Hybrid Monte Carlo (HMC) and Stochastic Tunneling HMC. These are discussed briefly in the following sections.

2.1 Multihit Metropolis

The Multihit Metropolis is an extension of the Metropolis algorithm, which is generally regarded as the "mother of Monte Carlo algorithms". The Metropolis algorithm is widely known and in this section, we briefly mention the steps in the context of lattice gauge theories. The algorithm basically gives a prescription to generate gauge field configurations with the probability distribution $\exp(-S[U])$, where $S[U]$ is the Euclidean lattice gauge action. The steps of the algorithm are as follows :

1. A gauge link $U_{x\mu}$ at a lattice site x and direction μ is selected randomly or in some order. A new gauge link $U'_{x\mu}$ is generated by a symmetric selection probability $T(U|U') = T(U'|U)$.

2. The change in the action ΔS, associated with introducing the new link, is calculated. The new link $U'_{x\mu}$ is accepted if $\exp(-\Delta S) > r$, where r is a random number uniformly distributed in $[0, 1)$. It is rejected otherwise.

3. The above steps are repeated for other sites and directions till the whole lattice has been updated. The updation of all the links is called a sweep. After each sweep, we obtain a new configuration over which the observables are measured.

In practice, the calculation of the sum of staples, required for computing the change in action ΔS (in step 2 above) for the Wilson gauge action S, is computationally costly. Hence, it is economical to update a link several times keeping the sum of staples fixed before moving on to another link. This is an implementation of the so-called *Multihit* Metropolis (MM) algorithm for gauge theories. The number of updates or *hits* at each site at a time is a tunable parameter. In the limit of infinite number of hits, the MM is theoretically equivalent to the Heat-bath algorithm.

It is important to note that both the Metropolis and the MM are local algorithms which update each link individually and therefore, may not be suitable for action densities which extend several sites beyond nearest neighbors.

2.2 Hybrid Monte Carlo

The Hybrid Monte Carlo (HMC) [45] is perhaps the most popular algorithm to study lattice gauge theories with fermion and gauge fields. The HMC is called "hybrid" since it combines different algorithms together to make an exact algorithm.

The Molecular Dynamics (MD) algorithm [46–48] is used to update the gauge fields. A fictitious quadratic momentum term is added to the action $S[U]$ to give it a look of a "Hamiltonian" $H[U, \pi] = S[U] + \pi^2/2$ that would evolve the system in "computer time". The conjugate momenta π are initialized by a Gaussian heat bath method. The gauge fields U and the momenta π are then updated in a MD trajectory by numerically solving the Hamilton's equations of motion in discrete steps of the computer time.

The discretization errors arising at the end of the MD trajectory are exactly corrected by the Metropolis Monte Carlo accept/reject step. This requires the MD trajectory to satisfy time-reversibility and conservation of the phase space volume. The common choice for the numerical method, satisfying the above conditions, is the Störmer-Verlet method, better known as Leapfrog method. The above steps satisfy the detailed balance condition and constitute the HMC algorithm for gauge fields. HMC is a global algorithm in the sense that all degrees of freedom are updated at the Metropolis accept/reject step after a MD trajectory. A priori this appears better suited for theories with complicated interactions and action densities spread over more than the nearest neighbors.

The updation of Grassmann-valued fermion fields is incorporated in HMC, using the pseudofermion method. The Grassmann integration can be done analytically to obtain the fermion determinant, which can be further converted exactly into an integral representation with complex-valued scalar fields, known as "pseudofermions", which have the same number of degrees of freedom as fermions. The pseudofermions are then updated in a Gaussian heat bath method. It is to be noted that this method is only applicable for a single fermion if the fermion determinant is real and positive or for even number of mass-degenerate fermions with real determinants.

The Hamiltonian for a theory with two mass-degenerate fermions and gauge fields, is thus

$$H = \mathcal{S}[U, \varphi] + \frac{1}{2} \sum_{x\mu} \mathrm{tr}(\pi_{x\mu})^2, \tag{2.1}$$

where $\mathcal{S}[U, \phi] = \mathcal{S}_W[U] - \varphi^\dagger (DD^\dagger)^{-1} \varphi$ is the effective action, with φ being the pseudofermion field, D being the Dirac operator matrix and $\mathcal{S}_W$ the usual Wilson plaquette action. π is the fictitious momentum conjugate to gauge fields. The steps of the HMC algorithm for a single MD trajectory, using leapfrog discretization of the MD trajectories, are as follows :-

1. **Pseudofermions** : Define $\chi = D^{-1}\varphi$. This makes $\exp(-\varphi^\dagger (DD^\dagger)^{-1} \varphi) = \exp(-\chi^\dagger \chi)$.

The χ fields are now generated by a Gaussian distribution and the pseudofermion field is extracted as $\varphi = D\chi$. The matrix D is obtained from the initial gauge field configuration U_0. The φ fields are held fixed for a given MD trajectory.

2. **Conjugate momenta** : The initial conjugate momenta fields π_0 are generated according to the Gaussian distribution $\exp(-\pi^2)$.

3. **Initial half step** : The initial Hamiltonian H_i is now computed with the previous field configuration and the momentum generated in the above step. The gauge fields are now updated half-step (ε being the step size), using the initial momentum and gauge configuration.
   $(U_{x\mu})_{\frac{1}{2}} = \exp\left((\varepsilon/2)(\mathrm{i}\pi_{x\mu})_0\right)(U_{x\mu})_0.$

4. **Intermediate steps** :
   Full step updates then follow for $k = 1, \ldots, n-1$ for both the gauge fields and the momenta in a leapfrog manner, where n is the total number of steps, in the following way:
   $(\mathrm{i}\pi_{x\mu})_k = (\mathrm{i}\pi_{x\mu})_{k-1} - \varepsilon F_{x\mu}[U,\varphi]\Big|_{U_{k-\frac{1}{2}}} \quad , \quad (U_{x\mu})_{k+\frac{1}{2}} = \exp\left(\varepsilon(\mathrm{i}\pi_{x\mu})_k\right)(U_{x\mu})_{k-\frac{1}{2}}.$
   $F[U,\varphi]$ is the derivative of the Hamiltonian with respect to the gauge link U, or in other words, the gauge field force term.

5. **Final half step** :
   $(\mathrm{i}\pi_{x\mu})_n = (\mathrm{i}\pi_{x\mu})_{n-1} - \varepsilon F_{x\mu}[U,\varphi]\Big|_{U_{n-\frac{1}{2}}} \quad , \quad (U_{x\mu})_n = \exp\left((\varepsilon/2)(\mathrm{i}\pi_{x\mu})_n\right)(U_{x\mu})_{n-\frac{1}{2}}.$

6. **Accept/Reject step** : The final Hamiltonian H_f at the end of the MD trajectory is now calculated with the updated gauge and momentum field configuration. The updated configuration is now accepted or rejected depending upon $\Delta H = H_f - H_i$, as is done for Metropolis algorithm.

The force F, which is calculated during each step in a MD trajectory, has a term proportional to the inverse of $DD^{\dagger}$, the computation of which is the most time-consuming part of HMC. Different Krylov space solvers, like Conjugate Gradient (CG), Minimal Residue, etc., are used to achieve this inversion iteratively.An important point to note that is the MD step size ε and the number of steps can be tuned to control the acceptance rates of the algorithm. Smaller step sizes and number of steps make the system move slowly in the configuration space with HMC time, resulting in higher acceptance but larger autocorrelations. On the other hand, the system changes too much with larger steps and step sizes, contributing to poor acceptance rates.

We have used the HMC algorithm extensively throughout this work for both the higher-derivative (HD) gauge-fixing of the pure $U(1)$ theory and also for the equivariantly gauge-fixed pure $SU(2)$ theory with ghost fields in the $SU(2)/U(1)$ coset. More details will be provided at the later chapters for the implementation of the HMC algorithm for these theories. However, it may be pointed out here that, the ghosts are treated very much like the fermions as discussed here, except that they are replaced by real-valued scalar fields, to be called pseudoghosts, with the same internal degrees of freedom as the original ghosts.

2.3 Stochastic Tunneling HMC

Originally proposed by Golterman and Shamir [22] in the context of overlap and domain-wall fermions, the Tunneling Hybrid Monte Carlo (THMC) is a modification of the HMC algorithm, to improve its ergodicity in situations where near-zero eigenmodes are present in the fermion probability weight. As we have mentioned in the previous section, the force term involves the inverse of the fermion matrix & therefore, near-zero eigenvalues of the matrix result in blowing up of the force. This leads to poor acceptance, ultimately bringing the updation process to a standstill. The exact zero eigenvalues, therefore, act as infinite barriers in the configuration space. Hence, HMC cannot scan the entire configuration space properly resulting in poor ergodicity.

The THMC algorithm proposes to factorize the fermion determinant in such a manner that the near-zero eigenmodes are separated out. The MD evolution then occurs with a different Hamiltonian H_{MD}, whereas the original Hamiltonian is

$$H = H_{\mathrm{MD}} + H_{\mathrm{corr}} \ . \tag{2.2}$$

The correction term H_{corr}, which consists of the contribution from the near-zero modes, is kept out of the MD evolution. This allows the system to tunnel across the infinite barriers without encountering difficulties. The error arising due to the exclusion H_{corr}, is corrected by considering the total Hamiltonian H in the accept/reject step.

In [22], the authors put forward both deterministic and stochastic implementations of THMC. The deterministic approach is computationally expensive, whereas the stochastic one is a more economical implementation. We have used a modified[1] stochastic implementation of THMC (sTHMC), which we will discuss explicitly for our system, later in Sec. 5.6.2.

[1]Suggested by the authors of [22], through private correspondence.

CHAPTER 3

NON-PERTURBATIVE GAUGE-FIXING OF COMPACT $U(1)$ LATTICE GAUGE THEORY

3.1 Introduction

As motivated in Chapter 1, although the lattice gauge formulation in the Wilson framework does not require gauge-fixing, there are situations where it is necessary to control the unphysical longitudinal gauge degrees of freedom (*lgdof* s). Since we have seen that fermions on the discrete lattice necessarily break chiral symmetry, [2–4, 7], the formulation of lattice chiral gauge theories in the Wilson approach[1] (without gauge-fixing) necessarily means strong coupling between the physical degrees of freedom and the *lgdof*s. The rough gauge problem and the undesired presence of *lgdof*s led to the failure of a full class of manifestly local lattice chiral gauge theories [34–37]. These failures gave rise to the understanding

[1] In a different approach of constructing lattice chiral gauge theory, the chiral symmetry on lattice is modified according to the Ginsparg-Wilson relation [7].

that controlling the dynamics of *lgdof*s in these theories (in other words, gauge-fixing) is essential to avoid undesirable results. A general gauge-fixing scheme for compact gauge fields associated with the lattice link fields, applicable at all strengths of the interaction including non-perturbative values, is thus very welcome.

However, the BRST scheme (discussed in Sec. 1.2.1), a standard mechanism for taking care of the redundancy related to the *lgdof*s, cannot be used in this general non-perturbative case with compact gauge fields. This is due to the No-Go theorem by Neuberger discussed in Sec. 1.3.2.

For the general non-Abelian case, the above theorem can be evaded by employing an equivariant BRST (eBRST) formalism [17,18] where gauge-fixing is done only in the coset space, leaving minimally a Cartan subgroup gauge-invariant. This is the topic of our study in this thesis in Chapter 5. This may be taken as a viable alternate non-perturbative scheme for defining a non-Abelian gauge theory.

Due to the no-go theorem, any BRST-type symmetry cannot also be maintained for the Abelian theory. As shown in Sec. 1.3.3, a naive lattice transcription of a covariant gauge fixing term results disastrously in a dense set of lattice Gribov copies. To overcome this issue, Shamir and Golterman [9,25] proposed to add, to the standard Wilson lattice gauge action for the compact $U(1)$ pure gauge case, a higher-derivative (HD) term (involving physical fields only), breaking gauge invariance explicitly. This term, as a first requirement, leads to a covariant gauge fixing term in the naive continuum limit, and, at the same time, is designed to ensure $U_{x\mu} = 1$ as a unique absolute minimum for the effective potential, thus avoiding the problem of the lattice Gribov copies and enabling weak-coupling perturbation theory (WCPT) around the unique vacuum. Counter-terms are possible to construct because of the emergence of a renormalizable gauge, and are required to restore gauge symmetry in the continuum limit.

WCPT analysis and numerical investigations performed earlier [10], only in the weak gauge coupling region of the above compact Abelian pure gauge theory, confirmed the existence of a new continuous phase transition between a regular ordered phase and a spatially modulated ordered phase, for sufficiently large value of the coefficient of the HD term. At this phase transition, gauge symmetry is restored and the scalar fields (*lgdof*s) decouple, leading to the desired emergence of massless free photons only, in the continuum limit taken from the regular broken phase.

Strong coupling of the *lgdof* with chiral fermions is what led to the failure of a prevalent class of non-perturbative chiral gauge theory proposal [5, 6]. With the success of the HD gauge-fixing model of the compact $U(1)$ lattice gauge theory in decoupling the *lgdof*, feasibility of manifestly local Abelian chiral gauge theories on lattice was shown for Wilson fermions [11, 12] and also for lattice domain wall fermions [13, 14]. It is worth mentioning here that, in the standard Wilsonian definition of a lattice gauge theory (that is, without gauge-fixing), the strong coupling of the unphysical *lgdof* with fermions (or with any physical degrees of freedom) in a gauge-noninvariant theory like a lattice chiral gauge theory, is irrespective of the strength of the usual gauge coupling. In fact, almost all studies in this area have been done in the so-called reduced model (i.e., in the limit of gauge coupling going to zero) and the basic problems are already present there.

All the success of the HD gauge-fixing approach for the Abelian theory is, so far, mainly in the reduced limit or in the weak gauge coupling region. The question naturally arises in a general framework as to what happens when the bare gauge coupling is not necessarily small. Obviously this question is linked with the issue of short distance behavior of $U(1)$ gauge theory and possibility of non-trivial physics. A comprehensive knowledge of the HD gauge-fixing scheme at a broad range of the gauge coupling is also desirable to understand the phase diagram and possible continuum limits of $U(1)$ chiral gauge theories constructed with this gauge-fixing approach.

A first preliminary account in this direction was presented, some time ago, in [49]. The novel FM-FMD[2] transition, that was responsible for the decoupling of the *lgdof* and the emergence of the original gauge symmetry, was still found to be present at stronger gauge couplings, with bare values larger than unity. With large gauge couplings, the FM-FMD transition was first order for small values of $\tilde{\kappa}$ (coefficient of the HD gauge-fixing term). Only at large $\tilde{\kappa}$, the transition was found to be continuous, with a tricritical point separating it from the first order transition. However, the nature of the possible continuum limit while approaching the continuous part of the transition from the FM-side was not studied. As a result the emerging physics at this transition was not clear.

In this chapter and the next, i.e., Chapter 4, we present results of our investigation of the HD gauge-fixed compact $U(1)$ lattice gauge theory at strong gauge couplings [15, 16]. In this chapter, in particular, we explore the phase diagram of the above compact $U(1)$ pure gauge theory with the HD gauge-fixing term and a suitable counter-term, *in the strong gauge coupling region* and present only the key findings at one value of strong gauge coupling ($g = 1.3$) regarding the nature of the possible continuum limits in that region [15]. A comprehensive account of the strong gauge coupling region, including a discussion of comparison of algorithms for the HD action [16] is presented in Chapter 4.

The chapter is organized as follows. In Sec. 3.2, the lattice action under investigation for the compact $U(1)$ gauge theory is presented. The main ideas of the HD gauge fixing action based on the theory at weak gauge coupling are reviewed. Sec. 3.2 also summarizes the main results from previous investigations of the theory at weak gauge couplings. Sec. 3.3 presents some of the details of our numerical investigations in the available parameter

[2] FM and FMD stand respectively for ferromagnetic and ferromagnetic directional phases. The nomenclature is derived from the phases of the theory in the so-called reduced limit, i.e., when the gauge coupling is zero, leaving the theory to be entirely a HD scalar theory.

space of the action, including the algorithms used in our investigation. The results of our investigation [15] at $g = 1.3$ are presented in Sec. 3.4 which identifies the tricritical point and determines the possible continuum limits. Finally, in Sec. 3.5, we present our conclusions on the possible continuum physics.

3.2 The Abelian Gauge Fixing Theory on Lattice

In this section, we briefly review the compact $U(1)$ gauge theory with the HD gauge-fixing term and mention its salient features validated mostly through analytic and numerical investigations, done earlier, at weak gauge couplings. Detailed accounts are found in [9, 10, 50].

The Euclidean action on a 4-dimensional hypercubic lattice is given by:

$$S = S_{\mathrm{W}} + S_{\mathrm{GS}} + S_{\mathrm{ct}}. \tag{3.1}$$

As we shall see in the following, the action S explicitly contains only physical fields and no ghost fields[3]. The gauge symmetry of the first term S_{W} is explicitly broken by the gauge-fixing second term S_{GS} and also by the third term S_{ct} in the above action.

The first term in (3.1), S_{W}, is the gauge-invariant standard Wilson term containing a summation over all gauge plaquettes $P_{x\mu\nu}$,

$$S_{\mathrm{W}} = \frac{1}{g^2} \sum_{x,\, \mu<\nu} (1 - \mathrm{Re}\, P_{x\mu\nu})\,, \tag{3.2}$$

the plaquette being the smallest Wilson loop around an elementary square at a lattice point

[3]The compact lattice $U(1)$ gauge fields are self-interacting and in principle the action could include ghost fields which would then be expected to decouple only in the continuum limit in the standard scenario.

x on the (μ, ν) plane.

The second term in (3.1), S_{GS}, is the Golterman-Shamir HD gauge-fixing term [9, 25] and is given by

$$S_{\text{GS}} = \tilde{\kappa} \left(\sum_{xyz} \Box_{xy}(U)\, \Box_{yz}(U) - \sum_{x} B_x^2 \right), \tag{3.3}$$

where the gauge-covariant Laplacian $\Box_{xy}(U)$ is given by,

$$\Box_{xy}(U) = \sum_{\mu} (\delta_{y,x+\mu} U_{x\mu} + \delta_{y,x-\mu} U^{\dagger}_{x-\mu,\mu} - 2\delta_{xy}), \tag{3.4}$$

and,

$$B_x = \sum_{\mu} (\mathcal{A}_{x-\mu,\mu} + \mathcal{A}_{x\mu})^2/4, \text{ with } \mathcal{A}_{x\mu} = \text{Im} U_{x\mu}. \tag{3.5}$$

The third term in (3.1), S_{ct}, generally represents a collection of all possible counter-terms, needed to ensure recovery of gauge symmetry at a *desirable* continuous phase transition. The counter-terms are determined by usual power counting which is validated by the construction of the term S_{GS} leading to a renormalizable (Lorentz covariant) gauge in the continuum. In principle, S_{ct} contains a dimension-2 gauge field mass counter-term, and five marginal counter-terms, allowed by the exact lattice symmetries [40]. Three of the five marginal counter-terms are field renormalization counter-terms for the gauge field, and the other two counter-terms are to nullify quartic gauge field self-interaction. It has been argued in [10] that all the marginal counter-terms in this theory can be perturbatively treated. However, being perturbative, they are not expected to give rise to a new phase transition.

We consider,

$$S_{\rm ct} = -\kappa \sum_{x\,\mu} \left(U_{x\mu} + U^{\dagger}_{x\,\mu} \right) , \tag{3.6}$$

which is a dimension-2 mass counter-term, as apparent from expanding the lattice gauge field $U_{x\mu} = \exp(iagA_\mu(x))$ for small lattice spacing a. As we shall witness later, the dimension-2 mass counter-term is the one responsible for the FM-FMD phase transition giving rise to a new universality class near that transition.

It can be explicitly shown [9] that the action (3.1) with the HD gauge-fixing term has a unique absolute minimum at $U_{x\mu} = 1$. In the naive continuum limit (i.e., lattice spacing $a \searrow 0$ in the action), the HD gauge-fixing term becomes the familiar covariant gauge fixing term

$$\tilde{\kappa} g^2 \int d^4x (\partial_\mu A_\mu)^2 = (1/2\xi) \int d^4x (\partial_\mu A_\mu)^2, \tag{3.7}$$

where ξ is defined as

$$\xi = 1/(2\tilde{\kappa} g^2). \tag{3.8}$$

The above considerations validate a weak coupling perturbation theory (WCPT) of the gauge fixed theory with $\xi \sim 1$ around $g = 0$ and large $\tilde{\kappa} \to \infty$.

From Eq. (3.8), it is clear that, to keep $\tilde{\kappa} g^2$ or ξ of $\mathcal{O}(1)$, we need to tune $\tilde{\kappa} \nearrow \infty$ as the gauge coupling $g \searrow 0$. In practice, for a given gauge coupling g, it needs to be seen how large the coefficient $\tilde{\kappa}$ of the HD gauge-fixing term needs to be in order for the gauge-fixing term to take discernible effect. It can be expected that for weak gauge couplings, there would be no significant effect of gauge-fixing for very small values of $\tilde{\kappa}$, since the effective coefficient of the gauge-fixing term given in Eq. (3.7) is then really tiny. With increase of the value of $\tilde{\kappa}$, but still with weak gauge couplings, gauge fixing can be expected to take effect, as has been found in investigations. However, what happens at strong gauge couplings cannot be guessed at all and is a major point of investigation of this chapter and Chapter 4. Numerical simulations can find out how large $\tilde{\kappa}$ needs to be for a given g in order for the gauge-fixing to take effect (to obtain a FM-FMD transition, as described above).

The theory is defined by the following functional integral for the partition function,

$$Z = \int \mathcal{D}U \exp(-S[U_{x\mu}]), \tag{3.9}$$

with $S[U_{x\mu}]$ given by (3.1) and

$$\mathcal{D}U = \prod_{x\mu} dU_{x\mu}, \tag{3.10}$$

where $dU_{x\mu}$ is the gauge invariant Haar measure.

Writing the gauge non-invariant part of the action (3.1) collectively as

$$S_{\mathrm{NI}}[U_{x\mu}] = S_{\mathrm{ct}}[U_{x\mu}] + S_{\mathrm{GS}}[U_{x\mu}], \tag{3.11}$$

let us consider a gauge transformation $U_{x\mu} \to \mathrm{g}_x U_{x\mu} \mathrm{g}^\dagger_{x+\mu}$ ($\mathrm{g}_x \in U(1)$) in the partition function (3.9) (remembering that $\mathcal{D}U$ and S_{W} are gauge-invariant while $S_{\text{NI}}[U_{x\mu}]$ is not),

$$
\begin{aligned}
Z &= \int \mathcal{D}U \exp\left(-S_{\text{W}} - S_{\text{NI}}[U_{x\mu}]\right) && (3.12)\\
&\to \int \mathcal{D}U \exp\left(-S_{\text{W}} - S_{\text{NI}}[\mathrm{g}_x U_{x\mu} \mathrm{g}^{\dagger}_{x+\mu}]\right) && (3.13)\\
&= \int \mathcal{D}\mathrm{g}\mathcal{D}U \exp\left(-S_{\text{W}} - S_{\text{NI}}[\mathrm{g}_x U_{x\mu} \mathrm{g}^{\dagger}_{x+\mu}]\right) && (3.14)\\
&= \int \mathcal{D}\phi\mathcal{D}U \exp\left(-S_{\text{W}} - S_{\text{NI}}[\phi^{\dagger}_x U_{x\mu} \phi_{x+\mu}]\right), && (3.15)
\end{aligned}
$$

where in the penultimate step, we multiply each side by $\int \mathcal{D}\mathrm{g} = \prod_x \int d\mathrm{g}_x = 1$ (normalized gauge volume at each site), and in the final step, $\phi_x \equiv \mathrm{g}^{\dagger}_x$ has been used.

As is apparent from the above steps, under a gauge transformation $U_{x\mu} \to \mathrm{g}_x U_{x\mu} \mathrm{g}^{\dagger}_{x+\mu}$, the gauge non-invariant terms pick up the *lgdof*, and the theory becomes a scalar-gauge system with $S_{\text{NI}}[\phi^{\dagger}_x U_{x\mu} \phi_{x+\mu}]$.

The action obtained after the gauge transformation (the so-called Higgs picture) involves both the gauge fields and the *lgdof* which are essentially radially frozen scalar fields ϕ_x.

The mass counter-term (3.6) takes the following form in the Higgs picture:

$$
S^{\phi}_{\text{ct}} = -\kappa \sum_{x\,\mu} \left(\phi^{\dagger}_x U_{x\mu} \phi_{x+\mu} + \phi^{\dagger}_{x+\mu} U^{\dagger}_{x\,\mu} \phi_x\right) \sim -\kappa \sum \phi^{\dagger} \Box(U) \phi, \tag{3.16}
$$

which is the usual kinetic term for the scalar field.

Similarly, the HD gauge-fixing term (3.3) becomes, in the Higgs picture,

$$
S^{\phi}_{\text{GS}} = \tilde{\kappa} \left(\sum \phi^{\dagger} \Box^2(U) \phi - \sum \mathcal{B}^2\right), \tag{3.17}
$$

where,

$$\mathcal{B}_x = \sum_{\mu} (\bar{\mathcal{A}}_{x-\mu,\mu} + \bar{\mathcal{A}}_{x\mu})^2/4, \text{ with } \bar{\mathcal{A}}_{x\mu} = \mathrm{Im}\left(\phi_x^\dagger U_{x\mu} \phi_{x+\mu}\right). \tag{3.18}$$

The total action, in the Higgs picture, thus assumes the form:

$$S^\phi = S_\mathrm{W} + S^\phi_\mathrm{GS} + S^\phi_\mathrm{ct} \tag{3.19}$$

where the standard Wilson term S_W is gauge invariant and hence does not pick up the *lgdof* when the functional integral integrates along the gauge orbit.

The gauge invariance as found in the standard Wilson term S_W alone is the target symmetry under the gauge transformations:

$$U_{x\mu} \to \mathsf{g}_x U_{x\mu} \mathsf{g}^\dagger_{x+\mu}, \quad \mathsf{g}_x \in U(1) \tag{3.20}$$

However, the total action (3.19) in the Higgs picture has enlarged, unphysical symmetry under the transformations

$$U_{x\mu} \to \mathsf{h}_x U_{x\mu} \mathsf{h}^\dagger_{x+\mu}, \quad \phi_x \to \mathsf{h}_x \phi_x, \quad \mathsf{h}_x \in U(1). \tag{3.21}$$

We would call the local symmetries given by (3.20) and (3.21) respectively as the g-symmetry (target physical symmetry) and the h-symmetry.

Putting $\phi_x = 1$ in the expression for the action S^ϕ in the Higgs picture (3.19) recovers the action (3.1), called the action in the vector picture. Given the Haar measure (3.10) of the functional integrals, theories given by the two actions (3.1) and (3.19) are completely equivalent.

With vanishing $\tilde{\kappa}$, the theory approaches an Abelian gauge-Higgs system.

With zero gauge coupling $g = 0$, we have $U_{x\mu} = 1$ for all the links of the lattice. This is known as the reduced limit. The reduced model is defined by the functional integral,

$$Z_{\text{red}} = \int \mathcal{D}\phi \, \exp\left(-S[\phi]\right), \tag{3.22}$$

with,

$$S[\phi] = -\kappa \sum_x \phi_x^\dagger \left(\Box\phi\right)_x + \tilde{\kappa} \sum_x \left\{\phi_x^\dagger \left(\Box^2\phi\right)_x - b_x^2\right\}, \tag{3.23}$$

where b_x is the appropriate modification of $\mathcal{B}_x$ of Eq. (3.18) with $U_{x\mu} = 1$.

The reduced model action is invariant under the global transformations

$$\phi_x \to \mathsf{h}\, \phi_x, \tag{3.24}$$

where $\mathsf{h} \in U(1)_{\text{global}}$ is independent of the lattice site.

At $\tilde{\kappa} = 0$, the reduced model is just the radially frozen scalar field theory in 4 dimensions with $U(1)$ global symmetry. This is also known as the XY model, or as the non-linear sigma model with global $U(1)$ symmetry, in 4 dimensions. The phase diagram of this theory is well known. At large κ, the system is frozen, i.e., $|\langle\phi_x\rangle| = 1$ with perfect ferromagnetic (FM) ordering. As κ is lowered, due to quantum fluctuations, there is a continuous phase transition of the system at $\kappa = \kappa_{\text{FM}-\text{PM}} = 0.15$ (numerically determined) into a paramagnetic (PM) phase where $|\langle\phi_x\rangle| = 0$. Because of the symmetry under $\kappa \to -\kappa$ and $\phi_x \to \phi_x^{\text{st}}$ where $\phi_x^{\text{st}} = (-1)^{\sum_\mu x_\mu}\phi_x$, there is also a continuous transition from the PM phase to an anti-ferromagnetic (AM) phase at $\kappa = -\kappa_{\text{PM}-\text{AM}} = -0.15$.

At non-zero $\tilde{\kappa}$, the reduced model is still symmetric under $\kappa \to -\kappa - 32\tilde{\kappa}$, $\tilde{\kappa} \to \tilde{\kappa}$, and

$\phi_x \to \phi_x^{\rm st}$. At small $\tilde{\kappa}$, it is reasonable to expect the phase structure to remain similar to that at $\tilde{\kappa} = 0$ with continuous FM-PM and PM-AM phase transitions, except that $\kappa_{\rm FM-PM}$ and $\kappa_{\rm PM-AM}$ would now depend on the value of $\tilde{\kappa}$. Analytic and numerical methods [50] yield results that are consistent with this expectation. As one approaches the FM-PM transition from the FM-side, the dimensionless vacuum expectation value $|\langle\phi_x\rangle| = a|\langle\Phi_x\rangle| = v$ decreases (where a and Φ are respectively lattice spacing and scalar field, both in physical units), and as a result, a radial mode (dimensionful) is developed dynamically and the unphysical *lgdof* are manifestly present in the continuum limit as usual scalar fields. In the reduced limit of lattice chiral gauge theories with fermions that break chiral symmetry explicitly on the lattice (e.g., Wilson fermions), the scalars couple to the fermions at such a phase transition through an effective Yukawa coupling and essentially spoil the chiral nature of the theory. The above is an undesirable outcome, and essentially leads to the failure of a large class of lattice chiral gauge theory proposals [5, 6]. If a lattice chiral gauge theory fails to produce chiral spectrum in the reduced limit, there is no hope in the full theory ($g \neq 0$) with the physical gauge fields back in the action.

The key idea of the non-perturbative gauge fixing proposal for the Abelian case (with the transverse gauge fields in the action) is to give rise to a new universality class where the unphysical degrees of freedom (*lgdof*) would decouple from the physical degrees of freedom in the continuum limit. From the development so far, it appears that the large $\tilde{\kappa}$-region is the place to look for such a possibility. For the *lgdof* to decouple from the physical sector, the desired new universality class in the large $\tilde{\kappa}$ region is to be identified with restoration of the original (target) g-symmetry (3.20). As has been found by WCPT around $g = 0$ and large $\tilde{\kappa}$, and by doing numerical simulations at weak gauge couplings [10], this happens at the FM-FMD transition and the spectrum of the continuum theory, achieved by approaching the FM-FMD transition from the FM-side, contains *only* free massless photons.

Following [9], we can gain useful insight into the phase diagram in the region of small g and large $\tilde{\kappa}$ by doing a simple-minded calculation. We start from the action (3.1) in the so-called vector picture, and use the property that the action has an absolute minimum at $U_{x\mu} = \exp\left(iagA_\mu(x)\right) = 1$. Near this point, the action can be expanded in powers g in the constant field approximation, i.e., by neglecting derivatives of the gauge field. This leads to an expression for a classical potential density in powers of the gauge coupling g:

$$V_{\text{cl}}(A_\mu) = \kappa\left(g^2 \sum_\mu A_\mu^2 + ...\right) + \frac{g^6}{2}\tilde{\kappa}\left\{\left(\sum_\mu A_\mu^2\right)\left(\sum_\mu A_\mu^4\right) + ...\right\}, \tag{3.25}$$

where terms with higher powers of g^2 are indicated by the ellipses. The classical potential density is expected to be a reasonable approximation at small g. However, as it turns out from numerical simulations, the classical potential density (3.25) produces a good qualitative picture of the new universality class in regions of the parameter space where the gauge coupling g is not very small and $\tilde{\kappa}$ is only sufficiently large, depending on the value of g.

Inspection of the expression for V_{cl} (3.25) immediately leads to a critical surface defined by

$$\kappa \equiv \kappa_{\text{FM}-\text{FMD}}(g, \tilde{\kappa}) = 0, \tag{3.26}$$

where the gauge boson (photon) is rendered massless.

Minimization of V_{cl} (3.25) with respect to gA_μ shows that the classical potential density has two different minima at $gA_\mu = 0$ for $\kappa \geq \kappa_{\text{FM}-\text{FMD}}$, and at $gA_\mu = \pm\left(\frac{|\kappa-\kappa_{\text{FM}-\text{FMD}}|}{6\tilde{\kappa}}\right)^{1/4}$ for $\kappa < \kappa_{\text{FM}-\text{FMD}}$. Hence, in the quantum theory at small g and large $\tilde{\kappa}$, it is expected that tuning κ to $\kappa_{\text{FM}-\text{FMD}}(g,\, \tilde{\kappa})$ signals a new *continuous* phase transition, within the *broken* phase, with a vector condensate as an order parameter:

$$\langle gA_\mu \rangle = \pm \left(\frac{|\kappa - \kappa_{\mathrm{FM-FMD}}|}{6\tilde{\kappa}} \right)^{1/4}, \ \forall \mu \quad \text{for} \quad \kappa < \kappa_{\mathrm{FM-FMD}} \tag{3.27}$$

$$\langle gA_\mu \rangle = 0, \ \forall \mu \quad \text{for} \quad \kappa \geq \kappa_{\mathrm{FM-FMD}} \tag{3.28}$$

The phase with the vector condensate is the novel phase and is called Ferromagnetic Directional (FMD) phase across all versions of the theory, including the theory in the reduced limit. Obviously the FMD phase breaks the rotational symmetry, and no Lorentz covariant continuum limit is obtainable from within the FMD phase. Hence, continuum limit is to be taken by approaching the continuous FM-FMD transition from the so-called Ferromagnetic (FM) phase.

Earlier investigations done in [10, 50] at weak gauge couplings are consistent with the above picture. For weak couplings, these studies confirmed a phase diagram with generic features as given in Fig. 3.1. The nomenclature of the phases in this theory has been taken as per the phases in the so-called reduced model [10]. The regular broken phase, FM (with ferromagnetic order) is characterized by a massive photon and a massive scalar, the PM (for paramagnetic) phase is the disordered (symmetric) phase having massless photons, and finally the new FMD (ferromagnetic-directional) phase is the spatially modulated ordered phase that breaks Euclidean rotational symmetry (there is also an anti-ferromagnetic or AM phase with staggered order, not to be discussed further in this study). Photon and scalar masses scale by approaching the continuous FM-PM transition from the FM phase, leading to a continuum gauge-Higgs theory. A sufficiently large $\tilde{\kappa}$ (and small g) ensures a satisfactory continuum limit with only the photon mass scaling (thereby recovering gauge symmetry and decoupling the scalars) at the FM-FMD phase transition by tuning a single parameter κ from the FM side.

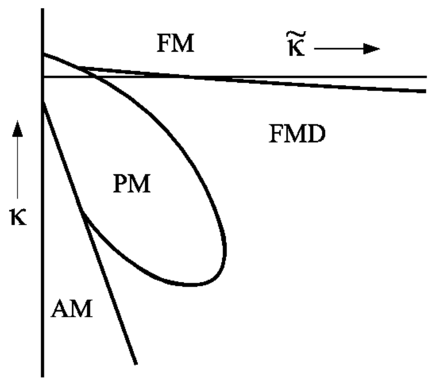

Figure 3.1: Schematic phase diagram in the $(\tilde{\kappa}, \kappa)$ plane at a given weak gauge coupling $(g < 1)$.

Given the above that this new formulation of a compact $U(1)$ gauge theory on lattice produces a correct continuum limit for weak gauge couplings, it is certainly worthwhile to ask about the nature of a continuum limit, if at all, for strong gauge couplings and also explore the possibilities of a non-trivial theory. The strong coupling region was first explored in [49, 51] with speculations of a few novel features. In this chapter, a completely independent and new investigation, a more careful and precise exercise has been carried out employing new methods (see Sec. 3.3 below). As a result, a clear picture of the phase diagram of the theory at strong gauge couplings has emerged. In the following, we present some of the key findings, principal among them is the existence of FM-FMD transition even at a strong gauge coupling, and a tricritical point on this transition.

3.3 Numerical simulations

Multihit Metropolis, a local update algorithm that was used in all previous numerical investigations of the theory (e.g. [10,49,51]), was discarded for the current work because at large g it produced results unstable against variation of the number of hits and also the particular order the lattice was swept. This is understandable, since with such a HD action density, spread over quite a few lattice sites, a local algorithm is bound to struggle, especially at large $\tilde{\kappa}$ (at strong gauge couplings, the FM-FMD transition is obtained at larger $\tilde{\kappa}$). In this chapter, we present results of numerical simulation done with Hybrid Monte Carlo (HMC), a global algorithm, and this marks a major difference with our previous work [49, 51] and produces new, reliable and numerically stable results at strong gauge couplings so that we now have a better understanding of the possible continuum limit at the FM-FMD transition at strong gauge couplings. A more detailed discussion and comparison of performance of the MM and the HMC algorithms, including a brief discussion on the implementation of the force terms in the Molecular Dynamics (MD) trajectory of the HMC algorithm, for the HD gauge-fixing action [16] is presented in Chapter 4.

Numerical simulation was done at gauge couplings $g = 1.0$, 1.1, 1.2, 1.3, 1.4, 1.5, 1.6 and 1.8 and also at weaker gauge couplings 0.6 and 0.8 (for comparing with available results in literature) at a variety of lattice volumes 8^4, 10^4, 12^4, 16^4, 20^4, 24^4, $8^3 24$ and $10^3 24$ to determine the phase diagrams in the $\kappa - \tilde{\kappa}$ plane at each fixed gauge coupling with κ-scans and $\tilde{\kappa}$-scans having intervals as fine as $\Delta\kappa = 0.001$, $\Delta\tilde{\kappa} = 0.005$ around the interesting phase transition regions. Each run in the scans typically has 5000 HMC trajectories for thermalization, and 10000 - 30000 HMC trajectories for measurement. Integrated auto-correlation times were measured and taken into account for error estimates. Error bars of all data points, wherever not shown explicitly, are smaller than the symbols. In this chapter we present only a small fraction of our results, namely at one gauge coupling $g = 1.3$ on 12^4, 16^4, 20^4 and $8^3 24$ lattices. In Chapter 4, in addition, we present results at gauge couplings $g = 0.6$, 1.0, 1.1, 1.2, 1.4 and 1.5 and also on 8^4 and 10^4 lattices, and build a comprehensive picture of the phase diagram and the emerging physics for a wide range of the parameters of the action. As already mentioned, there is also a comparative

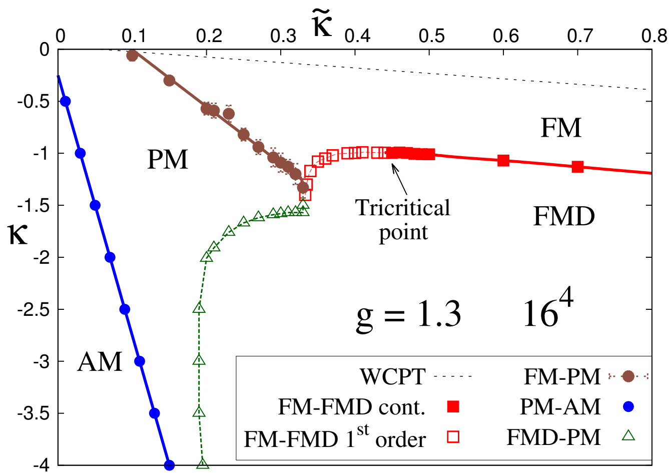

Figure 3.2: (Color online) Phase diagram in the $(\tilde{\kappa}, \kappa)$ plane at gauge coupling $g = 1.3$ on 16^4 lattice.

study of the performance of the MM and the HMC algorithms presented in Chapter 4.

The results presented in this chapter and in Chapter 4 generally have the most statistics. However, data at gauge coupling $g = 0.8$ and volumes $10^3 24$ and 24^4, not presented in these two chapters, while not having the same refinement level as the ones presented here because of lower statistics, help in some way for double-checking the conclusions made in this thesis.

Vacuum expectation values of quantities that were measured on equilibrated gauge field configurations on L^4 (or L^3T, $L \neq T$ for propagators) lattices, are the average plaquette

$$E_{\mathrm{P}} = \frac{1}{6L^4} \left\langle \sum_{x,\mu<\nu} \mathrm{Re}\, U_{\mathrm{P}_{\mu\nu}}(x) \right\rangle, \tag{3.29}$$

the gauge field mass term

$$E_\kappa = \frac{1}{4L^4} \left\langle \sum_{x,\mu} \mathrm{Re}\, U_{x\mu} \right\rangle, \tag{3.30}$$

and the lattice version of the vector condensate $\langle A_\mu \rangle$

$$V = \left\langle \sqrt{\frac{1}{4}\sum_{\mu}\left(\frac{1}{L^4}\sum_{x}\operatorname{Im} U_{x\mu}\right)^2} \right\rangle . \tag{3.31}$$

The vector condensate V is the order parameter for the FM-FMD transition. It is zero for all other phases except FMD. For first order FM-FMD transition, the quantity E_κ goes through a finite jump when plotted against κ. However, for continuous FM-FMD transition, the finite jump vanishes and E_κ is continuous across the transition.

To locate and determine the order of the phase transitions involving FMD, e.g., FM-FMD, AM-FMD and PM-FMD, the observables V and E_κ are very useful. To determine the location on a finite lattice, a suitable criterion has to be set. For all continuous phase transitions in our investigation, the location with the highest fluctuations in the data is taken as the approximate position of the phase transition. For all first order transitions, the standard histogram method, as used by us previously (e.g., look at Fig. 3.3 in Chapter 3), was employed. The location of the FM-PM and PM-AM phases are harder to determine, staying within the observables of the theory in the vector picture. However, we find that given the definition of V strictly as a positive quantity as in (3.31), the increased fluctuations of the fields around these continuous transitions are captured quite precisely around the phase transitions by the quantity V even though neither of these phases FM, PM and AM have a vector condensate. Out of all the phase transitions to be presented in this chapter and the next, the one of prime importance to us is the FM-FMD, and the location and nature of this transition including the tricritical points naturally attracted most of our attention.

In addition, vector propagators

$$G_{\mu\nu}(p) = \frac{1}{g^2 L^3 T} \left\langle \sum_{x,\,y} \mathrm{Im}\, U_{x\mu}\, \mathrm{Im}\, U_{y\nu} \exp[ip(x-y)] \right\rangle \tag{3.32}$$

and effective scalar propagators

$$H_{\mu\nu}(p) = \frac{1}{L^3 T} \left\langle \sum_{x,\,y} \mathrm{Re}\, U_{x\mu}\, \mathrm{Re}\, U_{y\nu} \exp[ip(x-y)] \right\rangle \tag{3.33}$$

were computed in momentum space as functions of the allowed momenta p on periodic lattices of volume L^3T with L and T respectively as spatial and temporal extensions. The operator $\mathrm{Re}\, U_{x\mu}$ carries quantum numbers of a scalar field and the expression given in Eq. (3.33) was used in the past in gauge-Higgs systems to compute Higgs mass [52]. Although we have discussed the operator for the scalar propagator here, the results for this propagator will be presented in Chapter 4.

No spontaneous chiral symmetry breaking is found in Quantum Electrodynamics (QED). As a probe for any non-trivial behavior in this gauge-fixed theory, we like to investigate the chiral condensate at the continuous part of the FM-FMD transition in the strong coupling region. The FM-FMD transition was thus probed with vectorially coupled quenched Kogut-Susskind fermions having $U(1)$ charge, by measuring the chiral condensate

$$\langle \overline{\chi}\chi \rangle_{m_0} = \frac{1}{L^4} \sum_x \left\langle M^{-1}_{xx} \right\rangle \tag{3.34}$$

as a function of a vanishing bare fermion mass m_0. The fermion matrix M is given by,

$$M_{xy} = \frac{1}{2} \sum_{\mu=1}^{4} \eta_\mu(x) \left(\delta_{y,x+\mu} U_{x\mu} - \delta_{y,x-\mu} U^\dagger_{x-\mu,\mu} \right) + m_0\, \delta_{x,y}, \tag{3.35}$$

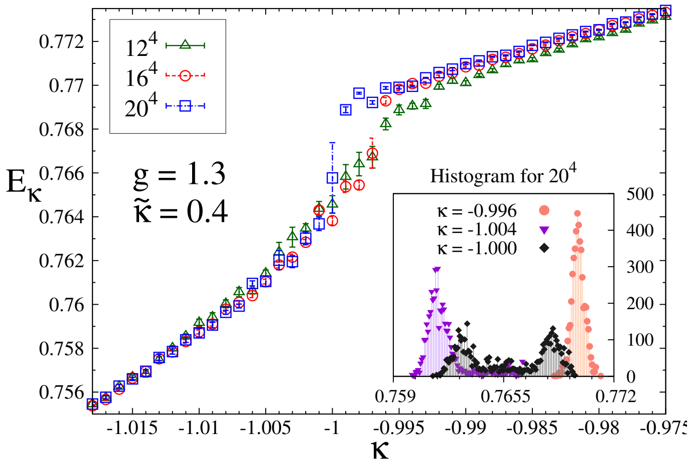

Figure 3.3: (Color online) E_κ versus κ plot on three different lattice volumes at $g = 1.3$ and $\tilde{\kappa} = 0.4$, showing a first order FM-FMD transition. Inset shows a histogram with a double peak structure at $\kappa = -1.000$.

with $\eta_\mu(x) \equiv (-1)^{x_1+\ldots+x_{\mu-1}}$ and $\eta_1(x) \equiv 1$. Noisy estimator method [53] with four noise vectors was used to compute the chiral condensate. Anti-periodic boundary conditions were used for the quenched fermions and the fermion matrix M was iteratively inverted using the standard Conjugate Gradient (CG) inverter. A more modern inverter, viz., BiCGStab was also tried, with no gains for the number of iterations needed for convergence; however, it had substantial computational overhead compared to CG and hence not used.

3.4 Results

In Fig. 3.2 we show the phase diagram at a fixed strong coupling $g = 1.3$ in the $\kappa - \tilde{\kappa}$ plane (with certain criteria, as discussed in the previous section, to determine the transitions on a finite lattice). Similar phase diagrams were also obtained for $g = 1.1, 1.2, 1.3, 1.5$. Contrast the above with that of Fig. 3.1. The FM-FMD phase transition in Fig. 3.1 for

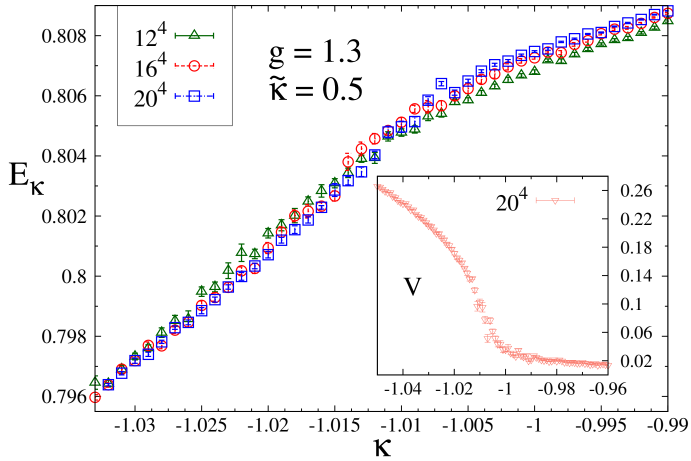

Figure 3.4: (Color online) E_κ versus κ plot on three different lattice volumes at $g = 1.3$ and $\tilde{\kappa} = 0.5$, showing a continuous FM-FMD transition. Inset shows V versus κ plots for the same parameters.

$g < 1$ is entirely a continuous transition [10, 49, 51], while for strong g (Fig. 3.2) there is a tricritical point separating a first order FM-FMD transition from a continuous transition. Fig. 3.2 shows the tricritical point for $g = 1.3$ at $\kappa = -0.99 \pm 0.01$ and $\tilde{\kappa} = 0.45 \pm 0.02$ for the lattice size 16^4. The change of location with lattice volumes bigger than 10^4 is small. The PM-FMD transition is found to be strongly first order, and ends at a critical end point [54] where the continuous FM-PM transition terminates at first order transitions. The first order FM-FMD transition weakens gradually as $\tilde{\kappa}$ is increased till the tricritical point where it becomes continuous.

The location of the tricritical point in the $\kappa - \tilde{\kappa}$ plane shifts to more negative κ and also to larger $\tilde{\kappa}$ with increasing g, evidence to be presented in Chapter 4. It also appears from our simulation, presented in Chapter 4, that, at a particular gauge coupling g^* between $g = 1.0$ and 1.1, the tricritical point tends to approach the critical end point. For $g < g^*$, the FM-FMD transition is fully continuous.

As already remarked, the plots in this chapter are all at $g = 1.3$.

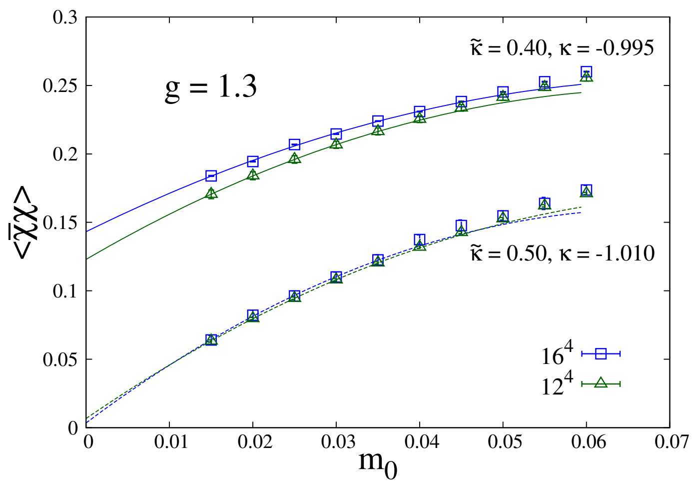

Figure 3.5: (Color online) Quenched chiral condensate in the FM phase near FM-FMD transition: non-zero at $\tilde{\kappa} = 0.4$ (first order FM-FMD), and consistent with zero at $\tilde{\kappa} = 0.5$ (continuous FM-FMD) at $g = 1.3$.

Figures 3.3 and 3.4 plot E_k, an observable similar to the entropy for the κ scan. With increasing volume, Fig. 3.3 shows a more distinct gap at $\kappa_{\mathrm{FM-FMD}} \sim -1.00$ for $\tilde{\kappa} = 0.4$, while Fig. 3.4 shows no discontinuity at $\kappa_{\mathrm{FM-FMD}} \sim -1.01$ for $\tilde{\kappa} = 0.5$. The inset of Fig. 3.3 shows a double peaked histogram at the critical κ, confirming the transition to be first order. The inset of Fig. 3.4 shows the corresponding V versus κ plot illustrating the FM-FMD transition at $\kappa \sim -1.01$ for $\tilde{\kappa} = 0.5$.

To understand the properties of the FM phase around the tricritical point, the region was further probed with quenched KS fermions. Fig.3.5 shows, for two lattice volumes, quenched chiral condensates in the FM phase near the FM-FMD transition at $\tilde{\kappa} = 0.4$ (where the transition is first order) and at $\tilde{\kappa} = 0.5$ (where the transition is continuous). Extrapolation to zero bare fermion mass m_0 was done with a phenomenological polynomial ansatz (keeping upto quadratic terms with five lowest masses fitted) and shows a condensate consistent with zero on the continuous side of the FM-FMD transition while clearly there is a non-zero condensate where the transition is first order. As we shall see comprehensively

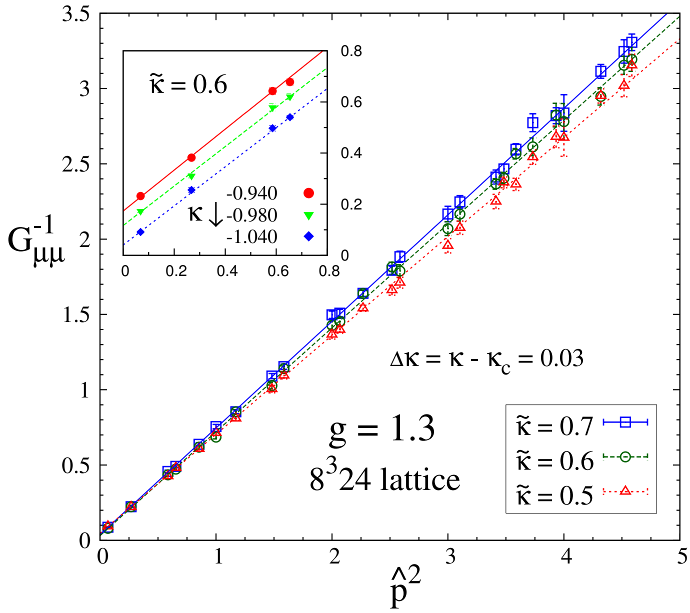

Figure 3.6: (Color online) Inverse photon propagators in the FM phase near FM-FMD transition at $g = 1.3$ and at three values of $\tilde{\kappa}$ for which the transition is continuous. Inset shows scaling of the photon mass as FM-FMD transition is approached from FM side.

in Chapter 4 that the continuous part of the FM-FMD transition is governed by the same perturbative point as the weak gauge coupling FM-FMD transition, the absence of any spontaneous chiral symmetry breaking in the continuous part of the FM-FMD transition at strong gauge coupling is a consistent result. There is a hint of non-zero chiral condensate as the tricritical point is approached from the FM side. However, confirmation on larger volumes is required. Probing the universality class of the tricritical point is important from the point of view of finding any non-trivial short distance property of the $U(1)$ gauge theory. However, it is outside the scope of the present study. At least, in the context of the HD gauge-fixed compact (1) lattice gauge theory, we have been able to exclude almost all regions of the parameter space, except a tricritical point (actually a line, in the 2 dimensional phase diagram, to be seen in Chapter 4), for any possible non-trivial behavior.

The inverse of photon propagator (2-point correlator of $\mathrm{Im}\, U_{x\mu}$) in momentum space was also measured and is plotted against the square of lattice momentum $\hat{p}^2$ (discrete on a finite box) in Fig. 3.6 for the continuous part of the FM-FMD transition, staying in the FM phase.[4] Inset shows a gradually vanishing photon mass (y-intercept), as κ approaches $\kappa_{\mathrm{FM-FMD}}$ (~ -1.07) for the given fixed $\tilde{\kappa}$ (0.6), suggesting an expected scaling of the photon mass at the transition and recovery of gauge symmetry. The slope of the fitted straight lines, in the main figure, suggests a field renormalization constant Z that is not unity. However, the figure shows that the slope increases with increasing $\tilde{\kappa}$. It seems reasonable to expect the slope to approach unity at large $\tilde{\kappa}$, consistent with WCPT at $g = 0$ or $\tilde{\kappa} = \infty$. In addition, the continuous FM-FMD transition line at all strong g is found in our simulations to be below but roughly parallel to the transition (the dotted line in Fig.3.2), obtained from 1-loop WCPT in [10]. Of course, the gap between them decreases as the coupling gets smaller.

3.5 Conclusion

The phase diagram of the compact $U(1)$ pure gauge theory in the non-perturbative gauge-fixing approach including the HD term and a mass counter-term has turned out to be somewhat more complex in the strong gauge coupling region ($g > 1$). Numerical simulation is also more difficult in this region, and local update algorithms struggle, forcing us to use global update algorithms with some care. However, after the algorithmic issues were sorted out, a clear picture of the possible continuum limits has emerged which is very relevant for all the major important issues discussed in Sec. 3.1, e.g., both Abelian and non-Abelian

[4] It may be mentioned here that the three data lines in the main part of Fig. 3.6 at three $\tilde{\kappa}$ are each at a value of κ which is at a fixed small distance away ($\Delta\kappa = \kappa - \kappa_{\mathrm{FM-FMD}} = 0.03$) from the FM-FMD transition.

lattice chiral gauge theories and short distance behavior of $U(1)$ gauge theories.

Existence of the FM-FMD transition at strong gauge couplings is confirmed. Evidence at gauge coupling $g = 1.3$ is presented in this chapter. The continuous part of this transition, away from the tricritical point, appears to produce familiar physics with free massless photons (and *lgdof*s decoupled) and zero chiral condensate.

The possibility for a non-trivial continuum limit in this pure compact U(1) lattice gauge theory at strong gauge couplings rests on the tricritical point with a new universality class.

Details of our study including results at other gauge couplings that help develop the overall picture in the strong gauge coupling region, will appear in Chapter 4.

CHAPTER 4

DETAILED PHASE DIAGRAM OF COMPACT GAUGE-FIXED $U(1)$ LATTICE GAUGE THEORY AT STRONG COUPLING

4.1 Introduction

In this Chapter, continuing our work from before [15], described in Chapter 3, we present a comprehensive account of our study of the non-perturbative gauge-fixing for the Abelian case as proposed in [9, 25]. The chapter is based on the results published in Ref. [16].

As mentioned in Chapter 3, we have realized the limitations of the configuration-generating algorithm, Multihit Metropolis (MM), used in all earlier studies in the weak gauge coupling region [10] and also in the earlier work at strong coupling [49]. As we have seen in the previous chapter in Sec. 3.2, the higher-derivative (HD) gauge-fixing term involves the square of the gauge-covariant lattice Laplacian, and as a result the action density at a lattice site involves significantly more lattice links than the usual Wilson plaquette. For a local updating algorithm like the MM, the accept/reject step is incorporated after each local update of the field. As a result, unless the coefficient $\tilde{\kappa}$ of the HD-term is sufficiently small, the algorithm would struggle to generate legitimate field-configurations. With stronger gauge couplings, the physically interesting continuous FM-FMD phase transition takes place only at larger values of $\tilde{\kappa}$, and this leads to the failure of the MM algorithm. In this chapter, we shall give a more detailed account of why we needed to abandon MM, irrespective of the number of hits and present a comparison with the Hybrid Monte Carlo (HMC), a global algorithm, generally adopted for generation of field configurations in this chapter.

In Chapter 3, results of the phase diagram and the emerging physics at the continuous part of the FM-FMD transition obtained with the newly employed HMC algorithm for the HD action were presented only at one value of the strong gauge coupling, viz., $g = 1.3$. The current chapter aims at a consistent and comprehensive picture applicable in general for a wide range of parameters to determine especially how the strong gauge coupling phase diagram gradually emerges from that of the weak gauge coupling region and how the two regions are related, if at all.

The main result of this chapter is that the Lorentz covariant physics emerging in the strong gauge coupling region, by approaching the FM-FMD transition from the FM-side, is actually governed by that at the phase transition at $g = 0$, $\tilde{\kappa} \to \infty$ and $\kappa \sim 0$, κ being the coefficient of a dimension-2 mass counter-term required to recover gauge symmetry (In the weak gauge coupling limit $g = 0$, the action has a unique global minimum). The chapter also establishes the inadequacy of a local algorithm like MM for larger $\tilde{\kappa}$ and bigger volumes, by comparing results with the HMC algorithm at different regions of the coupling parameter space. As remarked above, a tricritical line emerges for $g > 1$ in the 3-dimensional phase diagram separating the first order and the continuous FM-FMD transition surfaces. A detailed investigation of the universality class of the tricritical line is outside the scope of the current work.

It is worth mentioning here that the unfixed compact $U(1)$ lattice gauge theory, given by only the Wilson plaquette term (3.2), is known to produce a phase transition at gauge coupling $g \sim 1$ between a so-called Coulomb phase containing massless free photons and a phase with non-trivial properties like having confined gauge-balls in the spectrum. The phase transition, upon precision numerical studies, was revealed as a weak first order [55–57], and hence a quantum continuum limit does not strictly exist only with $U(1)$ Wilson plaquette action. As we shall find out in Sec 4.4, in the gauge-fixed theory under investigation with an expanded parameter space, while increasing the gauge coupling from $g < 1$ to $g > 1$, there is an emergence of a tricritical line at $g \sim 1$ separating a surface of continuous FM-FMD transition from a first order FM-FMD transition. The continuum limit obtained in the FM phase while approaching the continuous part of the FM-FMD transition even in the large gauge coupling ($g > 1$) region is found to consist of free massless photons only (with the *lgdof* decoupled).

The chapter is organized as follows. After briefly describing, in Sec. 4.2, the implementation of the force terms during the molecular dynamics trajectory of the HMC algorithm applied to the gauge-fixed theory with the HD action, we present a comparison in Sec. 4.3 of the MM and the HMC algorithms. In Sec. 4.4, we present results of the phase diagram at several values of the gauge coupling g including at the end a schematic 3-dimensional phase diagram covering a wide range of parameters from the weak gauge coupling to the strong gauge coupling regions. We collect results of various two point functions, and also the average plaquette value in Sec. 4.5 to understand the physics of the FM phase while approaching the FM-FMD transition at strong gauge couplings. We present our main conclusions in Sec. 4.6.

4.2 Implementation of the HMC algorithm

As indicated in the Introduction, we have written codes and tried both the MM and the HMC algorithms for generating the gauge field configurations. The MM was usually tried with 4 hits; however, various other values of hits were also tried, with very similar outcome.

In the following, we discuss implementation of the HMC algorithm. We skip any discussion on the Wilson plaquette term of the action, because that part is standard.

Writing the gauge link as $U_{x\mu} = \exp(i\theta_{x\mu})$, where $0 < \theta_{x\mu} \leq 2\pi$ is an angle (dimensionless), the HD gauge-fixing term (3.3) in the action (3.1) is expressed as follows

$$S_{\text{GS}} = \sum_{x\mu\nu} \Big(\cos(\theta_{x\mu} - \theta_{x\nu}) + \cos(\theta_{x-\mu,\mu} - \theta_{x-\nu,\nu}) + 2\cos(\theta_{x\mu} + \theta_{x-\nu,\nu}) \Big) \\ - \sum_{x\mu} 32\cos\theta_{x\mu} - \frac{1}{16} \sum_{x} \left(\sum_{\mu} (\sin\theta_{x\mu} + \sin\theta_{x-\mu,\mu})^2 \right)^2 + \text{constant terms} \quad (4.1)$$

The HMC algorithm, as discussed in Chap 3, employs a molecular dynamics trajectory, followed by a Metropolis accept/reject step that makes the algorithm exact. The molecular dynamics trajectory is an evolution in a fictitious time (computer time) of the system through a Hamiltonian that treats the fields of the action as generalized co-ordinates and includes quadratic terms for the conjugate momenta corresponding to the fields. The Hamilton's equations of motion are discretized and the equations for momenta update involves the force terms which are the derivatives of the action with respect to the corresponding field variable.

Contribution to the HMC force by the HD gauge-fixing term, calculated from (4.1) for the field $U_{x_0\rho}$, the link field directed from the site x_0 towards the neighboring site $x_0+\rho$ along the direction ρ, is given as

$$
\begin{aligned}
-F^{\rm GS}_{x_0\rho} &= \frac{\partial S_{\rm GS}}{\partial \theta_{x_0\rho}} \\
&= 2\tilde{\kappa}\sum_{\nu}\Big(\sin(\theta_{x_0\nu}-\theta_{x_0\rho})+\sin(\theta_{x_0+\rho-\nu,\nu}-\theta_{x_0\rho}) \\
&\quad -\sin(\theta_{x_0\rho}+\theta_{x_0-\nu,\nu})-\sin(\theta_{x_0\rho}+\theta_{x_0+\rho,\mu})\Big)+\ 32\tilde{\kappa}\,\sin\theta_{x_0\rho} \\
&\quad -\frac{\tilde{\kappa}}{4}\cos\theta_{x_0\rho}\sum_{\nu}\Big((\sin\theta_{x_0\rho}+\sin\theta_{x_0+\rho,\rho})(\sin\theta_{x_0+\rho-\nu,\nu}+\sin\theta_{x_0+\rho,\nu})^2 \\
&\quad +\ (\sin\theta_{x_0-\rho,\rho}+\sin\theta_{x_0,\rho})(\sin\theta_{x_0-\nu,\nu}+\sin\theta_{x_0\nu})^2\Big)
\end{aligned} \tag{4.2}
$$

A similar contribution to the force from the dimension-2 mass counter-term is easily found to be

$$
-F^{\rm ct}_{x_0\rho} = 2\kappa\sin\theta_{x\mu}. \tag{4.3}
$$

4.2.1 Numerical simulations

Details of all numerical simulations in this HD gauge-fixed compact $U(1)$ lattice gauge theory, including values of gauge couplings and lattice volumes at which simulations were performed, were presented in Sec. 3.3 of Chap. 3. In this chapter we present results at gauge coupling $g = 0.6,\ 1.0,\ 1.1,\ 1.2,\ 1.3$ and 1.5 and at lattice volumes 8^4, 10^4, 12^4, 16^4 and $8^3 24$. All observables measured were also enlisted in Sec. 3.3 of Chap. 3. Hence they will not be repeated here, except to mention that the scalar propagator, given by Eq. 3.33, the results of which was not shown in Chap. 3, will be presented here in Sec. 4.5.

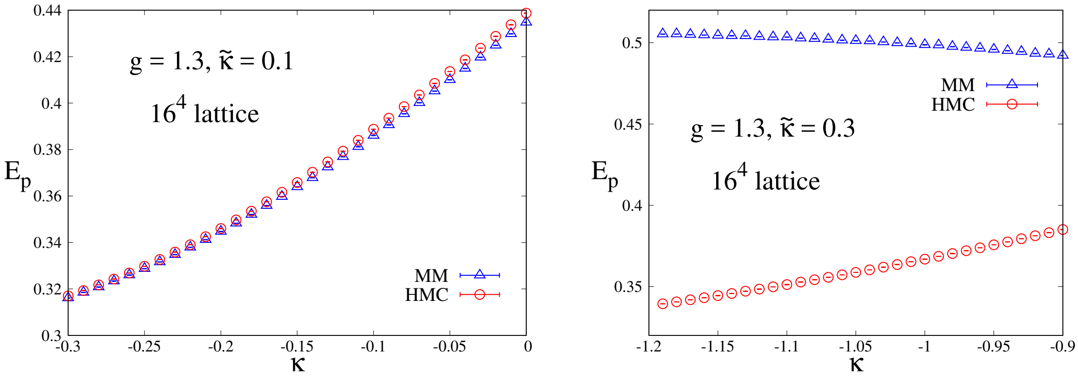

Figure 4.1: Comparison of average plaquette value E_p at $g = 1.3$ on 16^4 lattice at two values of $\tilde{\kappa}$ (= 0.1 and 0.3) in the two figures for a variety of values of κ around the FM-PM transition, obtained with MM and HMC algorithms.

4.3 Local versus Global Algorithm

In this section, we present results that show that a local algorithm like MM appears to be unreliable when the coefficient of the HD gauge-fixing term $\tilde{\kappa}$ is relatively large. Since the continuous part of the phase transition of interest (FM-FMD) takes place at a larger value of $\tilde{\kappa}$ when the gauge coupling is stronger, the problem is more apparent in the current work since it primarily deals with the fate of the theory at strong gauge couplings. We also show that the results with the MM algorithm are unstable as the volume increases.

In contrast, the HMC algorithm, a so-called global algorithm, generally appears to be more reliable and consistent, and undoubtedly a better algorithm for this theory with a HD term. First, it generally agrees with results in [10] obtained in the weak gauge coupling region for rather small volumes, mostly 4^4 and 6^4 and some data for 8^4. At larger $\tilde{\kappa}$, both for weak and strong gauge couplings, and for larger volumes, 10^4 and above, HMC gives stable results, as will be illustrated in the following.

In Fig. 4.1, we have compared average plaquette value E_p at a *strong* gauge coupling

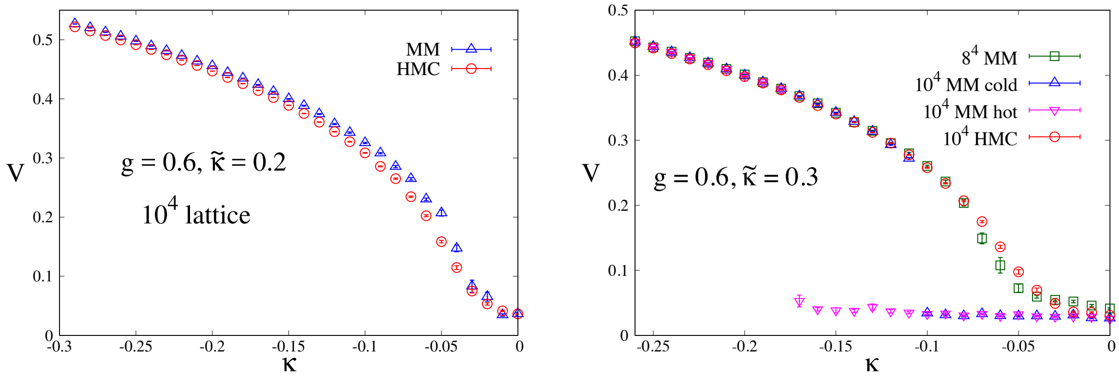

Figure 4.2: Comparison of the vector condensate V at $g = 0.6$ on 10^4 lattice at two values of $\tilde{\kappa}$ (= 0.2 and 0.3) in the two figures for a variety of values of κ around the FMD-FM transition, obtained with MM and HMC algorithms. The right figure also has values with MM algorithm on 8^4 lattices.

$g = 1.3$ on 16^4 lattice at two values of $\tilde{\kappa}$ (= 0.1 on the left and 0.3 on the right) for a variety of values of κ around the FM-PM transition, obtained with MM and HMC algorithms. The observable E_p does not show any noticeable signal for the transition. However, for $\tilde{\kappa} = 0.1$, the two algorithms produce nearly identical results for all values of κ presented, while for the larger $\tilde{\kappa} = 0.3$, results given by the two algorithms have no agreement anywhere.

Fig. 4.2 shows comparison of the observable V, an estimate of the vector condensate $\langle A_\mu(x) \rangle$ on the lattice, obtained with MM and HMC algorithms, at a *weak* gauge coupling $g = 0.6$ and two values of the coefficient $\tilde{\kappa}$ of the HD gauge-fixing term. On 10^4 lattices, we see general agreement of the two algorithms at smaller $\tilde{\kappa}$ in the left figure. However, for the same 10^4 lattices, the algorithms clearly give different results (indicating also a dependence on the initial configuration for the MM) at a slightly larger value of $\tilde{\kappa} = 0.3$ (in the right figure), suggesting a first-order-like discrete jump in the quantity V at a shifted location of the parameter κ, while the MM data on 8^4 lattices generally agree with the 10^4 HMC data signalling a smooth transition.

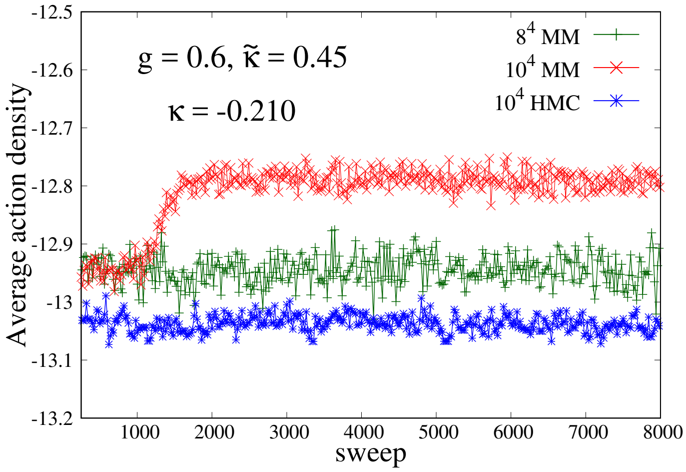

Figure 4.3: Average action density versus number of sweeps/trajectories just inside the FMD phase at a weak gauge coupling $g = 0.6$ with MM and HMC algorithms.

Average action density (value of action divided by volume) achieved after apparent equilibration is plotted in Fig. 4.3 against number of sweeps/trajectories at a weak gauge coupling $g = 0.6$ with both MM and HMC algorithms at a point in the coupling parameter space just inside the FMD phase. While the system settles at the lowest average action density with the HMC algorithm, the MM algorithm clearly produces unreliable results with the average action density above that obtained with HMC and showing instability with change of volume.

In fine, our findings are that, the MM algorithm struggles to generate reliable gauge field configurations with the HD action. It produces correct results only for sufficiently small coefficient $\tilde{\kappa}$ of the HD gauge-fixing term and on small lattices. The situation gets particularly worse on larger lattices, and at strong gauge couplings where one needs a large $\tilde{\kappa}$ for a continuous transition.

In contrast, the HMC algorithm agrees with the MM results at small values of $\tilde{\kappa}$ and small lattice volumes. In addition, the results with the HMC appear more consistent and stable with change of lattice volume and parameters of the algorithm. However, at times even the HMC can struggle with this HD action to move out of a local metastability because the changes of the fields and the momenta along a molecular dynamics trajectory are tiny with every differential 'time'-step. We have found it beneficial to use initially the MM algorithm for any configuration-generating run at a given point in the parameter space, and then feed the final configuration of the MM-run as the initial configuration of the HMC run, to make use of the best of both algorithms. This is because, even though the MM algorithm is unable to reach the true minima of the action, the changes of the values of the gauge fields are finite, unlike the differential changes during a trajectory of the HMC algorithm.

4.4 General study of the Phase Diagram at strong gauge couplings

As already mentioned in Sec. 4.1 the unfixed compact $U(1)$ lattice gauge theory ($\tilde{\kappa} = 0,\ \kappa = 0$), as formulated by the plaquette action of Wilson and given in (3.2), has been studied extensively in the past. At $g \sim 1$, the theory shows a phase transition from a so-called Coulomb phase (at weak gauge couplings, $g < 1$) having massless free photons, to a phase having non-trivial properties like confinement and existence of gauge-balls etc. at strong gauge couplings ($g > 1$). Through careful Monte Carlo simulations, the order of the transition was determined to be weakly first order. Hence a quantum continuum limit was not possible at this phase transition.

It is mentioned in Chapter 3 that the phase diagram of the theory (3.1) under investigation was studied for weak gauge couplings reasonably extensively in the past. From the point of view of quantum field theory, there are two continuous transitions of interest -

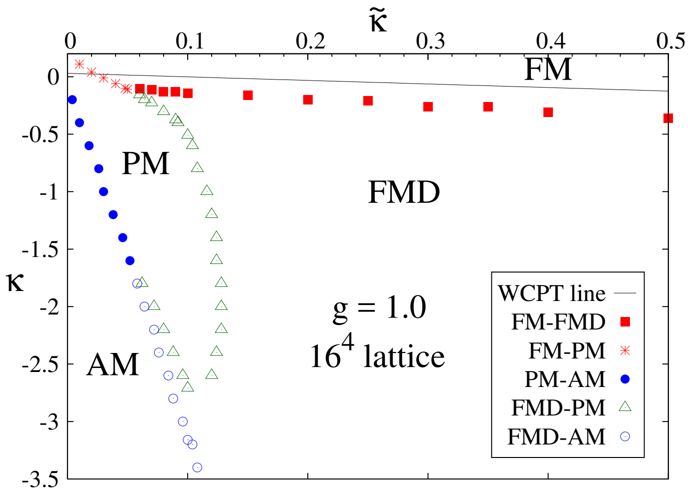

Figure 4.4: Phase diagram in the $(\tilde{\kappa}, \kappa)$ plane at gauge coupling $g = 1.0$ on 16^4 lattice.

the FM-PM transition and the FM-FMD transition. These transitions are illustrated in the phase diagram presented in Fig. 4.4 obtained in our numerical simulation at gauge coupling $g = 1$, approximately the largest gauge coupling exhibiting all the features of the phase diagram at weak gauge couplings ($g < 1$). As discussed in Sec. 3.2, a gauge-scalar (popularly known as gauge-Higgs) theory is expected to emerge in the continuum limit near the FM-PM transition at small values of $\tilde{\kappa}$. However, at larger values of $\tilde{\kappa}$, we find that, approaching the FM-FMD transition from the FM side makes the scalar fields (*lgdof*) decouple as gauge symmetry is recovered at that transition with emergence of massless free photons. The FMD phase is marked by a vector condensate, and hence approaching the FM-FMD transition from the FMD side cannot produce a Lorentz covariant theory.

In Fig. 4.4 and all phase diagrams to follow, all data points represented by solid (filled) symbols signify a continuous phase transition, while all data points represented by empty (unfilled) symbols signify a first order transition. Accordingly, one would find that FM-PM and PM-AM phase transitions are continuous and PM-FMD phase transition is first order, for all gauge couplings investigated in Chap. 3 and 4.

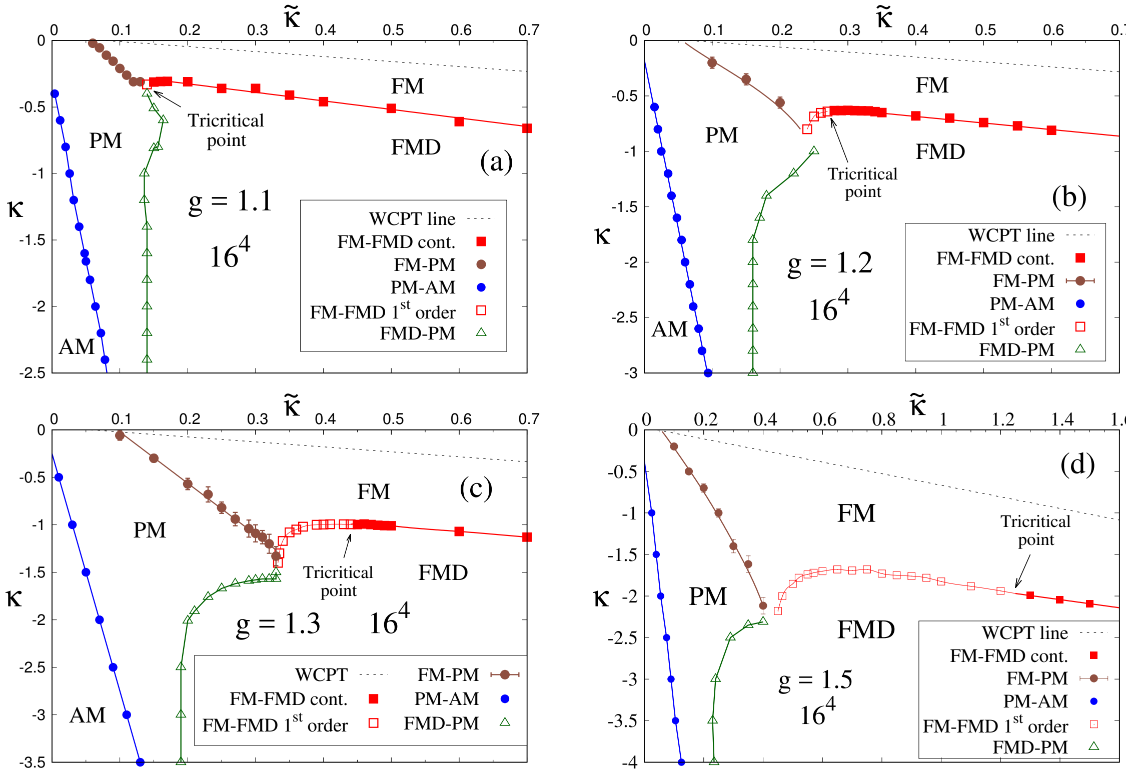

Figure 4.5: Phase diagram in the $(\tilde{\kappa}, \kappa)$ plane at gauge coupling $g = 1.1,\ 1.2,\ 1.3$ and 1.5 on 16^4 lattices. The dotted line shows the FM-FMD continuous transition calculated from WCPT around $g = 0$

However, for $g = 1.1$ and greater values of the gauge coupling g, the FM-FMD phase transition develops a first order part for smaller values of $\tilde{\kappa}$, as seen in Figs. 4.5(a), (b), (c) and (d). At $g = 1.1$ (Fig. 4.5(a)), in our simulations on 16^4 lattice, the FM-FMD phase transition first shows a little glimpse of its first order part for small values of $\tilde{\kappa}$ and then quickly turns itself into a continuous transition at a tricritical point at $(\tilde{\kappa},\ \kappa) \sim (0.14, -0.33)$ and remains continuous for larger values of $\tilde{\kappa}$. As the gauge coupling g is increased to $g = 1.2$ (Fig. 4.5(b)), $g = 1.3$ (Fig. 4.5(c)) and $g = 1.5$ (Fig. 4.5(d)), the location of the tricritical point in the $(\tilde{\kappa}, \kappa)$-plane shifts to larger $\tilde{\kappa}$ and more negative κ. In other words, the first order part of the FM-FMD phase transition extends quite rapidly with increase of the gauge coupling. However, it appears from our numerical simulations (which includes gauge couplings $g > 1.5$, corresponding data not shown here) that, given a large gauge coupling there is always a sufficiently large $\tilde{\kappa}$ beyond which the FM-FMD transition is continuous. In addition, the FM-FMD transition overall shifts to larger negative κ values at stronger gauge couplings.

The line joining the discrete data points at the phase transitions in the four plots of Fig. 4.5 are simple-minded interpolations with a purpose to guide the eye. The exact location of the meeting point of the three phases FM, FMD and PM are only roughly determined for a couple of the plots. However, such points where the continuous FM-PM transition ends at the joining of two (PM-FMD and FM-FMD) first order lines (for $g > 1$) have been described as critical end points in [54].

At weak gauge couplings studied for example in [10], the order of the continuous FM-FMD transition was expected to be second order from analytic considerations. In our case at strong gauge couplings, we conclude from numerical evidence of susceptibility peaks of the vector condensate at different volumes that the continuous part of the FM-FMD transition is also second order.

At $g = 1.1$, where in our numerical simulations on 16^4 lattices, the first order part of the FM-FMD transition makes an appearance for the first time, the discrete jump in the quantity E_κ across the transition is small, accordingly we conclude that the order of the transition is a weak first order. However, as the gauge coupling increases, the discrete jump in E_κ becomes quite pronounced, making the initial part (for smaller $\tilde{\kappa}$) of the FM-FMD transition strongly first order, which then becomes progressively weaker with increase of $\tilde{\kappa}$, until the transition line reaches the tricritical point, beyond which the transition is of course continuous.

The dotted straight line in each of the figures of Fig. 4.5 is obtained in bare WCPT near

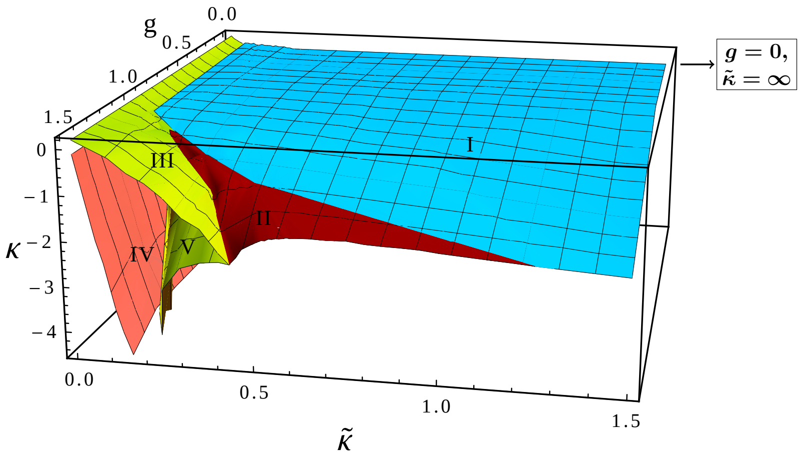

Figure 4.6: Schematic phase diagram in the 3-dimensional $(g,\, \tilde{\kappa},\, \kappa)$ parameter space at gauge coupling based on available data on 16^4 lattice. Surfaces of different phase transitions are labelled by: I: FM-FMD (continuous), II: FM-FMD (first order), III: FM-PM (continuous), IV: PM-AM (continuous), V: PM-FMD (first order). A tricritical line separating the first order and the continuous FM-FMD transitions emerges at $g > 1$ and continues to move towards larger $\tilde{\kappa}$ at stronger gauge coupling g. The arrow at the top right points to the WCPT corner ($g = 0,\ \tilde{\kappa} \to \infty$).

$g = 0$ by demanding recovery of gauge symmetry and is representative of the FM-FMD transition in $(\tilde{\kappa},\, \kappa)$-plane for a given gauge coupling g [10]. The dotted lines are always nearly parallel to the continuous parts of the FM-FMD transition for all gauge couplings in Fig. 4.5. However, the actual transitions run always lower in the $(\tilde{\kappa},\, \kappa)$-plane, and their distance from the WCPT lines increase with increasing gauge coupling.

In the next section, at strong bare gauge couplings, we shall explore the physics, achievable by approaching the continuous part of the FM-FMD phase transition from the FM phase, by computing the gauge field propagator, an effective scalar field propagator and chiral condensates. However, while the bare WCPT done around the point $g = 0$ and $\tilde{\kappa} = \infty$ has limited range of applicability, there exists no phase transitions between the WCPT corner of the 3-dimensional coupling parameter space (viz., $g = 0$ and $\tilde{\kappa} = \infty$)

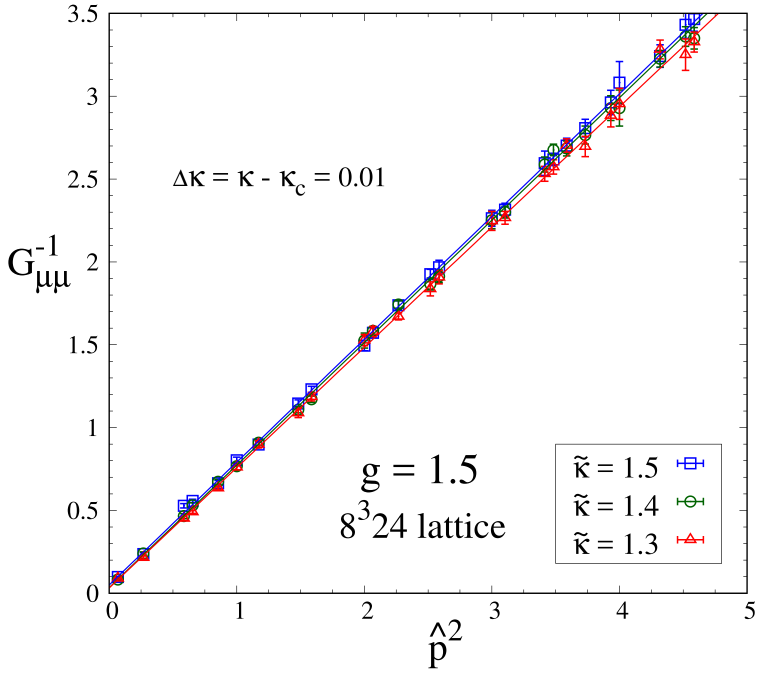

Figure 4.7: The inverse of the gauge field propagator versus $\hat{p}^2$ at $g = 1.5$ lattices near the continuous FM-FMD transition on $8^3 24$ lattices indicating emergence of free massless photons.

and any point on the continuous part of the FM-FMD transition at a strong gauge coupling and a large enough $\tilde{\kappa}$. The schematic phase diagram in the 3-dimensional parameter space $(g,\, \tilde{\kappa},\, \kappa)$ is displayed in Fig. 4.6. Kindly note that $\kappa = 0$ surface is located slightly below the top surface of the 3-dimensional box presented in the figure. The diagram is drawn based on available data on phase transitions and interpolations and extrapolations. The continuity of the entire FM-FMD transition surface (bounded by the tricritical line starting at $g = 1.1$) up to the WCPT corner is clearly evident when we look at the 3-dimensional phase diagram. Hence it is natural to expect that this whole region falls under the same universality class and the continuum physics obtainable should be no different from that near the weak gauge coupling region.

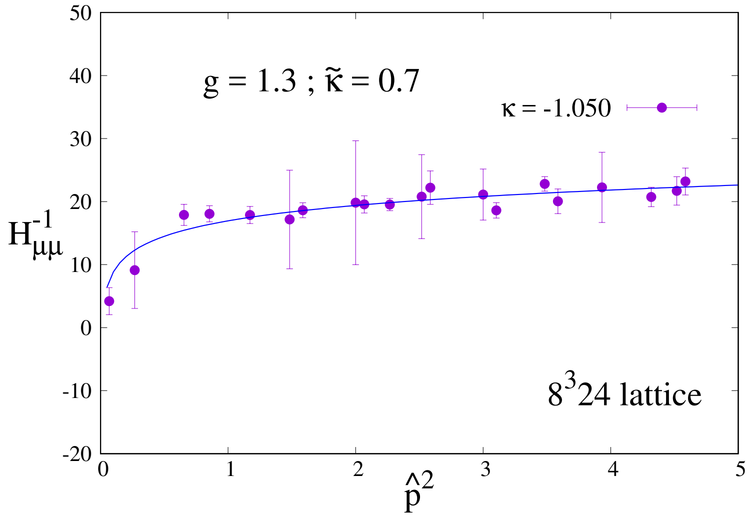

Figure 4.8: The inverse of the effective scalar propagator versus $\hat{p}^2$ at $g = 1.3$ lattices near the continuous FM-FMD transition on $8^3 24$ lattices indicating decoupling of *lgdof*.

4.5 Vector and Scalar propagators, Chiral Condensates and the Plaquette

The inverse of the gauge field propagator, as given by Eq. 3.32, for $\mu = \nu$, is plotted in Fig. 4.7 against the lattice momentum $\hat{p}^2 = 2\sum_\mu \sin^2 p_\mu/2$ at $g = 1.5$ and $\tilde{\kappa} = 1.3, 1.4, 1.5$ on $8^3 24$ lattices. The κ values are chosen to stay very close to the FM-FMD transition (continuous for the above $\tilde{\kappa}$ values). The linear behavior of the fits passing nearly through the origin clearly indicates a vanishing photon mass at the transition. At each $\tilde{\kappa}$ value, although not shown in the plot, the photon mass scales with decreasing κ approaching the transition from the FM side. As $\tilde{\kappa}$ increases from 1.3 to 1.5, there is a small but monotonic increase of the slope of the fit. The corresponding figure at $g = 1.3$ in [15], presented in this thesis in Fig. 3.6 of Chap. 3, also has the same trend with increasing $\tilde{\kappa}$. Consistency of this trend in these two figures and in data at other gauge couplings (not

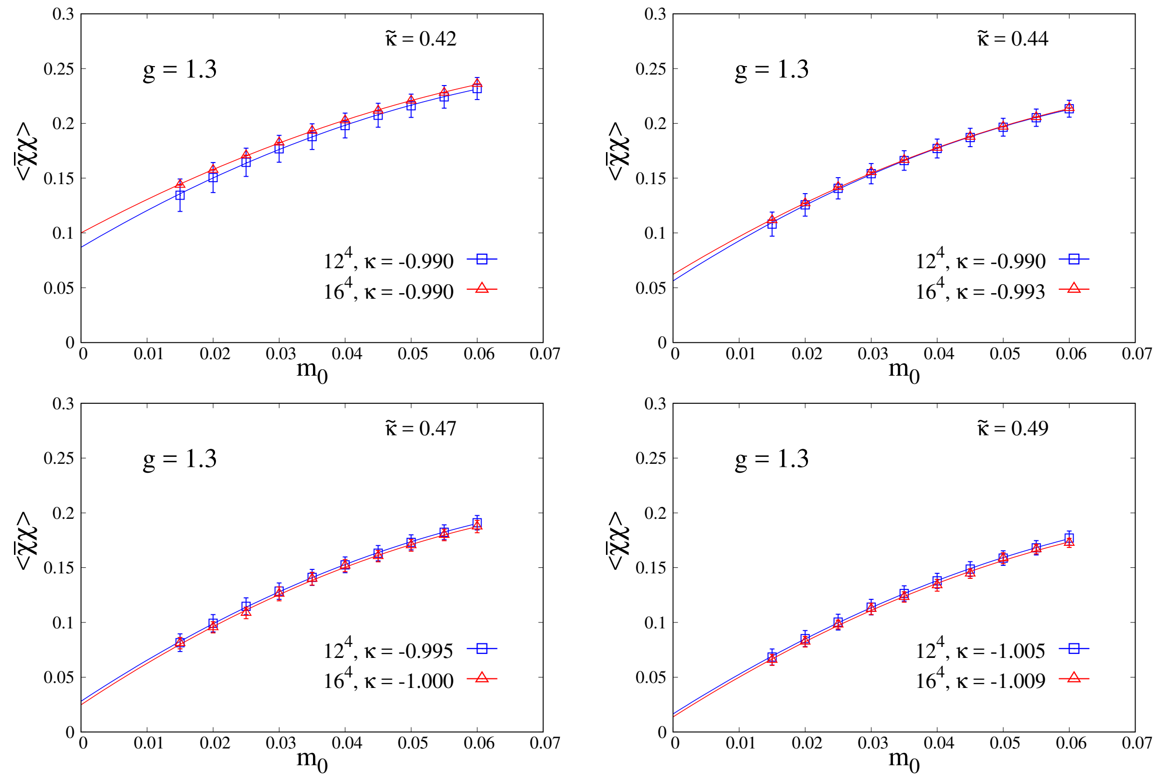

Figure 4.9: Quenched chiral condensates versus bare fermion mass at four values of $\tilde{\kappa}$ around the tricritical point at $g = 1.3$ on two lattice volumes 12^4 and 16^4.

shown here) suggests that at larger $\tilde{\kappa}$ the slope is likely to approach unity, in tune with theoretical expectations, rendering the photons perfectly free.

The scalar propagator was not presented in Chap. 3. With the expression given in Eq. 3.33, in Fig. 4.8, we plot its inverse with $\mu = \nu$ against $\hat{p}^2$ at $g = 1.3$ in the FM phase very close to the continuous part of the FM-FMD transition. The scalar propagator is noisy, consistent with observations made in [10], despite having about 50000 equilibrated field configurations, far more than our usual number. However, the non-linearity of the inverse propagator at small momenta suggests absence of a pole. The non-linearity in the inverse propagator at small momenta was also observed at weak coupling studies in [10], both through WCPT and numerical studies and was accepted as an indication of the decoupling

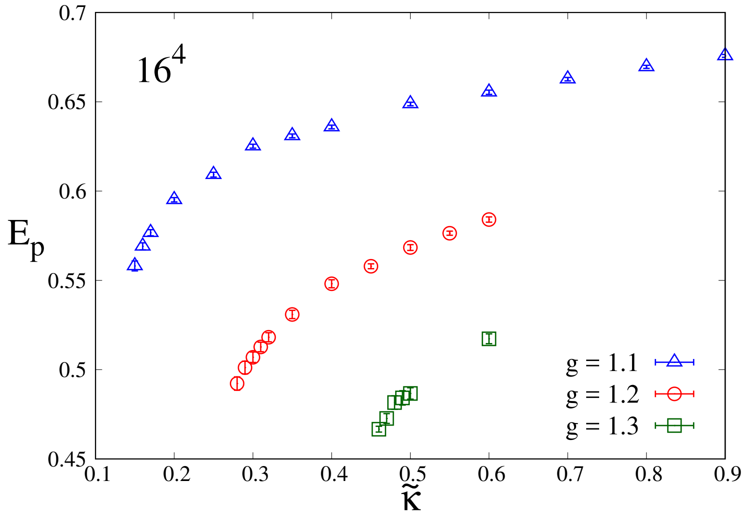

Figure 4.10: Average plaquette near the continuous FM-FMD transition versus $\tilde{\kappa}$ at gauge couplings $g = 1.1$, 1.2 and 1.3 on 16^4 lattice.

of the *lgdof*. The smooth curve in Fig. 4.8 is essentially to guide the eye, and not a fit. However, we have observed that our inverse propagator data for small lattice momentum $\hat{p}^2$ are roughly consistent with a non-linear behavior like $(\log\, p^2)^{-1}$, as found perturbatively in [10].

In [15] at $g = 1.3$, presented in this thesis in Fig. 3.5 of Chap. 3, a chiral transition, when probed with quenched Kogut-Susskind fermions, was observed roughly around the tricritical point. While the tricritical point was found to be around $\tilde{\kappa} = 0.45$ and $\kappa = -1.000$, the chiral transition around the same values of κ near the FM-FMD transition was determined to be between $\tilde{\kappa} = 0.40$ and 0.50. In this chapter, we have probed the chiral transition with more precision, and our results are summarized in the four plots of Fig. 4.9. While we observe that the chiral condensate gradually dips towards zero as $\tilde{\kappa}$ increases, the volume dependence of the plots, especially at lower fermion masses, are very different for the lower two $\tilde{\kappa}$ values as opposed to the higher $\tilde{\kappa}$ values. In Fig. 4.9, for $\tilde{\kappa} \leq 0.44$, the 16^4

data and their chiral extrapolation always lie above that of the 12^4 lattice, while the trend appears to be opposite for data at $\tilde{\kappa} \geq 0.47$. The opposite trend of volume dependence in the chiral limit is, however, very clearly seen in the corresponding plots in [15] at $\tilde{\kappa} = 0.40$ and 0.50 (Fig. 3.5 of Chap. 3 in this thesis). From the numerical evidence, it appears that the chiral transition takes place very near, if not coincident with, the tricritical point where the order of the FM-FMD transition changes from first order to continuous (second order). The vanishing chiral condensate at the continuous part of the FM-FMD transition is taken as an evidence of absence of non-trivial physics from this transition, although the chiral condensates do not exactly vanish on our finite lattices.

All our numerical investigations at strong gauge couplings indicate that, given any bare gauge coupling, there always exists a continuous FM-FMD transition for a sufficiently large $\tilde{\kappa}$ and the emerging physics while approaching the transition from the FM-side is governed by the WCPT point at $g = 0$ and $\tilde{\kappa} \to \infty$. Fig. 4.10 shows the average plaquette in the FM phase near the continuous FM-FMD transition increasing with increasing $\tilde{\kappa}$ for gauge couplings $g = 1.1$, 1.2 and 1.3. It is reasonable to expect that as $\tilde{\kappa}$ is increased, the average plaquette eventually would approach unity, the value of the plaquette at the perturbative point, in a behavior similar to that of the slope of the gauge field propagator.

4.6 Conclusion

A non-perturbatively gauge-fixed compact $U(1)$ lattice gauge theory is an alternate formulation of the pure $U(1)$ gauge theory on lattice. It is not only important because it provides a quantum continuum limit (unlike the standard Wilson formulation) and a possible probe at short distance behavior of a perturbatively non-asymptotically free theory (for example, by examining the universality class of the tricritical line obtained by us), but particularly for a manifestly local lattice formulation of Abelian chiral gauge theory with lattice fermions which explicitly break chiral symmetry. It obviously is very important to know the phase diagram of the theory for wide range of all its parameters so that all possible continuum limits and the universality classes can be traced.

We have carried out an extensive numerical investigation of the theory, especially at strong gauge couplings ($g > 1$). In the previous chapter (Chapter 3), results were presented for a single gauge coupling $g = 1.3$. The approach in this chapter is to scan a wide range of the 3-dimensional parameter space, generating gauge field configurations for a very large number of points in that parameter space to locate and determine the nature of the phase transitions and come up with an overall picture. The results of Chapter 3 and this have been published in Refs. [15] and [16] respectively, and all the diagrams have been taken from them.

We find that there is no lack of continuity between the FM-FMD phase transition near the perturbative point at $g = 0$ and $\tilde{\kappa} \to \infty$ and the FM-FMD transition at strong gauge couplings up to the edge of the tricritical line. The continuous part of the FM-FMD transition surface (blue surface, marked I in Fig. 4.6) is one continuous surface, and the results of all our measurements help build the emergence of a single universality class, obtained by approaching the transition near $g = 0$, $\tilde{\kappa} \to \infty$ from the FM side. Hence irrespective of the bare gauge coupling being weak or strong, at a strong enough coefficient $\tilde{\kappa}$ of the HD gauge-fixing term, the physics obtained by approaching the continuous FM-FMD transition from the FM side is governed by the perturbative point and is a Lorentz covariant theory of free massless photons, with the redundant *lgdof* decoupling at that transition.

The tricritical line at strong gauge couplings is potentially the only place where a different universality class with non-trivial physics may appear. However, a detailed investigation in that direction deserves a dedicated study and is outside the scope of the current work, given its vast and extensive nature. Precise determination of the critical exponents near the tricritical line would settle the issue.

The action with the HD gauge-fixing term poses its own problems in the Monte Carlo importance sampling. We found that a local algorithm like MM is poor in generating gauge field configurations (corresponding to quantum fluctuations around the global minimum of the classical action), especially on large values of the coefficient $\tilde{\kappa}$ of the HD term and at relatively larger lattices. A global algorithm like HMC was generally found to produce faithful field configurations and was used to generate the ensembles at the vast number of points in the 3-dimensional parameter space.

CHAPTER 5

EQUIVARIANT BRST GAUGE-FIXING OF NON-ABELIAN THEORIES

5.1 Introduction

The equivariant BRST gauge-fixing scheme, which circumvents the no-go theorem, was first proposed by Schaden [17] in 1998 for $SU(2)$ gauge theory. It was later extended for $SU(N)$ gauge theories by Golterman and Shamir [18], who thereby proposed a prescription for constructing $SU(N)$ chiral lattice gauge theories (ChLGT) for anomaly-free fermion representations. The eBRST gauge-fixing scheme basically amounts to gauge-fixing in a coset space G/H of the gauge group G, keeping a subgroup H (consisting of the maximal Abelian subgroup) invariant. Due to the presence of quartic ghost terms in such a theory, this scheme successfully evades the no-go theorem. It potentially provides a theoretically valid alternate formulation of non-Abelian gauge theories on the lattice. For constructing ChLGT, one then requires to gauge-fix the remaining Abelian subgroup in the scheme described in Chapter 3. A critical point can be found in the extended phase diagram of the gauge-fixed theory, by tuning a finite number of counter-terms, where the desired ChLGT can be constructed.

Apart from the importance of the eBRST scheme in the construction of ChLGT, it has been also suggested [20, 21] that the phase diagram of the eBRST gauge-fixed theory can accommodate a novel Higgs phase with no mass gap, due to strong dynamics in the *lgdof* sector. Evidence for the novel phase was provided through a combination of strong coupling and mean field techniques. It was also shown that the eBRST gauge-fixing coupling is asymptotically free [19], dimensional transmutation takes place in the longitudinal sector (from large-N calculations [21]), and at an infra-red scale the coupling gets strong.

In this chapter, we embark on the first time numerical study of the eBRST gauge-fixing method. We have based our study on the pure $SU(2)$ gauge theory, since it is the simplest case. Our key result has been the verification of the eBRST formalism as a valid alternative of the Wilsonian approach. We have strong evidence of a phase with a spontaneously broken global continuous symmetry in the reduced model (the theory with transverse gauge fields frozen to zero), which is also a topological field theory.

The chapter is organized as follows. In Sec. 5.2, we review the basic theory of the eBRST gauge-fixing scheme for $SU(N)$ theories in the continuum. The concept of anti-eBRST is also discussed, which leads to the extended eBRST algebra. We end the section with a discussion of the eBRST theory for the $SU(2)$ case. Next, the lattice eBRST symmetry and the construction of the gauge-fixing action on the lattice is reviewed in Sec. 5.3. This is followed by a brief sketch of the proof of how the eBRST theory evades the Neuberger's no-go theorem, and a discussion of its consequences, in Sec. 5.4. The eBRST gauge-fixed action of the pure $SU(2)$ theory and its reduced model is now explicitly studied in Sec. 5.5. Results of previous analytic work in this theory about the novel Higgs phase is also briefly reviewed. With this action, we now proceed to explain in detail about our numerical implementation of the theory, using Hybrid Monte Carlo (HMC) and the first-time implementation of stochastic Tunneling HMC [22], in Sec. 5.6. The results in the reduced model are now discussed in Sec. 5.7, followed by the results obtained in the full theory, in Sec. 5.8. Finally, we present our conclusions in Sec. 5.9.

5.2 Equivariant BRST Symmetry in the Continuum

In the equivariant BRST (eBRST) prescription of gauge-fixing, the gauge-fixing is done in the coset of a non-Abelian gauge group of the Yang-Mills theory, keeping minimally a Cartan subgroup invariant. In this section, we will discuss the eBRST gauge-fixing for a general $SU(N)$ gauge theory, after which we will construct the action explicitly for the $SU(2)$ case in the continuum. The following discussion is based on the Refs. [17, 18].

The Lagrangian density for a pure $SU(N)$ gauge theory in Euclidean spacetime is

$$\mathcal{L}(x) = \frac{1}{2g^2}\mathrm{tr}\left(F_{\mu\nu}(x)F_{\mu\nu}(x)\right) \ , \tag{5.1}$$

where g is the gauge coupling. The field strength tensor is given by,

$$F_{\mu\nu} = \partial_\mu V_\nu - \partial_\nu V_\mu + i[V_\mu, V_\nu] \ , \tag{5.2}$$

where V_μ is the $SU(N)$ gauge field. The spacetime dependence of the fields have been dropped for convenience. The components of the algebra-valued gauge field V_μ are

$$V_\mu = V_\mu^a T_a, \quad a = 1, 2, \ldots, N^2 - 1, \tag{5.3}$$

where T_a are the generators of the $SU(N)$ group. The generators are traceless Hermitian matrices and they satisfy the Lie algebra, $[T_a, T_b] = if_{abc}T_c$, with the normalization condition $\mathrm{tr}(T_aT_b) = \frac{1}{2}\delta_{ab}$. Note that, the indices $a, b, \ldots$ always run over all the generators of G, if not mentioned otherwise.

Let us now denote the $SU(N)$ group by G and the subgroup by $H \subset G$, with their corresponding algebras being denoted by $\mathcal{G}$ and $\mathcal{H}$ respectively. The eBRST gauge-fixing is now done in the coset G/H. The components of the gauge field are now written separately as

$$V_\mu = W_\mu^\alpha T_\alpha + A_\mu^i T_i \ , \quad \text{where} \ \ T_\alpha \in \mathcal{G}/\mathcal{H}, \ T_i \in \mathcal{H} \ . \tag{5.4}$$

In our discussion, the H generators will be represented by the indices $i, j, \ldots$, whereas the Greek indices $\alpha, \beta, \ldots$ will be used to indicate the generators lying in $\mathcal{G}/\mathcal{H}$. From the consistency check that the commutator of two elements in the subgroup $\mathcal{H}$ must lie in $\mathcal{H}$ itself, we find the following structure constants to be

$$f_{i\alpha j} = -f_{ij\alpha} = -f_{\alpha ij} = 0 \ . \tag{5.5}$$

Here, we have used the fact that the structure constants are completely antisymmetric.

Similar to the BRST formalism, the eBRST formalism too involves ghost fields $(C, \overline{C})$ and an auxiliary field B, which now reside in the coset space,

$$C = C^\alpha T_\alpha, \quad \overline{C} = \overline{C}^\alpha T_\alpha, \quad B = B^\alpha T_\alpha. \tag{5.6}$$

The ghost sector fields are $\mathcal{G}/\mathcal{H}$-valued and therefore, $\mathrm{tr}(CT_i) = 0$, for example. They transform under infinitesimal H gauge transformations in the same way as a field in the adjoint representation :

$$\delta_\omega C = -i[\omega, C], \quad \omega \in \mathcal{H}. \tag{5.7}$$

In order for Eq. 5.7 to be consistent, $[\omega, C]$ must belong to $\mathcal{G}/\mathcal{H}$, since the ghost fields belong to $\mathcal{G}/\mathcal{H}$. Using Eq. 5.5, we observe that $[\omega, C] = i\,\omega^j C^\alpha f_{j\alpha\beta} T_\beta \in \mathcal{G}/\mathcal{H}$, as it should be.

5.2.1 eBRST Transformations

We shall now discuss the eBRST variations, denoted by s, of the different fields of the theory. The physical fields have similar transformations to the ones for BRST (see Eqs. 1.81, 1.82 in Sec. 1.2.1). For the gauge field, we have $sV_\mu = D_\mu(V)C = \partial_\mu C + i[V_\mu, C]$. However, the transformations of the different parts of the gauge field are now different. From the transformation of V_μ, we have,

$$sV_\mu = sA_\mu + sW_\mu = \partial_\mu C + i\,[A_\mu, C] + i\,[W_\mu, C]\ , \tag{5.8}$$

from which we get,

$$sA_\mu = i\,[W_\mu, C]_{\mathcal{H}} \quad \text{and} \quad sW_\mu = D_\mu(A)C + i\,[W_\mu, C]_{\mathcal{G}/\mathcal{H}}\ . \tag{5.9}$$

Here, we have used $[A_\mu, C] \in \mathcal{G}/\mathcal{H}$ as can be seen from Eq. 5.5. Note that, the notations $[\cdots]_{\mathcal{H}}$ and $[\cdots]_{\mathcal{G}/\mathcal{H}}$ denote the projections of the commutator in $\mathcal{H}$ and $\mathcal{G}/\mathcal{H}$, respectively. In case of $SU(2)$, where gauge-fixing is done in the coset $SU(2)/U(1)$, the transformation rules for the different parts of the gauge field reduce to

$$sA_\mu = i\,[W_\mu, C], \quad sW_\mu = D_\mu(A)C. \tag{5.10}$$

Such simplifications occur for special cases, where $[W_\mu, C]$ is entirely contained in $\mathcal{H}$. We will discuss about them later. The matter fields ψ and $\bar{\psi}$ has the same transformation as BRST,

$$
\begin{aligned}
s\psi &= -iC\psi, \\
s\bar{\psi} &= i\bar{\psi}C \ .
\end{aligned}
\tag{5.11}
$$

The eBRST transformation rule for the ghost field C is obtained by projecting the BRST transformation rule (Eq. 1.86) onto the coset space $\mathcal{G}/\mathcal{H}$. Requiring the eBRST transformation to have components only in the coset space and since $\mathrm{tr}(sCT_i) = 0, \ \forall \ T_i \in \mathcal{H}$, we have

$$
sC = \left(-\,i\,C^2\right)_{\mathcal{G}/\mathcal{H}} = -\,i\,C^2 + X, \tag{5.12}
$$

where

$$
X \equiv (-\,i\,C^2)_{\mathcal{H}} = 2\,i\,T_j \mathrm{tr}\left(C^2 T_j\right). \tag{5.13}
$$

The above modification makes the eBRST nilpotency condition different from the usual BRST one, $\delta_B^2 = 0$. For the ghost field $\overline{C}$, the eBRST transformation rule is similar to the BRST rule,

$$
s\overline{C} = -iB \ , \tag{5.14}
$$

since the auxiliary field B already belongs to $\mathcal{G}/\mathcal{H}$.

For usual BRST variation, we have $\delta_B^2 C = 0$, but for eBRST, there would be extra terms for the X part. First, using Eq. 5.12 and the Grassmann nature of s and C, we see that

$$
\begin{aligned}
s\,\mathrm{tr}\left(C^2T_j\right) &= \mathrm{tr}\left((sC)CT_j - C(sC)T_j\right) \\
&= \mathrm{tr}\left(\left\{(-iC^2+X)C - C(-iC^2+X)\right\}T_j\right) \\
&= \mathrm{tr}\left((XC-CX)T_j\right) \\
&= X^iC^\alpha\mathrm{tr}\left([T_i,T_\alpha]T_j\right) \\
&= if_{i\alpha\beta}X^iC^\alpha\mathrm{tr}\left(T_\beta T_j\right) = 0\ ,
\end{aligned} \tag{5.15}
$$

where the trace vanishes in the last line. Therefore, putting Eq. 5.15 in Eq. 5.13, we obtain $sX = 0$. Using these results, we thus obtain the double eBRST variation of the ghost field C to be

$$s^2C = -isC^2 + sX = -i[X,C] = \delta_X C, \tag{5.16}$$

which does not vanish and is, instead, equal to an infinitesimal gauge transformation in the subgroup H, with the parameter X. The gauge transformation is denoted by δ_ω where ω is the parameter of transformation and an element of the gauge group algebra. Similarly, for the ghost field $\overline{C}$, we require

$$s^2\overline{C} = \delta_X\overline{C}, \tag{5.17}$$

which, using Eq. 5.14, gives us

$$-\,isB = -\,i\left[X,\overline{C}\right] \implies sB = \left[X,\overline{C}\right]. \tag{5.18}$$

The above eBRST transformation for the auxiliary field B, is non-vanishing unlike the

BRST one (compare Eq. 1.93). The double eBRST variation of B now gives

$$s^2 B = s\left(X\overline{C} - \overline{C}X\right) = X(-iB) - (-iB)X = -i[X, B] = \delta_X B, \tag{5.19}$$

where we have used $sX = 0$, and Eq. 5.17. Thus, we see that requiring all the ghost sector fields to have the same rule for their double variation, i.e. an "equivariant nilpotency" condition, makes their eBRST transformations consistent.

For the gauge field, the double eBRST variation is also non-vanishing as it has contributions from the X term in the variation of C and is similarly, equal to a H gauge transformation with parameter X. Explicitly, we have

$$\begin{aligned} s^2 V_\mu &= s\left(D_\mu(V)C\right) = \partial_\mu(sC) + i\left[V_\mu, sC\right] + i\left[sV_\mu, C\right] \\ &= -i\partial_\mu C^2 + \partial_\mu X + i\left[V_\mu, -iC^2 + X\right] + i\left[D_\mu(V)C, C\right] \\ &= D_\mu(V)X - iD_\mu(V)C^2 + i\left[D_\mu(V)C, C\right] \\ &= D_\mu(V)X = \delta_X V_\mu, \end{aligned} \tag{5.20}$$

where we have used Eqs. 5.9, 5.12 and the definition of the covariant derivative in section 5.2. In the last line, the two terms were cancelled using the following relation,

$$\begin{aligned} \partial_\mu C^2 &= (\partial_\mu C^\alpha)C^\beta T_\alpha T_\beta + C^\alpha(\partial_\mu C^\beta)T_\alpha T_\beta \\ &= (\partial_\mu C^\alpha)C^\beta [T_\alpha, T_\beta] = [\partial_\mu C, C] \end{aligned} \tag{5.21}$$

which is derived using the anti-commuting nature of the Grassmann variable C. The double eBRST variations of the $\mathcal{H}$ and $\mathcal{G}/\mathcal{H}$ components of V can now be easily read off from Eq.

5.20,

$$s^2 A_\mu = D_\mu(A)X = \delta_X A_\mu \ ,$$
$$s^2 W_\mu = -i\,[X, W_\mu] = \delta_X W_\mu. \tag{5.22}$$

where the A_μ and W_μ fields transform in the fundamental and adjoint representations of H, respectively.

The physical field ψ also has the similar double eBRST variation as above, i.e. a H gauge transformation in the fundamental representation,

$$s^2\psi = -i(sC)\psi + iC(s\psi) = -\left(-\,i\,C^2 + X\right)\psi + iC\,(-iC\psi)$$
$$= -iX\psi = \delta_X\psi \tag{5.23}$$

Thus, it has been consistently established that the eBRST symmetry is equivariantly nilpotent, which means the double variation of eBRST is a gauge transformation in the subgroup H with a commuting parameter $\omega = X \in \mathcal{H}$,

$$s^2 = \delta|_{\omega\to X}. \tag{5.24}$$

An important observation is that eBRST is still nilpotent on any H invariant object.

It is useful to note that the eBRST variation of a polynomial of the fields is given by a graded Leibnitz rule,

$$s(A\cdot B) = (sA)\cdot B + (-1)^{n(A)}A\cdot(sB) \tag{5.25}$$

where A and B are polynomials in the fields and $n(A)$ is the number of Grassmann fields in A.

Finally, we remark that the eBRST transformation s commutes with the H gauge transformation δ_ω,

$$[s, \delta_\omega] = 0. \tag{5.26}$$

This is an important property which will help us in our construction of the eBRST-invariant gauge-fixing action in the next section.

5.2.2 eBRST-invariant Action

The first step in the construction of the gauge-fixing action, is to take a local gauge-fixing condition, which gauge-fixes the coset space G/H and keeps the H-subgroup invariance of the action. The gauge-fixing condition, $F(V) = 0$, should be invariant under H, i.e.,

$$F(V) = 0 \implies F(V^h) = 0, \ \forall \ h \in H \subset G \tag{5.27}$$

where V^h is the vector potential obtained after a gauge transformation under H. Following Ref. [17], we choose a gauge-fixing function,

$$F(V) = D_\mu(A)W_\mu = \partial_\mu W_\mu + i[A_\mu, W_\mu], \tag{5.28}$$

which is covariant under H. From the fact that, $W_\mu \in \mathcal{G}/\mathcal{H}$, and by Eq. 5.5, we see that $F(V) \in \mathcal{G}/\mathcal{H}$. It thus transforms in the adjoint representation under H-gauge transformations, as

$$\delta_\omega F(V) = -i\,[\omega, F(V)]. \tag{5.29}$$

To construct the gauge-fixing action now, we have to choose a term invariant under both the eBRST and local H transformations. The generic form of such an action would be

$$S_{GF} = s\Sigma_{GF} \ , \tag{5.30}$$

where Σ_{GF} is H-invariant. The invariance of the above action under the desired symmetries can be easily seen as,

$$\begin{aligned} sS_{GF} &= s^2\Sigma_{GF} = \delta_X \Sigma_{GF} = 0, \\ \delta_\omega S_{GF} &= s\delta_\omega \Sigma_{GF} = 0, \end{aligned} \tag{5.31}$$

with $X, \omega \in \mathcal{H}$. These follow from the fact that Σ_{GF} is invariant under H and from Eq. 5.26. The gauge-fixing action is also eBRST-exact. With these symmetries, a general form of the gauge-fixing Lagrangian density is

$$\begin{aligned} \mathcal{L}_{GF}(\alpha, \tilde{g}) &= s\,\mathrm{tr}\left(2\alpha \overline{C} F + i\tilde{g}^2 \overline{C} B\right) \\ &= \mathrm{tr}\left(-2\alpha(iBF + \overline{C} sF) + \tilde{g}^2(B^2 - i\overline{C}[X, \overline{C}])\right), \end{aligned} \tag{5.32}$$

where $F \equiv F(V)$ is the gauge-fixing function and α and $\tilde{g}$ are two real dimensionless coefficients. The parameter α can, however, be scaled away by field redefinitions. This can be easily seen by plugging the following field redefinitions, $B \to B/\alpha, C \to \alpha^{\gamma-1}C, \overline{C} \to \alpha^{-\gamma}\overline{C}$, for any γ, in Eq. 5.32, which turns $\mathcal{L}_{GF}(\alpha, \tilde{g})$ into $\mathcal{L}_{GF}(1, \tilde{g}/\alpha)$. So, the parameter α can be set to 1.

The gauge invariance of the above action under H can be seen explicitly by taking the

H-variation of Σ_{GF},

$$\begin{aligned}\delta_\omega \Sigma_{GF} &= \delta_\omega \,\mathrm{tr}\left(2\,\overline{C}F + i\tilde{g}^2\overline{C}B\right)\\ &= \mathrm{tr}\left(-2\,i[\omega,\overline{C}]F - 2\,i\overline{C}[\omega,F] + \tilde{g}^2[\omega,\overline{C}]B + \tilde{g}^2\overline{C}[\omega,B]\right)\\ &= 0,\end{aligned} \tag{5.33}$$

where we have used Eq. 5.7 and the cyclic property of trace to arrive at the last line. It can be seen that both the terms in the first line of Eq. 5.32 are individually gauge invariant.

The above action in Eq. 5.32 is, however, not the most general action possible. We will now see how it can be made more general, by making it invariant under the extended eBRST symmetry.

5.2.3 Anti-eBRST

The usual BRST invariant Lagrangian of Yang-Mills theory can also be shown to be invariant under an anti-BRST transformation. This was found out independently by Curci, Ferrari [58] and Ojima [59]. The anti-BRST transformations are obtained by the ghost flip operation,

$$C \to \overline{C} \quad \text{and} \quad \overline{C} \to -C. \tag{5.34}$$

The physical fields are unaffected by this operation. The anti-BRST variation $\bar{\delta}_B$ is also nilpotent, i.e. $\bar{\delta}_B^2 = 0$.

The anti-BRST symmetry can also be incorporated into the equivariant BRST formalism similarly, as done earlier for BRST, by restricting the ghost sector fields to the coset space and defining an anti-eBRST transformation $\bar{s}$ [18]. By the ghost flip operation (Eq. 5.34) and keeping in mind that $C, \overline{C} \in \mathcal{G}/\mathcal{H}$, the anti-eBRST transformations for the matter and gauge fields can be found to be

$$\begin{aligned}
\bar{s}\,\psi &= -i\overline{C}\psi, \\
\bar{s}\,\bar{\psi} &= i\,\bar{\psi}\,\overline{C}, \\
\bar{s}\,V_\mu &= D_\mu(V)\overline{C}, \\
\bar{s}\,A_\mu &= i\,[W_\mu, \overline{C}]_{\mathcal{H}}, \\
\bar{s}\,W_\mu &= D_\mu(A)\overline{C} + i\,[W_\mu, \overline{C}]_{\mathcal{G}/\mathcal{H}}.
\end{aligned} \tag{5.35}$$

By requiring the equivariant nilpotency condition for anti-eBRST (compare Eq. 5.24) to be

$$\bar{s}^2 = \delta|_{\omega\to\overline{X}}, \quad \text{where } \overline{X} = 2\,i\,T_j \mathrm{tr}\left(\overline{C}^2 T_j\right) \in \mathcal{H}, \tag{5.36}$$

we find the anti-eBRST transformation rules for the ghost sector fields to be

$$\begin{aligned}
\bar{s}\,\overline{C} &= -i(\overline{C}^2)_{\mathcal{G}/\mathcal{H}} = -i\,\overline{C}^2 + \overline{X}, \\
\bar{s}\,C &= iB - i\{C, \overline{C}\}_{\mathcal{G}/\mathcal{H}} = iB - i\{C, \overline{C}\} + \widetilde{X}, \\
\bar{s}\,B &= [\widetilde{X}, \overline{C}] - i\,[\overline{C}, B]_{\mathcal{G}/\mathcal{H}},
\end{aligned} \tag{5.37}$$

where

$$\widetilde{X} = 2\,i\,T_j\,\mathrm{tr}\left(\{C, \overline{C}\}T_j\right) \in \mathcal{H} \tag{5.38}$$

The above anti-eBRST and eBRST transformation rules together form the *extended* eBRST algebra,

$$s^2 = \delta_X, \quad \bar{s}^2 = \delta_{\overline{X}}, \quad \{s, \bar{s}\} = \delta_{\widetilde{X}}, \tag{5.39}$$

which closes when acting on the physical and ghost sector fields. Denoting the ghost flip operation in Eq. 5.34 by f, the extended eBRST algebra also satisfies

$$f s = \bar{s} f, \qquad f \bar{s} = -s f, \tag{5.40}$$

for all fields. The anti-eBRST variation $\bar{s}$ also satisfies the similar Leibniz rule as in the case of eBRST, given in Eq. 5.25.

5.2.4 Extended eBRST gauge-fixing action

With the extended eBRST symmetry, we can now construct the most general gauge-fixing action. The first term in the eBRST invariant Lagrangian, in Eq. 5.32, can now be rewritten in a way so that, the anti-eBRST invariance becomes explicit :

$$s\,\mathrm{tr}\left(2\alpha\overline{C}F\right) = -s\bar{s}\,\mathrm{tr}\left(W^2\right). \tag{5.41}$$

In the above equation, the pre-potential $\mathrm{tr}\left(W^2\right)$ is invariant under the H gauge symmetry.

The most general extended eBRST-invariant Lagrangian (restricting to terms of engineering dimension 4) with local H gauge symmetry is thus the following,

$$\begin{aligned}\mathcal{L}^{e}_{GF} &= -s\bar{s}\,\mathrm{tr}\left(W^2 + \tilde{g}^2\,\overline{C}C\right) \\ &= \bar{s}s\,\mathrm{tr}\left(W^2 + \tilde{g}^2\,\overline{C}C\right),\end{aligned} \tag{5.42}$$

where a coefficient for the first term can be similarly scaled away as in Eq. 5.32. The second line in Eq. 5.42 is obtained using the commutation relation of s and $\bar{s}$ given in Eq. 5.39, and the H-symmetry of the pre-potential. The above Lagrangian is also invariant under the discrete ghost flip symmetry f (see Eqs. 5.34, 5.40). In the terminology of [60], where the most general BRST and anti-BRST invariant action was constructed, the above Lagrangian in Eq. 5.42 is "hermitian" under the following operations,

$$C^\dagger = \overline{C}, \qquad \overline{C}^\dagger = C, \qquad B^\dagger = -B + \{\overline{C}, C\}_{\mathcal{G}/\mathcal{H}}, \qquad (V^a_\mu)^\dagger = V^a_\mu. \tag{5.43}$$

We now apply the eBRST and anti-eBRST transformations explicitly in Eq. 5.42 to obtain the expanded Lagrangian. Using Eqs. 5.35, 5.14, 5.9, the cyclic property of trace and an integration by parts, we obtain for the first term,

$$\begin{aligned} -s\bar{s}\,\mathrm{tr}\left(W^2\right) &= -2s\,\mathrm{tr}\left((D_\mu(A)\overline{C})W_\mu + i\,[W_\mu, \overline{C}]_{\mathcal{G}/\mathcal{H}} W_\mu\right) \\ &= 2s\,\mathrm{tr}\left(\overline{C} D_\mu(A) W_\mu\right) \\ &= -2\,i\,\mathrm{tr}\left(B D_\mu(A) W_\mu\right) - 2\,\mathrm{tr}\left(\overline{C} D_\mu(A) D_\mu(A) C\right) \\ &\quad - 2\,i\,\mathrm{tr}\left(\overline{C} D_\mu(A)[W_\mu, C]_{\mathcal{G}/\mathcal{H}}\right) + 2\,\mathrm{tr}\left([W_\mu, \overline{C}]_{\mathcal{H}}[W_\mu, C]_{\mathcal{H}}\right). \end{aligned} \tag{5.44}$$

The second term in Eq. 5.42 expands to the following terms (omitting the coefficient $\tilde{g}^2$ for now),

$$\bar{s}s\,\mathrm{tr}\left(\overline{C}C\right) = \mathrm{tr}\left((\bar{s}s\overline{C})C\right) + \mathrm{tr}\left((s\overline{C})(\bar{s}C)\right) - \mathrm{tr}\left((\bar{s}\overline{C})(sC)\right) + \mathrm{tr}\left(\overline{C}(\bar{s}sC)\right) \tag{5.45}$$

using the Leibnitz rule (Eq. 5.25) for both s and $\bar{s}$. Using the extended eBRST transformation rules and a bit of algebra, the above terms can be further expanded to obtain

$$\begin{aligned}
\mathrm{tr}\left((\bar{s}s\overline{C})C\right) &= -\mathrm{tr}\left(\widetilde{X}^2\right) + \mathrm{tr}\left(B\{C,\overline{C}\}\right),\\
\mathrm{tr}\left((s\overline{C})(\bar{s}C)\right) &= \mathrm{tr}\left(B^2\right) - \mathrm{tr}\left(B\{C,\overline{C}\right),\\
-\mathrm{tr}\left((\bar{s}\overline{C})(sC)\right) &= \mathrm{tr}\left((\overline{C}^2)_{\mathcal{G}/\mathcal{H}}(C^2)_{\mathcal{G}/\mathcal{H}}\right),\\
\mathrm{tr}\left(\overline{C}(\bar{s}sC)\right) &= -\mathrm{tr}\left(B\{C,\overline{C}\right) + \mathrm{tr}\left(\{C,\overline{C}_{\mathcal{G}/\mathcal{H}}\right)^2,
\end{aligned} \tag{5.46}$$

which together becomes,

$$\begin{aligned}
\bar{s}s\,\mathrm{tr}\left(\overline{C}C\right) = {}& \mathrm{tr}\left(B^2\right) - \mathrm{tr}\left(B\{C,\overline{C}\}\right)\\
&+ \mathrm{tr}\left((\overline{C}^2)_{\mathcal{G}/\mathcal{H}}(C^2)_{\mathcal{G}/\mathcal{H}}\right) + \mathrm{tr}\left(\{\overline{C},C\}_{\mathcal{G}/\mathcal{H}}\right)^2 - \mathrm{tr}\left(\widetilde{X}^2\right).
\end{aligned} \tag{5.47}$$

The auxiliary field B can now be integrated out to arrive at the on-shell Lagrangian density. The terms of the action containing B are given as,

$$\begin{aligned}
&\tilde{g}^2\mathrm{tr}(B^2) - \tilde{g}^2\mathrm{tr}\left(B\{C,\overline{C}\}\right) - 2\,i\,\mathrm{tr}\left(BD_\mu(A)W_\mu\right)\\
&= \mathrm{tr}\left(\tilde{g}B - \frac{i}{\tilde{g}}D_\mu(A)W_\mu - \frac{\tilde{g}}{2}\{C,\overline{C}\}_{\mathcal{G}/\mathcal{H}}\right)^2 + \frac{1}{\tilde{g}^2}\mathrm{tr}\left(D_\mu(A)W_\mu\right)^2\\
&\quad - \frac{\tilde{g}^2}{4}\mathrm{tr}\left(\{C,\overline{C}\}_{\mathcal{G}/\mathcal{H}}\right)^2 - i\,\mathrm{tr}\left((D_\mu(A)W_\mu)\{C,\overline{C}\}\right),
\end{aligned} \tag{5.48}$$

where the $\mathcal{G}/\mathcal{H}$ projection of $\{C,\overline{C}\}$ in the last term is unnecessary as $D_\mu(A)W_\mu \in \mathcal{G}/\mathcal{H}$. One can now eliminate B by putting in its equation of motion,

$$B = \frac{i}{\tilde{g}^2}D_\mu(A)W_\mu + \frac{1}{2}\{C,\overline{C}\}_{\mathcal{G}/\mathcal{H}}. \tag{5.49}$$

The last term in the second line of Eq. 5.48 can be rewritten after an integration by parts and by the cyclic property of trace as,

$$-\,i\,\mathrm{tr}\left((D_\mu(A)\overline{C})[W_\mu, C]\right) + i\,\mathrm{tr}\left([W_\mu, \overline{C}](D_\mu(A)C)\right). \tag{5.50}$$

Collecting all the terms, the total on-shell gauge-fixing Lagrangian density is thus,

$$\mathcal{L}_{GF}^{o.s.} = \frac{1}{\tilde{g}^2}\mathrm{tr}\,(D_\mu(A)W_\mu)^2 + \mathcal{L}_{gh}^{(2)} + \tilde{g}^2\mathcal{L}_{gh}^{(4)}, \tag{5.51}$$

where the terms bilinear in ghost fields, $\overline{C}$ and C, are

$$\begin{aligned}\mathcal{L}_{gh}^{(2)} =& -2\,\mathrm{tr}\left(\overline{C}D_\mu(A)D_\mu(A)C\right)\\ &+ i\,\mathrm{tr}\left((D_\mu(A)\overline{C})[W_\mu, C] + [W_\mu, \overline{C}](D_\mu(A)C)\right)\\ &+ 2\,\mathrm{tr}\left([W_\mu, \overline{C}]_{\mathcal{H}}[W_\mu, C]_{\mathcal{H}}\right),\end{aligned} \tag{5.52}$$

and the 4-ghost terms are

$$\mathcal{L}_{gh}^{(4)} = -\mathrm{tr}\left(\widetilde{X}^2\right) + \mathrm{tr}\left((\overline{C}^2)_{\mathcal{G}/\mathcal{H}}(C^2)_{\mathcal{G}/\mathcal{H}}\right) + \frac{3}{4}\mathrm{tr}\left(\{\overline{C}, C\}_{\mathcal{G}/\mathcal{H}}\right)^2. \tag{5.53}$$

Combining all the terms in 5.52 and defining them as $\overline{C}MC$, it can be seen that the bilinear ghost operator M is real and symmetric. The novel 4-ghost interaction terms, which are not present in the usual BRST gauge-fixing action, are actually responsible for avoiding the Neuberger's no-go theorem. This will be described in Sec. 5.4.

Integrating out the auxiliary field modifies the eBRST variation $s\overline{C}$ (Eq. 5.14) and anti-eBRST variation $\bar{s}C$ (Eq. 5.37), as

$$s\overline{C} = -\bar{s}C = \frac{1}{\tilde{g}^2}D_\mu(A)W_\mu + \frac{1}{2}\{C, \overline{C}\}_{\mathcal{G}/\mathcal{H}} \tag{5.54}$$

where we have used the equation of motion for B given in Eq. 5.49.

Although the $SU(N)$ gauge symmetry is explicitly broken by the gauge-fixing terms, the extended eBRST gauge-fixing action still remains invariant under the skewed permutation group $\widetilde{S}_N$, which is a discrete subgroup of $SU(N)$. The action is also invariant under a ghost-$SU(2)$ symmetry, which transform C and $\overline{C}$ as a doublet. Details of these symmetries can be found in Refs. [18, 61].

5.2.5 $SU(2)/U(1)$

For the $SU(2)$ group, the only way of fixing the gauge in an eBRST invariant manner, is by fixing the coset $SU(2)/U(1)$ and keeping the subgroup $U(1)$ invariant. This belongs to the *special class* of gauge-fixed theories for which the structure constants $f_{\alpha\beta\gamma}$ are equal to zero, i.e., the commutator of any two generators in the coset $\mathcal{G}/\mathcal{H}$ always belong in $\mathcal{H}$. This leads to several simplifications, for example $sC = \bar{s}\overline{C} = 0$, and as a result, the extended eBRST Lagrangian $\mathcal{L}^e_{GF}$ in Eq. 5.42 becomes the same as the eBRST one in Eq. 5.32. This can be seen for the second term in Eq. 5.42, from the following equation,

$$\bar{s}\,\mathrm{tr}\left(\overline{C}C\right) = -i\mathrm{tr}\left(\overline{C}B\right), \tag{5.55}$$

where we have used the anti-eBRST transformation rule $\bar{s}C = iB$ for the special class.

For the $SU(2)$ Yang-Mills theory, the gauge field is split as in the following,

$$V^a_\mu \tau_a = A^i_\mu \tau_i + W^\alpha_\mu \tau_\alpha, \quad \text{with} \;\; a = 1, 2, 3, \;\; i = 3 \;\&\; \alpha = 1, 2. \tag{5.56}$$

The generators $\tau_a = \sigma_a/2$, where σ_a are the Pauli matrices. The ghost sector fields are a linear combination of the generators τ_1 and τ_2. With the auxiliary field integrated out, the total Lagrangian for the gauge-fixing part is

$$\begin{aligned}\mathcal{L}_{GF}^{SU(2)} = & \frac{1}{\tilde{g}^2}\mathrm{tr}\left(D_\mu(A)W_\mu\right)^2 \\ & -2\,\mathrm{tr}\left(\overline{C}D_\mu(A)D_\mu(A)C\right) + 2\,\mathrm{tr}\left([W_\mu,\overline{C}][W_\mu,C]\right) \\ & -\mathrm{tr}\left(\widetilde{X}\right)^2 .\end{aligned} \tag{5.57}$$

One may compare the above with Eqs. 5.51, 5.52, 5.53.

This concludes the discussion of eBRST gauge-fixing in the continuum. The eBRST construction on the lattice for the general case is now described below.

5.3 Equivariant BRST on the lattice

The eBRST and anti-eBRST gauge-fixing action can be formulated on the lattice by respecting all the internal symmetries. Following Ref. [18], we review the lattice transcription for the choice of eBRST gauge-fixing with $G = SU(N)$ and $H = U(1)^{N-1}$, which is the maximal Abelian subgroup containing only diagonal generators. Another choice of gauge-fixing could be with $G = SU(N)$ and $H = SU(N-1)\times U(1)$, where the subgroup still contains the maximal Abelian subgroup. Note that to evade the no-go theorem, one needs to have the maximal Abelian subgroup, $U(1)^{N-1}$ as a subgroup of H.

The gauge link on the lattice $U_{x\mu}$ is, as usual, related to the continuum gauge field $V_\mu(x)$ as

$$U_{x\mu} = \exp(i\,V_\mu(x)). \tag{5.58}$$

For convenience, it is repeated once again that the gauge field is decomposed as $V_\mu^a T_a = W_\mu^\alpha T_\alpha + A_\mu^i T_i$, where the index a runs over the generators in $\mathcal{G}$, the index i runs over generators in $\mathcal{H}$ and the Greek index α over the generators in the coset $\mathcal{G}/\mathcal{H}$.

The eBRST and the anti-eBRST transformation rules for the lattice gauge links are

$$
\begin{aligned}
sU_{x\mu} &= i\left(U_{x\mu}C_{x+\mu} - C_x U_{x\mu}\right), \\
\bar{s}U_{x\mu} &= i\left(U_{x\mu}\overline{C}_{x+\mu} - \overline{C}_x U_{x\mu}\right).
\end{aligned} \tag{5.59}
$$

The ghost sector fields are defined the same way as in the continuum, but with discrete spacetime indices, and hence have the same eBRST transformations as in the continuum.

The lattice equivalent of the coset gauge field $W_\mu(x)$ is $\mathcal{W}_{x\mu}$, given as

$$
\begin{aligned}
\mathcal{W}_{x\mu} &= -i\left[U_{x\mu}T_iU^\dagger_{x\mu}, T_i\right] \\
&= -i\left[(1+iV_{x\mu})T_i(1-iV_{x\mu}), T_i\right] + O(V^2) \\
&= \left[\left[V_{x\mu}, T_i\right], T_i\right] + O(V^2) \\
&= W_{x\mu} + O(V^2).
\end{aligned} \tag{5.60}
$$

In the last line of the above equation, we have used the following relation, for any element $\mathcal{A} \in \mathcal{G}$,

$$
\begin{aligned}
\left[\left[\mathcal{A}, T_i\right], T_i\right] &= if_{jik}\mathcal{A}^j_{\mathcal{H}}\left[T_k, T_i\right] + if_{\alpha i\beta}\mathcal{A}^\alpha_{\mathcal{G}/\mathcal{H}}\left[T_\beta, T_i\right] \\
&= -f_{\alpha i\beta}f_{\beta i\gamma}\mathcal{A}^\alpha_{\mathcal{G}/\mathcal{H}}T_\gamma = \mathcal{A}_{\mathcal{G}/\mathcal{H}}
\end{aligned} \tag{5.61}
$$

where the first term on the right hand side of the first line vanishes since H is Abelian, and in the second line, we have used the identity

$$
\sum_{i\alpha} f_{i\alpha\beta}f_{i\alpha\gamma} = \delta_{\beta\gamma}. \tag{5.62}
$$

With the definition of forward and backward lattice covariant derivatives, for any field Φ, as

$$D_\mu^+\Phi_x = U_{x\mu}\Phi_{x+\mu}U_{x\mu}^\dagger - \Phi_x,$$
$$D_\mu^-\Phi_x = \Phi_x - U_{x-\mu,\mu}^\dagger\Phi_{x-\mu}U_{x-\mu,\mu}, \tag{5.63}$$

we can now construct the lattice equivalent of the continuum gauge-fixing function, given in Eq. 5.28. The lattice gauge-fixing function,

$$D_\mu^-\mathcal{W}_{x\mu} = \mathcal{W}_{x\mu} - U_{x-\mu,\mu}^\dagger\mathcal{W}_{x\mu}U_{x-\mu,\mu} \tag{5.64}$$

goes to $D_\mu(A)W_\mu$ in the classical continuum limit. It belongs to the coset $\mathcal{G}/\mathcal{H}$ and hence, transforms covariantly under H gauge transformations. The first term in Eq. 5.64 belongs to the coset, since

$$\mathrm{tr}\left(\mathcal{W}_{x\mu}T_j\right) = -i\,\mathrm{tr}\left(U_{x\mu}T_iU_{x\mu}^\dagger\left[T_i,T_j\right]\right) = 0. \tag{5.65}$$

The above follows from the general relation, $\mathrm{tr}([A,B]C) = \mathrm{tr}(A[B,C])$ and the fact that the commutator of generators of the maximal Abelian subgroup vanishes. The second term in Eq. 5.64 also resides in the coset, as seen from

$$\mathrm{tr}(T_jU_{x\mu}^\dagger[U_{x\mu}T_iU_{x\mu}^\dagger,T_i]U_{x\mu}) = \mathrm{tr}([U_{x\mu}T_jU_{x\mu}^\dagger,U_{x\mu}T_iU_{x\mu}^\dagger]T_i) = \mathrm{tr}([T_j,T_i]U_{x\mu}^\dagger T_iU_{x\mu}) = 0\,. \tag{5.66}$$

The lattice off-shell gauge-fixing Lagrangian, invariant under eBRST and anti-eBRST, is now taken as

$$\mathcal{L}^{L}_{GF} = -s\bar{s}\,\mathrm{tr}\left(-2U_{x\mu}T_iU^{\dagger}_{x\mu}T_i + \tilde{g}^2\overline{C}C\right). \tag{5.67}$$

In the näive continuum limit, it goes to the gauge-fixing Lagrangian, given in Eq. 5.42. An important relation, used in deriving the continuum limit, is

$$\mathrm{tr}\left([T_i, A][T_i, B]\right) = -\mathrm{tr}\left(A_{\mathcal{G}/\mathcal{H}}B_{\mathcal{G}/\mathcal{H}}\right), \tag{5.68}$$

which uses the relation in Eq. 5.62. The first term in the Lagrangian can be expanded by applying the s and $\bar{s}$ variations, to obtain,

$$\begin{aligned}
2s\bar{s}\,\mathrm{tr}\left(U_{x\mu}T_iU^{\dagger}_{x\mu}T_i\right) = &-2\,i\,\mathrm{tr}(B_xD^{-}_{\mu}\mathcal{W}_{x\mu}) \\
&-2\,\mathrm{tr}\left(\left[T_i, D^{+}_{\mu}C_x\right]\left[U_{x\mu}T_iU^{\dagger}_{x\mu}, D^{+}_{\mu}\overline{C}_x\right]\right) \\
&-2\,i\,\mathrm{tr}\left(\{D^{+}_{\mu}C_x, \overline{C}_x\}\mathcal{W}_{x\mu}\right).
\end{aligned} \tag{5.69}$$

The second term, $-s\bar{s}\,\mathrm{tr}\left(\tilde{g}^2\overline{C}C\right)$, has the same expansion as in the continuum, given in Eq. 5.47.

Following the discussion in the continuum, we now obtain the on-shell lattice Lagrangian density, by integrating out the auxiliary field B, to be

$$\begin{aligned}
\mathcal{L}^{L,o.s.}_{GF} = &\frac{1}{\tilde{g}^2}\mathrm{tr}\left(D^{-}_{\mu}\mathcal{W}_{x\mu}\right)^2 \\
&+2\,\mathrm{tr}\left(\left[T_i, D^{+}_{\mu}C_x\right]\left[U_{x\mu}T_iU^{\dagger}_{x\mu}, D^{+}_{\mu}\overline{C}_x\right]\right) \\
&-i\,\mathrm{tr}\left(2\{D^{+}_{\mu}C_x, \overline{C}_x\}\mathcal{W}_{x\mu} + \{\overline{C}_x, C_x\}D^{-}_{\mu}\mathcal{W}_{x\mu}\right) \\
&+\tilde{g}^2\Big(\mathrm{tr}\left((\overline{C}^2_x)_{\mathcal{G}/\mathcal{H}}(C^2_x)_{\mathcal{G}/\mathcal{H}}\right) + \frac{3}{4}\mathrm{tr}\left(\{\overline{C}_x, C_x\}_{\mathcal{G}/\mathcal{H}}\right)^2 - \mathrm{tr}(\widetilde{X}^2)\Big).
\end{aligned} \tag{5.70}$$

Since the quartic ghost terms in the last line of Eq. 5.70 are not amenable to numerical simulations, we can introduce new set of auxiliary fields through a Hubbard-Stratonovich transformation to do away with the four-ghost terms.

5.4 Avoiding the No-Go theorem

We discussed the proof of Neuberger's no-go theorem in Sec. 1.3.2. The partition function of a BRST-invariant gauge-fixed theory with compact gauge fields vanishes identically, rendering the expectation value of a gauge-invariant operator to the indeterminate $0/0$ form. A crucial property of the eBRST framework is that it evades the no-go theorem and we shall now demonstrate how this is achieved.

Introducing a parameter t as earlier, we can define the functional integral,

$$Z_{\mathrm{eBRST}}(t) = \int \mathcal{D}\Xi \, \mathrm{e}^{-S_{GI}(U) - S^L_{GF}(t;U,C,\overline{C},B)}, \tag{5.71}$$

from which the partition function of the eBRST gauge-fixed theory can be obtained by setting $t = 1$. The measure $\mathcal{D}\Xi \equiv \mathcal{D}U \, \mathcal{D}B \, \mathcal{D}C \, \mathcal{D}\overline{C}$ is eBRST-invariant. The term S_{GI} is taken to be the gauge-invariant Wilson plaquette action and the eBRST gauge-fixing action S^L_{GF}, corresponding to the Lagrangian density in Eq. 5.67, is found by setting $t = 1$ in the function,

$$S^L_{GF}(t) = \sum_x \left(t \, s \, \mathrm{tr}(2\,\overline{C}F(U)) - \tilde{g}^2 \, s\bar{s} \, \mathrm{tr}(\overline{C}C) \right). \tag{5.72}$$

For the following discussion, the gauge-fixing function $F(U)$ can be chosen arbitrarily, given it satisfies the basic requirements discussed in Sec. 5.2.2. One can note that, similar to as mentioned in Sec. 1.3.2, the parameter t cannot be multiplied to the second term in

Eq. 5.72, as it contains the B-dependent terms, and setting $t = 0$ in that case would be ill-defined.

Proceeding similarly as in Eq. 1.102, we again find that $dZ_{\text{eBRST}}(t)/dt = 0$, due to integration over a total eBRST variation. Now, setting $t = 0$, we find that

$$Z_{\text{eBRST}}(0) = \int \mathcal{D}U\, \mathrm{e}^{-S_{GI}(U)} \int \mathcal{D}B\, \mathcal{D}C\, \mathcal{D}\overline{C}\, \exp\left[\tilde{g}^2 \sum_x s\bar{s}\, \mathrm{tr}(\bar{C}C)\right], \tag{5.73}$$

which shows that ghost fields are present in the integrand, unlike the case for BRST. It can now be shown that the above partition function does not vanish. The proof of this statement is technical and the reader is referred to Refs. [17, 18]. An essential ingredient for the partition function to be non-vanishing, is the presence of the quartic ghost terms in the eBRST action. An important point to note here is that the proof holds on the condition that the subgroup H contains the maximal Abelian subgroup of the $SU(N)$ gauge group.

Since $dZ_{\text{eBRST}}(t)/dt = 0$, we, finally, have $Z_{\text{eBRST}}(0) = Z_{\text{eBRST}}(1) \neq 0$, and as a result, the eBRST theory successfully circumvents the no-go theorem.

An important corollary of the above exercise is the existence of an *invariance* theorem [17, 18], which states that the expectation value of a gauge-invariant operator obtained in a gauge theory without gauge-fixing, is exactly equal to that obtained for the same operator in an eBRST gauge-fixed theory. This result is rigorous for a finite lattice. The partition function Z_{eBRST} is equal to the partition function of the unfixed theory up to a non-zero multiplicative constant, since the lattice gauge fields are decoupled from the ghost sector in Eq. 5.73 and $Z_{\text{eBRST}}(0) = Z_{\text{eBRST}}(1)$. We will demonstrate the validity of the invariance theorem explicitly through our numerical investigation, at least for a region of the parameter space of the $SU(2)$ eBRST theory.

Another consequence of the above proof is that the reduced model of the theory (obtained by switching off the transverse degrees of freedom) is a topological field theory, as it does not depend on the gauge-fixing coupling [17, 18]. It then follows rigorously that, the eBRST theory is unitary if the underlying unfixed theory is.

For constructing chiral gauge theories with the eBRST prescription, one also needs to gauge-fix the unfixed Abelian subgroup H. This can now be done in the gauge-fixing approach described in Chapter 3. The construction of ChLGT for the general $SU(N)$ case is described in Ref. [18]. It is remarked that gauge-fixing the remaining invariant subgroup breaks the eBRST invariance explicitly and apparently, unitarity in a finite volume. However, unitarity in the total gauge-fixed theory was established to all orders in perturbation theory [18]. The question of non-perturbative unitarity can only be answered through non-perturbative calculations. Our present work on the lattice is for a pure $SU(2)$ gauge theory gauge-fixed in the coset $SU(2)/U(1)$, in the eBRST prescription.

5.5 eBRST $SU(2)$ gauge theory on the lattice

The lattice gauge-fixing action for $SU(2)$ simplifies considerably from the general $SU(N)$ case. As we have seen in Sec. 5.2.5, the extended eBRST algebra reduces to the eBRST algebra for the special case of $SU(2)$. For the $SU(2)$ theory, the lattice gauge link is $U_{x\mu} = \exp(iV_\mu(x))$, where the algebra-valued gauge field is given by Eq. 5.56. Note that the convention for the indices still remains the same. The on-shell gauge-fixing action is given by (cf. Eq. 5.70),

$$\mathcal{S}_{gf}^{o.s.} = \frac{1}{\tilde{g}^2}\sum_x \mathrm{tr}\left(D_\mu^- \mathcal{W}_{x\mu}\right)^2$$
$$- 2\sum_x \mathrm{tr}\Big(\left[U_{x\mu}\tau_3 U_{x\mu}^\dagger, D_\mu^+ \overline{C}_x\right]\left[\tau_3, D_\mu^+ C_x\right] + i\{\overline{C}_x, D_\mu^+ C_x\}\mathcal{W}_{x\mu}\Big)$$
$$- \tilde{g}^2 \sum_x \mathrm{tr}(\widetilde{X}_x^2). \tag{5.74}$$

The four-ghost term can now be traded off for an auxiliary field ρ and a bilinear ghost term, by the following Hubbard-Stratonovich transformation,

$$-\tilde{g}^2\sum_x \mathrm{tr}(\widetilde{X}_x^2) = -\frac{\tilde{g}^2}{2}\sum_{x,i}(f_{\alpha\beta i}\overline{C}_{x\alpha}C_{x\beta})^2 \to \sum_{x,i}\Big(\frac{\tilde{g}^2}{2}\rho_{xi}^2 + \tilde{g}\rho_{xi}f_{\alpha\beta i}\overline{C}_{x\alpha}C_{x\beta}\Big), \tag{5.75}$$

where $f_{\alpha\beta i}$ are the real antisymmetric structure constants of $SU(2)$ algebra. This transformation now makes the action suitable for numerical investigation. It is to be noted that, for our case of $SU(2)$, the auxiliary field has only one component, i.e., $\rho_x = \rho_{x3}\tau_3$.

The total eBRST gauge-fixed $SU(2)$ action on the lattice, with the auxiliary field ρ, is thus given as

$$\mathcal{S} = \mathcal{S}_W + \mathcal{S}_{gf}, \tag{5.76}$$

where $\mathcal{S}_W$ is the usual Wilson plaquette action,

$$\mathcal{S}_W = \frac{\beta}{2}\sum_{x,\mu<\nu} \mathrm{Re}\ \mathrm{tr}\left[\mathbb{1} - U_{x\mu\nu}\right], \tag{5.77}$$

where $\beta = 4/g^2$. The eBRST gauge-fixing term is given as

$$\begin{aligned}
\mathcal{S}_{gf} &= \frac{1}{2\tilde{g}^2}\sum_{x\alpha}(\mathcal{D}^-_\mu \mathcal{W}_{x\mu})^2_\alpha + \frac{1}{2\tilde{g}^2}\sum_{x}(\rho_{x3})^2 + \sum_{xy\alpha\beta}\overline{C}_{x\alpha}M_{x\alpha,y\beta}C_{y\beta} \\
&= \tilde{\kappa}\sum_{x\alpha}(\mathcal{D}^-_\mu \mathcal{W}_{x\mu})^2_\alpha + \tilde{\kappa}\sum_{x}(\rho_{x3})^2 + \sum_{xy\alpha\beta}\overline{C}_{x\alpha}M_{x\alpha,y\beta}C_{y\beta},
\end{aligned} \tag{5.78}$$

where $\tilde{\kappa} \equiv 1/2\tilde{g}^2 = 1/2\xi g^2$, has been introduced as in the convention of Chap. 3. The second line in the right hand side above is the starting point of the numerical calculation. The simulation is done using the parameters β and $\tilde{\kappa}$. This will be denoted as the *full theory* from now onwards, as opposed to the *reduced model* to be discussed in the next section.

A mass term for the lattice coset gauge field $\mathcal{W}_{x\mu}$ and for the ghost field C_x, together invariant under on-shell eBRST transformations, can be added in the action in Eq. 5.76, as

$$\mathcal{S}_{mass} = m^2\sum_{x}\left[-4\,\tilde{\kappa}\,\mathrm{tr}(U_{x\mu}\tau_3U^\dagger_{x\mu}\tau_3) + 2\,\mathrm{tr}(\overline{C}_xC_x)\right]. \tag{5.79}$$

The ghost matrix, $M(U,\rho) = \Omega(U) + R(\rho)$, is real, with the gauge-field dependent Ω being symmetric and $R_{x\alpha,y\beta} = \delta_{xy}\rho_{x3}f_{3\alpha\beta}$ being antisymmetric in the coset indices. The matrix element $\Omega_{x\alpha,y\beta}$ is explicitly given by

$$\begin{aligned}
\Omega_{x\alpha,y\beta} = {} & 2\delta_{\alpha\beta}\delta_{xy}\mathrm{tr}\left(U^\dagger_{y-\mu,\mu}\tau_3U_{y-\mu,\mu}\tau_3 + U_{y\mu}\tau_3U^\dagger_{y\mu}\tau_3\right) \\
& - 2\epsilon_{\alpha\delta}\epsilon_{\beta\gamma}\delta_{x,y-\mu}\mathrm{tr}\left(U_{y\mu}\tau_\gamma U^\dagger_{y\mu}\tau_\delta\right) \\
& - 2\epsilon_{\alpha\gamma}\epsilon_{\beta\delta}\delta_{x,y+\mu}\mathrm{tr}\left(U_{y\mu}\tau_\gamma U^\dagger_{y\mu}\tau_\delta\right).
\end{aligned} \tag{5.80}$$

A parameterization of the $SU(2)$ group-valued gauge link U used later in our numerical simulation is

$$a_0\mathbb{1} + i\,a_j\sigma_j = \begin{pmatrix} a_0 + i\,a_3 & a_2 + i\,a_1 \\ -a_2 + i\,a_1 & a_0 - i\,a_3 \end{pmatrix} \quad \text{with} \quad a_0^2 + a_1^2 + a_2^2 + a_3^2 = 1, \tag{5.81}$$

where σ_j are the Pauli matrices and $\mathbb{1}$ is the 2×2 identity matrix. This requires 4 numbers to be stored in the computer for each gauge link $U_{x\mu}$.

5.5.1 Reduced model

The so-called reduced model is the theory on the orbit, i.e., an interacting theory of the longitudinal gauge degrees of freedom (*lgdof*s) and ghost fields. The reduced limit is taken by setting the gauge coupling $g = 0$. As a consequence of the invariance theorem, the reduced model is found to be topological field theory (TFT), as the partition function of the reduced model is just a number independent of the gauge-fixing coupling $\tilde{g}$.

As described in Chapters 1 and 3, the full theory action $\mathcal{S}[U]$ is given a gauge transformation to obtain $\mathcal{S}[\phi^\dagger U \phi]$ with *lgdof*s ϕ. The gauge fields U are then set to 1 to arrive at the reduced model action $\mathcal{S}^{\text{red}}$. The action of the reduced model of the eBRST gauge-fixed $SU(2)$ theory, with *lgdof*s as group-valued ϕ fields, is given as follows:

$$\mathcal{S}^{\text{red}} = \mathcal{S}^{\text{red}}_{gf}, \tag{5.82}$$

where

$$
\begin{aligned}
\mathcal{S}_{gf}^{\rm red} = 2\tilde{\kappa} \sum_x {\rm tr} \Big[&-2 \left(\phi_x \phi^\dagger_{x+\mu} \tau_3 \phi_{x+\mu} \phi^\dagger_x \tau_3 + \phi_x \phi^\dagger_{x-\mu} \tau_3 \phi_{x-\mu} \phi^\dagger_x \tau_3 \right) \times (\nu\texttt{-term}) \\
&+ \frac{1}{2} \left(\phi_x \phi^\dagger_{x+\mu} \tau_3 \phi_{x+\mu} \phi^\dagger_x + \phi_x \phi^\dagger_{x-\mu} \tau_3 \phi_{x-\mu} \phi^\dagger_x \right) \times (\nu\texttt{-term}) \Big] \\
+ \tilde{\kappa} \sum_x (\rho_{x3})^2 &+ \sum_{xy\alpha\beta} \overline{C}_{x\alpha} M^{\rm red}_{x\alpha,y\beta} C_{y\beta},
\end{aligned}
\tag{5.83}
$$

The ϕ-field version of the eBRST-invariant mass term of the full theory (see Eq. 5.79),

$$
\mathcal{S}_{mass}^{\rm red} = m^2 \sum_x \left[-4\, \tilde{\kappa}\, {\rm tr} \left(\phi_x \phi^\dagger_{x+\mu} \tau_3 \phi_{x+\mu} \phi^\dagger_x \tau_3 \right) + 2\, {\rm tr} \left(\overline{C}_x C_x \right) \right]. \tag{5.84}
$$

can also be added to the action in Eq. 5.82.

The real and symmetric reduced-model-ghost matrix $M^{\rm red}_{x\alpha,y\beta}$ acting on any coset vector, such as the ghost field C, produces

$$
C'_{x\alpha} = M^{\rm red}_{x\alpha,y\beta} C_{y\beta}. \tag{5.85}
$$

The new vector $C'_{x\alpha}$ can be written explicitly in several parts, as follows:

Diagonal part :

$$
C'_{x\alpha} = 2\, {\rm tr} \left(\phi_x \phi^\dagger_{x-\mu} \tau_3 \phi_{x-\mu} \phi^\dagger_x \tau_3 + \phi_x \phi^\dagger_{x+\mu} \tau_3 \phi_{x+\mu} \phi^\dagger_x \tau_3 \right) C_{x\alpha} + \rho_{x3}\, f_{3\alpha\beta}\, C_{x\beta}\ , \tag{5.86}
$$

Off-diagonal part :

$$
\begin{aligned}
C'_{x1} =& -2\,\mathrm{tr}\,\left(\phi_{x+\mu}\phi^\dagger_{x+2\mu}\tau_2\phi_{x+2\mu}\phi^\dagger_{x+\mu}\tau_2\right)C_{x+\mu,1}\\
&+2\,\mathrm{tr}\,\left(\phi_{x+\mu}\phi^\dagger_{x+2\mu}\tau_1\phi_{x+2\mu}\phi^\dagger_{x+\mu}\tau_2\right)C_{x+\mu,2}\\
&-2\,\mathrm{tr}\,\left(\phi_{x-\mu}\phi^\dagger_{x}\tau_2\phi_{x}\phi^\dagger_{x-\mu}\tau_2\right)C_{x-\mu,1}\\
&+2\,\mathrm{tr}\,\left(\phi_{x-\mu}\phi^\dagger_{x}\tau_2\phi_{x}\phi^\dagger_{x-\mu}\tau_1\right)C_{x-\mu,2}\ , \qquad (5.87)\\
C'_{x2} =& \quad 2\,\mathrm{tr}\,\left(\phi_{x+\mu}\phi^\dagger_{x+2\mu}\tau_2\phi_{x+2\mu}\phi^\dagger_{x+\mu}\tau_1\right)C_{x+\mu,1}\\
&-2\,\mathrm{tr}\,\left(\phi_{x+\mu}\phi^\dagger_{x+2\mu}\tau_1\phi_{x+2\mu}\phi^\dagger_{x+\mu}\tau_1\right)C_{x+\mu,2}\\
&+2\,\mathrm{tr}\,\left(\phi_{x-\mu}\phi^\dagger_{x}\tau_1\phi_{x}\phi^\dagger_{x-\mu}\tau_2\right)C_{x-\mu,1}\\
&-2\,\mathrm{tr}\,\left(\phi_{x-\mu}\phi^\dagger_{x}\tau_1\phi_{x}\phi^\dagger_{x-\mu}\tau_1\right)C_{x-\mu,2}\ . \qquad (5.88)
\end{aligned}
$$

The eBRST transformation rules are modified for the reduced model. In the absence of the gauge link U, the ϕ fields now have an eBRST transformation,

$$s\phi_x = -iC_x\phi_x\ , \tag{5.89}$$

under which the action is eBRST-invariant.

The reduced model is invariant under the remnant local $U(1)$ symmetry, corresponding to the unfixed part of the theory. The local $U(1)$ transformation in the reduced model acts on the ϕ field from the left, hence denoted here as $U(1)_L$:

$$\phi'_x = \mathsf{h}_x\phi_x, \qquad \mathsf{h}_x = \exp(\mathrm{i}\theta_x\tau_3) \in U(1)_L. \tag{5.90}$$

The action is also invariant under a global $SU(2)_R$ transformation, acting on the ϕ fields from the right, since all the terms have the ϕ fields present as $\phi\phi^\dagger$ combination:

$$\phi'_x = \phi_x \mathsf{g}, \qquad \mathsf{g} \in SU(2)_R. \tag{5.91}$$

5.5.2 Possible spontaneous symmetry breaking in the reduced model

Being a TFT, the partition function of the reduced model is independent of the gauge-fixing coupling. This raises the question that, whether the effective potential of the reduced model can develop new minima as a function of the coupling, or in other words, whether the reduced model can display a spontaneous symmetry breaking (SSB).

To understand why one should even consider the possibility of a SSB in a TFT like the reduced model, we have to note that it has been shown by analysis of perturbative 1-loop renormalization group (RG) equations in [19] that the coupling $\tilde{g}$ in the gauge fixing sector ($\tilde{g}^2 = \xi g^2 = 1/(2\tilde{\kappa})$, where ξ is the gauge fixing parameter) is also asymptotically free, just like the non-Abelian gauge coupling g. Hence, dimensional transmutation takes place and both these couplings can effectively become strong at infrared scales Λ and $\tilde{\Lambda}$ corresponding to g and $\tilde{g}$. According to the findings in [19], two possibilities exist: one where the Λ parameters are of the same order, the other where the $\tilde{\Lambda} \gg \Lambda$. Obviously, it is an interesting question to ask about the nature of the strong coupling theory on the orbit, i.e., the reduced model. Can strong dynamics of the *lgdof* lead to a SSB?

It was demonstrated in Ref. [20] through a toy model, that a phase transition can indeed occur in a TFT through a non-trivial effective potential. A seed is necessary to force the symmetry breaking. Similarly in the reduced model, the broken phase can be obtained in a finite volume with a symmetry breaking seed, which is then turned off in the thermodynamic limit and the system stays in the broken phase. The authors provided evidence of the existence of a broken phase in the reduced model through a combination of strong coupling and mean-field techniques: the global $SU(2)_R$ symmetry of the action spontaneously breaks in the manner, $SU(2)_R \rightarrow U(1)_R$. Although the existence of the SSB can only be verified through a controlled non-perturbative calculation, this and its effect on the full theory raises very interesting possibilities. The numerical simulations in this thesis are aimed at finding the truth about these possibilities.

The quantity $\tilde{A}_x$ [20] can be used to signal the symmetry breaking of the global $SU(2)_R \rightarrow U(1)_R$. The expectation value

$$\langle \tilde{A}_x \rangle = \langle \phi_x^\dagger \tau_3 \phi_x \rangle \tag{5.92}$$

transforms in the adjoint representation of $SU(2)_R$ and is invariant under the local $U(1)_L$ transformation. It is to be noted that, $\tilde{A}_x$ is not invariant under the modified eBRST transformation, but since it is not a total eBRST variation, it cannot signal a possible spontaneous breaking of eBRST symmetry.

The object $\tilde{A}_x$ is a 3-vector of norm 0.5 (see Eq. 5.97), defined at every lattice point x, with components $\frac{1}{2}\mathrm{tr}(\tilde{A}_x \tau_i), i = 1, 2, 3$. In an unbroken $SU(2)_R$ symmetric phase, the $\tilde{A}_x$ vectors, at the lattice sites, point at random directions in 3 dimensions. As a result, the average $\tilde{A}$ vector (averaged over all the lattice sites), for a single configuration, is a null vector. On the other hand, in the broken phase, the average $\tilde{A}$ is a vector, with non-zero components, pointing in a certain direction. If the system is frozen, i.e., devoid of any quantum fluctuations, each and every $\tilde{A}_x$ vector in a configuration points in the same direction. As we approach the phase transition from the broken to unbroken phase, some of the $\tilde{A}_x$ vectors start to deviate from the direction, in which rest of the vectors are pointing, and become random. Consequently, the length of the average $\tilde{A}$ vector starts to diminish from 0.5. Hence, we can characterize the two different phases by studying the length of the average $\tilde{A}$ vector averaged over many ensembles, given for a lattice volume V by

$$\langle|\tilde{A}|\rangle = \left\langle \sqrt{\sum_{i=1}^{3}\left(\frac{1}{V}\sum_{x}\pi_{xi}\right)^2} \right\rangle, \quad \text{where} \;\; \pi_{xi} = \frac{1}{2}\mathrm{tr}\left(\tilde{A}_x\,\tau_i\right). \tag{5.93}$$

The values of $\langle|\tilde{A}|\rangle$ would be

$$\begin{aligned} \langle|\tilde{A}|\rangle = 0 \quad & \text{in the unbroken phase,} \\ \leq 0.5 \text{ (explained below)} \quad & \text{in the broken phase.} \end{aligned} \tag{5.94}$$

As is usually done in a numerical study, a symmetry breaking seed

$$\mathcal{S}_{seed} = -h\,\mathrm{tr}\left(\tau_3\tilde{A}_x\right), \tag{5.95}$$

is introduced in the reduced model action (Eq. 5.82). The term explicitly breaks the $SU(2)_R$ symmetry and forces the $\tilde{A}_x$ vectors to point along the τ_3 direction. It is invariant under the local $U(1)$ symmetry and breaks the eBRST symmetry. At a fixed lattice volume, the order parameter is now studied with the seed being tuned to zero. The process is then ideally repeated at different volumes, to conclusively identify a given phase. If a seed is used, it is sufficient to compute the expectation value of π_3, the τ_3 component of the average $\tilde{A}$ for each configuration.

The ϕ_x fields can also be parameterized the same way as in Eq. 5.81. In this parameterization, the components π_i of $\tilde{A}_x$ are

$$\begin{aligned} \pi_1 &= a_0 a_2 + a_1 a_3 \, , \\ \pi_2 &= a_2 a_3 - a_0 a_1 \, , \\ \pi_3 &= \frac{1}{2}(a_0^2 - a_1^2 - a_2^2 + a_3^2) \, . \end{aligned} \tag{5.96}$$

From above, we can see that at each site

$$|\tilde{A}| = \sqrt{\pi_1^2 + \pi_2^2 + \pi_3^2} = \frac{1}{2}(a_0^2 + a_1^2 + a_2^2 + a_3^2) = 0.5 \, , \tag{5.97}$$

since $\sum_i a_i^2 = 1$.

5.5.3 Effect on the Full theory

With the gauge coupling turned on for the full theory, the $SU(2)_R$ symmetry becomes local from global, as it was in the reduced model and therefore, there is no local order parameter. Point to note here is that, the $SU(2)_R$ symmetry of the full theory becomes explicit only in the Higgs picture, using the language of Chapter 3, i.e., after giving a gauge transformation to the action and the gauge non-invariant terms thereby picking up the *lgdof*s. It is interesting to ask now is whether the SSB in the reduced model has any effect on the phase diagram of the full theory. This basically amounts to asking whether the strong dynamics of the *lgdof* affects physics in any way. From the invariance theorem, which is a rigorous result on a finite lattice, one can argue that such a scenario is not possible, since the physical observables of the eBRST gauge-fixed theory are exactly the same as in the unfixed theory in any finite volume.

However, this may not be the complete answer. By introducing an explicit eBRST symmetry breaking term, the invariance theorem ceases to hold in the eBRST theory. If we now take the thermodynamic limit and then turn off the symmetry breaking term, there can be two possible outcomes. Either the invariance theorem again becomes applicable and the system gives the physics of the usual confining phase or, the system enters a new phase different from the previous one. The question of whether the invariance theorem still holds or not, is a dynamical one and can only be addressed through a non-perturbative calculation. In Ref. [20], through a combination of strong coupling and mean field techniques, evidence was shown for the existence of a novel phase in the full theory. In this novel phase denoted as the Higgs phase, the two Nambu-Goldstone bosons, associated with spontaneous symmetry breaking of the global $SU(2)_R \to U(1)_R$, are eaten up through a Higgs mechanism to generate two massive W bosons (gauge bosons in the coset space) and a massless photon as evidence of the local $U(1)$-invariance. As seen in Eq. 5.79, the mass of the W bosons is allowed by the eBRST symmetry, provided an appropriate mass for the ghost fields is also generated. The existence of the eBRST symmetry is desirable, because it is necessary for the theory to be unitary.

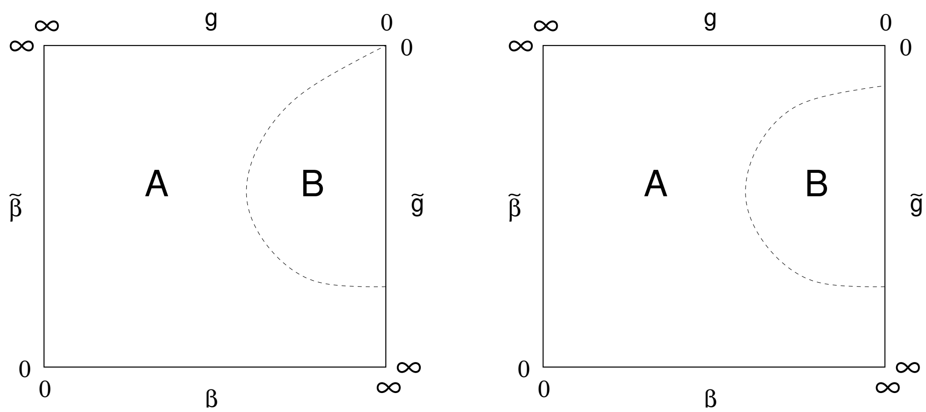

Figure 5.1: Possible scenarios of phase diagrams [20] of the eBRST gauge-fixed $SU(2)$ theory. The horizontal axes denote the bare gauge coupling and the vertical axes stand for the bare gauge-fixing coupling of the theory.

In Ref. [20], from where Fig. 5.1 has been taken, the authors employed a combination of strong coupling and mean field methods and speculated the existence of the two scenarios for the phase diagram of the eBRST gauge-fixed theory. In Fig. 5.1, the phase A denotes the usual confining phase of the $SU(2)$ theory, and the phase B indicates the novel Higgs phase. As already introduced, the coupling β is related to the gauge coupling g as $\beta = 4/g^2$, whereas $\tilde{\beta}$ is associated to the gauge-fixing coupling $\tilde{g}$ through the relation $\tilde{\beta} = 1/\tilde{g}^2$. The phase diagram on the left panel shows that the Higgs phase extends to the critical point, $g = \tilde{g} = 0$, where a continuum limit can be taken from within the Higgs phase. On the other hand, the figure on the right panel shows that the B phase does not extend to the critical point and ends at some non-zero $\tilde{g}$ for vanishing g, meaning that the new phase in the right panel is just a lattice artefact. It has been argued that both these scenarios are possible and the correct one can only be found out through non-perturbative numerical investigation. It is instructive to note that the reduced model lies along the right vertical axis in both the panels in the above figure.

5.6 Details of the numerical implementation

In this section, we discuss the numerical implementation of the full theory and the reduced model. As we will see, there exist serious challenges with regard to simulating the eBRST theory on the computer, making it a very hard problem. We have used Hybrid Monte Carlo (HMC) to study both the full theory and the reduced model, including the ghosts dynamically. For the full theory, the stochastic Tunneling HMC (sTHMC) algorithm has also been employed, which is a first-time implementation of the algorithm. For the ghost matrix inversions, we have employed the BiCGStab algorithm. We have used Message Passing Interface (MPI), to parallelize our algorithms for computational efficiency. Using

MPI, the lattice is distributed among several computational nodes of the computer and the local computations in each node are done in parallel. For calculations that require information of the lattice from neighboring nodes, the instructions for message passing between different nodes need to be explicitly encoded in the numerical program, which is a rather non-trivial task. The basic MPI framework of the coding has been partly based on Ref. [23].

5.6.1 HMC

The ghost fields are Grassmann-valued and are not directly implemented in the computer. As discussed in Sec. 2.2, they can be replaced by real-valued fields in the pseudofermion method. The integration of the ghost fields in the partition function can be done as follows,

$$\int \mathcal{D}C\mathcal{D}\overline{C}\,\exp(-\overline{C}MC) = \mathrm{det}M = |\mathrm{det}M|\,\mathrm{sign}(\mathrm{det}M). \tag{5.98}$$

Since elements of M are real, $|\mathrm{det}M|$ can be simulated using HMC by introducing a real-valued scalar ("pseudo-ghost") field φ,

$$|\mathrm{det}M| = \sqrt{\mathrm{det}(MM^T)} = \int \mathcal{D}\varphi\,\exp\left(-(1/2)\varphi^T(MM^T)^{-1}\varphi\right). \tag{5.99}$$

Note that the notation φ has also been used for pseudofermions in Sec. 2.2 and, is different from the reduced model ϕ field.

The partition function of the full theory now becomes

$$Z_{\text{full}} = \int \mathcal{D}U\mathcal{D}\varphi\mathcal{D}\rho \exp\Bigg(- [\mathcal{S}_W + \tilde{\kappa}\sum_{x\alpha}(\mathcal{D}^-_\mu \mathcal{W}_{x\mu})^2_\alpha + \tilde{\kappa}\sum_x(\rho_{x3})^2 + \frac{1}{2}\sum_{xy\alpha\beta}\varphi_{x\alpha}(MM^T)^{-1}_{x\alpha,y\beta}\,\varphi_{y\beta}]\Bigg)\,\text{sign}(\det M). \qquad (5.100)$$

From the above, we see that the sign of the determinant of M can be kept out of the Molecular Dynamics (MD) evolution but, the sign has to be tracked for calculating any expectation value. It can be noted that we only need to track the sign-changes, since the overall sign gets canceled among the numerator and denominator of the expectation value. However, tracking the sign of the determinant is not an easy task. Calculating the determinant explicitly is not a solution since the computational cost is outrageously high. Since we have no prior knowledge about the eigenvalue distribution of the ghost matrix, the question of effectively applying different sign-tracking numerical methods, is still an open one. Moreover, close to a sign change of the ghost determinant, the ghost matrix will have near-zero eigenvalues creating problems in the HMC updation process. We have tried the sTHMC algorithm in the hope that it can address these issues, to be discussed in the next section.

In our HMC code, we use a slightly modified partition function Z', the same as (5.100) except $\text{sign}(\det M)$,

$$Z' \equiv \int \mathcal{D}U\mathcal{D}\varphi\mathcal{D}\rho \exp\left(-[\mathcal{S}_W + \mathcal{S}'_{gf} + \frac{1}{2}\varphi^T(M^TM)^{-1}\varphi]\right) \qquad (5.101)$$

where $\mathcal{S}'_{gf} = \tilde{\kappa}\sum\limits_{x\alpha}(\mathcal{D}^-_\mu\mathcal{W}_{x\mu})^2_\alpha + \tilde{\kappa}\sum\limits_x(\rho_{x3})^2$. If the ghost determinant does not change sign in a simulation, we will be able to obtain exact results with the above partition function Z'. We have used the HMC algorithm ignoring the sign of the ghost determinant, to calculate expectation value of a gauge-invariant operator, the plaquette, in a reasonably wide region of the parameter space of the full theory, and checked if the invariance theorem is satisfied. If the determinant changes sign, the plaquette value thus computed would be different from that in the unfixed theory. The above procedure gives us a handle to identify regions of parameter space where sign changes of the determinant are more likely.

The gauge and the auxiliary fields need to be updated in the HMC algorithm with their corresponding conjugate momenta. The Hamiltonian used in the HMC algorithm, for the full theory, is thus

$$
\begin{aligned}
H &= \mathcal{S}[U,\rho] + \frac{1}{2}\sum_{x\mu} \mathrm{tr}(\pi_{x\mu})^2 + \frac{1}{2}\sum_{x} (\widetilde{\pi}_{x3})^2 \\
&= \mathcal{S}[U,\rho] + \sum_{x\mu a} (\pi^a_{x\mu})^2 + \frac{1}{2}\sum_{x} (\widetilde{\pi}_{x3})^2
\end{aligned}
\tag{5.102}
$$

where $\mathcal{S}[U,\rho] = \mathcal{S}_W + \mathcal{S}'_{gf} + \frac{1}{2}\phi^T(M^TM)^{-1}\phi$. The momentum, conjugate to the link variable $U_{x\mu}$, is a 2×2 matrix denoted by $\pi_{x\mu} = \pi^a_{x\mu}\sigma_a$, which is algebra-valued and has components for all the generators of $SU(2)$ group. But the auxiliary field ρ_x has a conjugate momentum with only one component with respect to τ_3, given as $\widetilde{\pi}_x = \widetilde{\pi}_{x3}\tau_3$. Henceforth, by $\widetilde{\pi}_x$ we will mean $\widetilde{\pi}_{x3}$, and ρ_x will mean ρ_{x3} unless explicitly mentioned.

The implementation of HMC is done similarly for the reduced model where the ϕ fields are updated along with the corresponding momenta in a MD trajectory, instead of the gauge link U. The ghost fields are updated exactly as described for the full theory. We generally used quite small time-steps in the MD trajectory, as this was necessary to obtain reasonable acceptance rates. However, this helped us identify regions of the parameter space in the reduced model (and also in the full theory) where one or more eigenvalues of the ghost matrix are approaching zero, since this approach will be signalled by a divergence in the number of iterations for the matrix inversion during a MD trajectory.

5.6.2 Stochastic Tunneling HMC

To track the sign of the determinant of the ghost matrix, we have done a first-time implementation of the stochastic tunneling HMC algorithm (sTHMC) proposed by Golterman and Shamir in [22]. The basic aspects of the algorithm have been discussed earlier in Chapter 2 Sec. 2.3.

In the partition function Z, the integration of ghost fields is done as in Eq. 5.98, to obtain

$$\begin{aligned} Z &= \int \mathcal{D}U\mathcal{D}\rho \exp\left(-[\mathcal{S}_W + \mathcal{S}'_{gf}]\right) \det M \\ &= \int \mathcal{D}U\mathcal{D}\rho \exp\left(-\mathcal{S}\right) \det M. \end{aligned} \tag{5.103}$$

Following the THMC prescription, the determinant of the ghost matrix M can be decomposed as

$$\det M = \alpha^{-k} \det D \det A. \tag{5.104}$$

The matrix D is also a $n \times n$ matrix like M, while A is a $k \times k$ matrix ($k < n$), given as

$$D = M + \alpha P Q^T, \quad A = \alpha - \alpha^2 Q^T D^{-1} P, \tag{5.105}$$

where P and Q are $n \times k$ "blocking" matrices, and α is a constant. For our case of $SU(2)$ theory, n is equal to $2V$, where V is the lattice volume. Rewriting the partition function Z, by using the split form of the determinant in Eq. 5.104 and a Boltzmann weight for the blocking matrices, we get

$$\begin{aligned}Z &= \alpha^{-k} \int \mathcal{D}\Theta \; \exp\Big(- \mathcal{S}[U,\rho] - \mathcal{S}_{\text{ker}}[P,Q]\Big) \times (\det D) \times (\det A) \\ &= \alpha^{-k} \int \mathcal{D}\Theta \, \mathcal{D}\varphi \; \exp\left(-[\mathcal{S} + \frac{1}{2}\varphi^T (D^T D)^{-1} \varphi + \mathcal{S}_{\text{ker}}]\right) \, |\det A| \, \text{sign}(\det A \times \det D) \\ &= \alpha^{-k} \int \mathcal{D}\Theta \, \mathcal{D}\varphi \; \exp\left(-[\mathcal{S} + \frac{1}{2}\varphi^T (D^T D)^{-1} \varphi - \log|\det A| + \mathcal{S}_{\text{ker}}]\right) \\ &\qquad \times \text{sign}(\det A \times \det D), \end{aligned} \tag{5.106}$$

where $\mathcal{D}\Theta = \mathcal{D}U \mathcal{D}\rho \mathcal{D}P \, \mathcal{D}Q$ and $\mathcal{S}_{\text{ker}}$ is explained below.

We aim to decompose the determinant of M in such a way, that the near-zero eigenvalues of the ghost determinant, which are responsible for sign changes, are captured by A. The deterministic version of THMC [22] is based on the construction of the blocking vectors, through explicit determination of the lowest eigenvectors. In that process, the ghost matrix would be deflated exactly, thereby, lifting the lowest eigenmodes. The zero-crossings of the near-zero eigenvalues are tracked explicitly to account for the sign changes. However, the above process requires calculation of the eigenmodes at every MD step, requiring a heavy computational overhead.

To overcome the above difficulty, a stochastic version of THMC was proposed in Ref. [22]. Here, the near-zero eigenmodes need to be computed only twice, once before and once after, in a MD trajectory. The blocking matrices are obtained as a combination of stochastically generated vectors and the initial computed eigenvectors. However, the probability distribution of the constituent blocking vectors depends on a parameter γ, which is of the order of the lattice volume. For the stochastic process to have a reasonable acceptance, γ should be $O(1)$. Having $\gamma \propto V$, therefore, means vanishing acceptance.

A way out[1] is by simply taking the normalized blocking vectors from a purely Gaussian distribution. We have used this modified version, denoted by sTHMC, in our work.

The sTHMC algorithm, that we use, implements blocking vectors, independent of the eigenvalue spectrum of the ghost matrix. Tuning the parameters α and k, we may obtain non-zero overlap of the Gaussian blocking vectors with the near-zero eigenmodes of the ghost matrix, thereby deflating the matrix. If all the near-zero eigenvalues are thus captured by the matrix A, we can explicitly calculate the sign of the determinant of A to determine the overall sign of the ghost determinant. However, in practical situations, only a fraction of the eigenvalues would be present in A and the remaining in D. If there are remnant near-zero modes in D, the zero-crossings would generally be avoided by the MD evolution, due to the reasons discussed in Sec. 2.3 and would lead to loss of ergodicity. However, we have the invariance theorem as a check and we can estimate the degree of deviation. Since we have no idea about the eigenvalue distribution of the ghost matrix, the above procedure may shed light on the nature of the eigenvalues near zero. Similar to HMC, we simulate using another partition function,

$$Z'' = \alpha^{-k} \int \mathcal{D}\Theta\, \mathcal{D}\varphi\, \exp\left(-[\mathcal{S} + \frac{1}{2}\varphi^T (D^T D)^{-1} \varphi - \log|\det A| + \mathcal{S}_{\text{ker}}] \right) \tag{5.107}$$

which is Z sans the sign of determinant of A times D. By tracking the sign of determinant of matrix A, the observable with respect to Z can be calculated by a reweighting procedure described later.

In sTHMC, the $n \times k$ blocking matrices P and Q are composed of k number of unit norm n-vectors $p(x)$ and $q(x)$ respectively. To generate normalized Gaussian random n-vector $p(x)$, one needs to pick each element from the distribution $\exp(-np(x)^2/2)$, which

[1] Pointed out by the authors of Ref. [22] through private communication.

has a standard deviation $\sigma = 1/\sqrt{n}$. The blocking kernel action,

$$\mathcal{S}_{\text{ker}} = \frac{n}{2} \sum_{x} \left(p(x)^2 + q(x)^2 \right) , \tag{5.108}$$

in the partition function Z'' (and also Z) remains unchanged throughout, in a given MD trajectory since it does not depend on the gauge fields. Hence, it does not affect the acceptance rate and one ignores the blocking kernel action for the final accept/reject step.

The accept/reject step is finally done with the Hamiltonian, given as

$$H = H_{MD} - \log |\text{det} A|, \tag{5.109}$$

where the Hamiltonian for the MD evolution, H_{MD}, is given by

$$H_{MD} = \mathcal{S} + \frac{1}{2} \varphi^T (D^T D)^{-1} \varphi + \frac{1}{2} \sum_{x\mu} \text{tr}(\pi_{x\mu})^2 + \frac{1}{2} \sum_{x} (\widetilde{\pi}_{x3})^2. \tag{5.110}$$

The fields π and $\widetilde{\pi}$ are the corresponding conjugate momenta of the gauge and auxiliary field ρ respectively. One, therefore, needs to exactly calculate the determinant of the $k \times k$ matrix, A, twice, once at the start of the MD steps and once at the end. Before calculating the determinant of A, one also needs to perform k number of matrix inversions of D with respect to k number of $p(x)$ vectors, as can be seen from equation 5.105. Hence, taking k too large would mean longer computational time and also, poorer acceptance rate as the matrix D changes too much from M.

The steps of the sTHMC algorithm for each MD trajectory is as follows (cf. Sec. 2.2):

1. At the beginning of each MD step, the n-vectors, k in number for each blocking matrices P and Q, are generated from a Gaussian distribution, along with the conjugate

field momenta.

2. The initial Hamiltonian H_i is then computed with the D matrix in the ghost term, instead of matrix M. The determinant of the initial $k \times k$ matrix, A, is calculated. The blocking matrices remain constant throughout the MD steps and hence, the blocking kernel action does not require to be computed.

3. The MD steps are now performed with leapfrog update of the fields and conjugate momenta respectively. All the force calculations are done with D matrix instead of M.

4. At the end of the MD steps, the final Hamiltonian H_f with the determinant of the final A matrix is now computed. The accept/reject step is now performed with the following probability,

$$\exp(-\Delta H) = \exp(H_{i,MD} - H_{f,MD}) \frac{\det A_i}{\det A_f}\,, \tag{5.111}$$

with $\Delta H = H_f - H_i$ being the change in the Hamiltonian.

The expectation value of an operator $\mathcal{O}$ with respect to the partition function Z can now be obtained as

$$\begin{aligned} \langle \mathcal{O} \rangle_Z &= \frac{\langle\, \text{sign}(\det A \times \det D)\, \mathcal{O} \rangle_{Z''}}{\langle\, \text{sign}(\det A \times \det D) \rangle_{Z''}} \\ &\simeq \frac{\langle\, \text{sign}(\det A)\, \mathcal{O} \rangle_{Z''}}{\langle\, \text{sign}(\det A) \rangle_{Z''}}, \end{aligned} \tag{5.112}$$

where in the second step, we have used the assumption that the sign of $\det D$, whether positive or negative, does not change over the MD trajectories and therefore, cancels.

The sign of the determinant of A for each MD step, to be used in Eq. 5.112, can be extracted as follows. The following steps are implemented only after the simulation has equilibrated and the measurements of the observable is to be started :

1. At the start of the first MD trajectory, the matrix $A_{i,1}$ is constructed from the blocking vectors P_1 and Q_1 on the initial gauge configuration $\{U_{i,1}\}$ and its determinant is calculated explicitly.

2. At the end of the trajectory, on the final gauge configuration $\{U_{f,1}\}$, the matrix $A_{f,1}$ is again constructed from the same constant blocking vectors P_1 and Q_1. The determinant of $A_{f,1}$ is computed which is required for the accept/reject step (Eq. 5.111).

3. For the first measurement, the sign of the determinant A_1 to be used for measurement is

$$\mathrm{sign}(\det A_1) \equiv \mathrm{sign}(\det A_{i,1}) \times \mathrm{sign}(\det A_{f,1}). \tag{5.113}$$

4. For the nth measurement, if the configuration $U_{f,n}$ at the end of the nth MD trajectory is accepted, the sign of the determinant A_n is taken to be

$$\mathrm{sign}(\det A_n) \equiv \mathrm{sign}(\det A_{n-1}) \times \mathrm{sign}(\det A_{i,n}) \times \mathrm{sign}(\det A_{f,n}). \tag{5.114}$$

   If rejected, the sign of the last accepted MD step is taken.

5. After N measurements, we obtain the expectation value of gauge-invariant $\mathcal{O}$ in Eq.

5.112 from the following,

$$\langle\, \mathrm{sign}(\det A)\, \mathcal{O} \rangle_{Z''} = \frac{1}{N} \sum_{l=1}^{N} \mathrm{sign}(\det A_l)\, \mathcal{O}_l \ , \tag{5.115}$$

$$\langle\, \mathrm{sign}(\det A) \rangle_{Z''} = \frac{1}{N} \sum_{l=1}^{N} \mathrm{sign}(\det A_l) \ . \tag{5.116}$$

From the above, we see that the overall sign of the determinant is not taken into consideration and only the change in sign is tracked. The overall sign can be taken out of the numerator and denominator of the expectation value in Eq. 5.112 and thus can be cancelled.

5.6.3 Force terms in full theory

The force terms of the full theory, used in the MD trajectory (cf. Sec. 2.2), are explicitly given in the following subsections. The HMC and sTHMC force terms are exactly the same, except that the ghost matrix M in case of HMC is replaced by the deflated ghost matrix D for sTHMC.

Gauge field force

The gauge force term $F[U, \varphi]$, obtained by differentiating the MD Hamiltonian by the gauge fields, is given as the sum of the following terms,

$$F_{z\nu}[U, \varphi] = \left(F_W[U] + F_{gf}[U, \varphi] + F_{\mathrm{mass}}[U]\right)_{z\nu} \ , \tag{5.117}$$

where F_W corresponds to the Wilson action and F_{gf} to the gauge-fixing term in the action. The force term corresponding to mass term in the action (Eq. 5.79) is also shown here. The expression for F_W is given as follows

$$(F_W)_{z\nu} = \frac{\beta}{4}\left((U_{z\nu}A_{z\nu} - A^\dagger_{z\nu}U^\dagger_{z\nu}\right) - \frac{\beta}{8}\mathrm{tr}\left((U_{z\nu}A_{z\nu} - A^\dagger_{z\nu}U^\dagger_{z\nu}\right), \tag{5.118}$$

where A is the sum of adjacent staples.

The F_{gf} term in (5.117) contains two contributions - one from the gauge-fixing term and another from the ghost term. The contribution from the gauge-fixing term is given as

$$(F_{gf})_{x\mu} = 2\tilde{\kappa}\left(\left[U_{x\mu}\tau_3 U^\dagger_{x\mu}, (4\tau_3 A_x - B_x)\right] + \left[U_{x\mu}(4\tau_3 C_{x\mu} - D_{x\mu})U^\dagger_{x\mu}, \tau_3\right]\right), \tag{5.119}$$

where

$$\begin{aligned}
B_x &= \sum_\nu \left(U_{x\nu}\tau_3 U^\dagger_{x\nu} + U^\dagger_{x-\nu,\nu}\tau_3 U_{x-\nu,\nu}\right), \\
D_{x\mu} &= \sum_\nu \left(U_{x+\mu,\nu}\tau_3 U^\dagger_{x+\mu,\nu} + U^\dagger_{x,\nu}\tau_3 U_{x,\nu}\right), \\
A_x &= B_x\tau_3 \quad \text{and} \quad C_{x\mu} = D_{x\mu}\tau_3.
\end{aligned} \tag{5.120}$$

The contribution to the gauge force from the ghost term is given as

$$(F_{gf})_{x\mu} = 2F^{33}_{x\mu} - \left(F^{11} + F^{12} + F^{21} + F^{22}\right)_{x\mu}, \tag{5.121}$$

where

$$F^{33}_{x\mu} = \left[U_{x\mu}\tau_3 U^\dagger_{x\mu}, \tau_3\right] \sum_\alpha \left\{(M^T X)_{x\alpha} X^T_{x\alpha} + (M^T X)_{x+\mu,\alpha} X^T_{x+\mu,\alpha}\right\}, \tag{5.122}$$

$$F^{11}_{x\mu} = \left[U_{x\mu}\tau_1 U^\dagger_{x\mu}, \tau_1\right] \Big\{(M^T X)_{x2} X^T_{x-\mu,2} + (M^T X)_{x2} X^T_{x+\mu,2}$$
$$+X_{x2}(M^T X)^T_{x-\mu,2} + X_{x2}(M^T X)^T_{x+\mu,2}\Big\}, \qquad (5.123)$$
$$F^{22}_{x\mu} = \left[U_{x\mu}\tau_2 U^\dagger_{x\mu}, \tau_2\right] \Big\{(M^T X)_{x1} X^T_{x-\mu,1} + (M^T X)_{x1} X^T_{x+\mu,1}$$
$$+X_{x1}(M^T X)^T_{x-\mu,1} + X_{x1}(M^T X)^T_{x+\mu,1}\Big\}, \qquad (5.124)$$
$$F^{12}_{x\mu} = -\left[U_{x\mu}\tau_1 U^\dagger_{x\mu}, \tau_2\right] \Big\{(M^T X)_{x2} X^T_{x-\mu,1} + (M^T X)_{x1} X^T_{x+\mu,2}$$
$$+X_{x2}(M^T X)^T_{x-\mu,1} + X_{x1}(M^T X)^T_{x+\mu,2}\Big\}, \qquad (5.125)$$
$$F^{21}_{x\mu} = -\left[U_{x\mu}\tau_2 U^\dagger_{x\mu}, \tau_1\right] \Big\{(M^T X)_{x1} X^T_{x-\mu,2} + (M^T X)_{x2} X^T_{x+\mu,1}$$
$$+X_{x1}(M^T X)^T_{x-\mu,2} + X_{x2}(M^T X)^T_{x+\mu,1}\Big\}. \qquad (5.126)$$

In the above, $X = (MM^T)^{-1}\varphi$. The calculation of the vector X requires BiCGStab inversion of the matrix product $(MM^T)^{-1}$ at every MD step.

The force for the mass term in Eq. 5.79 is given as

$$(F_{\text{mass}})_{x\mu} = 4\tilde{\kappa} m^2 \left[U_{x\mu}\tau_3 U^\dagger_{x\mu}, \tau_3\right]. \qquad (5.127)$$

Auxiliary field force

The auxiliary field force term is obtained only from the gauge-fixing term as

$$\begin{aligned}
\widetilde{F}_z[\rho,\varphi] &= \frac{\partial}{\partial\rho_z}\left(\mathcal{S}_{gf}\right) \\
&= \frac{\partial}{\partial\rho_z}\left(\tilde{\kappa}\sum_x (\rho_x)^2 + \frac{1}{2}\sum_{xy\alpha\beta}\varphi_{x\alpha}(MM^T)^{-1}_{x\alpha,y\beta}\,\varphi_{y\beta}\right) \\
&= 2\tilde{\kappa}\rho_z - \frac{1}{2}\sum_{xy}\left((MM^T)^{-1}\varphi\right)^T_x \left(\frac{\partial R}{\partial\rho_z}M^T + M\frac{\partial R^T}{\partial\rho_z}\right)_{xy}\left((MM^T)^{-1}\varphi\right)_y .
\end{aligned} \qquad (5.128)$$

The derivative $\partial R/\partial\rho$ is given as

$$\begin{aligned}\frac{\partial R_{x\alpha;y\beta}}{\partial\rho_z} &= \frac{\partial}{\partial\rho_z}(\delta_{xy}\epsilon_{\alpha\beta}\rho_x) \\ &= \delta_{xy}\epsilon_{\alpha\beta}\delta_{xz}\ .\end{aligned} \tag{5.129}$$

Using (5.129) and the definition of X from above, we get

$$\widetilde{F}_z = 2\tilde{\kappa}\rho_z - \left\{X_{z1}(M^T X)_{z2} - X_{z2}(M^T X)_{z1}\right\}\ . \tag{5.130}$$

5.6.4 Force terms in Reduced model

In the MD trajectory, the reduced model updation Hamiltonian is

$$\mathcal{H} = \mathcal{S}_{red}[\phi,\rho] + \frac{1}{2}\sum_x \mathrm{tr}(\pi_x^2) + \frac{1}{2}\sum_x (\widetilde{\pi}_x)^2, \tag{5.131}$$

where $\pi_x = \pi_x^a\sigma^a$ is the conjugate momentum to the ϕ field and $\widetilde{\pi}$ is that to the ρ field. The discretized equations of motion in MD time for the fields and conjugate momenta are

$$\begin{aligned}\phi_x(t+\varepsilon) &= \phi_x(t) + i\varepsilon\phi_x(t), \quad i\pi_x(t+\varepsilon) = i\pi_x(t) - \varepsilon F_x(t)\ , \\ \rho_x(t+\varepsilon) &= \rho_x(t) + \varepsilon\widetilde{\pi}_x(t), \quad \widetilde{\pi}_x(t+\varepsilon) = \widetilde{\pi}_x(t) - \varepsilon\widetilde{F}_x(t)\ ,\end{aligned} \tag{5.132}$$

where t denotes the MD time index and ε is a small discrete time step.

ϕ field force

The force term F_x required for the updation of π_x fields in Eq. 5.132 can be written as two major terms corresponding to the reduced model action in Eq. 5.82,

$$F_x = (F_{gf})_x + (F_{\text{mass}})_x . \tag{5.133}$$

The F_{gf} term consists of

$$F_{gf} = F^{I}_{gf} + F^{gh}_{gf} , \tag{5.134}$$

where F^{I}_{gf} corresponds to the first term, and F^{gh}_{gf} to the third term i.e. ghost term, in the reduced model action in Eq. 5.83. Explicitly, we have

$$F^{I}_{gf} = F^{Ia}_{gf} + F^{Ib}_{gf} + F^{Ic}_{gf} , \tag{5.135}$$

with

$$\begin{aligned}
(F^{Ia}_{gf})_x &= 8\tilde{\kappa}\,[B_x, \tau_3 B_x \tau_3] \ , \\
(F^{Ib}_{gf})_{x-\mu} &= 2\tilde{\kappa} \sum_{\mu} \left[\phi_{x-\mu}\phi^{\dagger}_{x}(4\tau_3 B_x \tau_3 - B_x)\phi_x \phi^{\dagger}_{x-\mu}, \tau_3\right] \ , \\
(F^{Ic}_{gf})_{x+\mu} &= 2\tilde{\kappa} \sum_{\mu} \left[\phi_{x+\mu}\phi^{\dagger}_{x}(4\tau_3 B_x \tau_3 - B_x)\phi_x \phi^{\dagger}_{x+\mu}, \tau_3\right] \ ,
\end{aligned} \tag{5.136}$$

where

$$B_x = \sum_{\mu} \left(\phi_x \phi^{\dagger}_{x+\mu}\tau_3 \phi_{x+\mu}\phi^{\dagger}_{x} + \phi_x \phi^{\dagger}_{x-\mu}\tau_3 \phi_{x-\mu}\phi^{\dagger}_{x}\right) , \tag{5.137}$$

and for the ghost force term, we have (dropping the subscript gf and superscript gh on the right hand side for convenience)

$$
\begin{aligned}
F_{gf}^{gh} = &\left(F^{Ia} + F^{Ib} + F^{Ic}\right) \\
&+ \frac{1}{2}\left(F^{IIa} + \overline{F}^{IIa} + F^{IIb} + \overline{F}^{IIb}\right) \\
&+ \frac{1}{2}\left(F^{IIIa} + \overline{F}^{IIIa} + F^{IIIb} + \overline{F}^{IIIb}\right) ,
\end{aligned} \tag{5.138}
$$

where

$$
\begin{aligned}
F_x^{Ia} &= 2\sum_{\alpha} \left[B_x, \tau_3\right] X_{x\alpha}^T (M^T X)_{x\alpha} , \\
F_x^{IIa} &= -2 \sum_{\mu,\alpha\beta\gamma\delta} \epsilon_{\alpha\delta}\epsilon_{\beta\gamma} \left[\phi_x \phi_{x+\mu}^\dagger \tau_\gamma \phi_{x+\mu} \phi_x^\dagger, \tau_\delta\right] X_{x-\mu,\alpha}^T (M^T X)_{x\beta} , \\
\overline{F}_x^{IIa} &= -2 \sum_{\mu,\alpha\beta\gamma\delta} \epsilon_{\alpha\delta}\epsilon_{\beta\gamma} \left[\phi_x \phi_{x-\mu}^\dagger \tau_\gamma \phi_{x-\mu} \phi_x^\dagger, \tau_\delta\right] (M^T X)_{x\alpha}^T X_{x-\mu,\beta} , \\
F_x^{IIIa} &= -2 \sum_{\mu,\alpha\beta\gamma\delta} \epsilon_{\alpha\delta}\epsilon_{\beta\gamma} \left[\phi_x \phi_{x-\mu}^\dagger \tau_\gamma \phi_{x-\mu} \phi_x^\dagger, \tau_\delta\right] X_{x\alpha}^T (M^T X)_{x-\mu,\beta} , \\
\overline{F}_x^{IIIa} &= -2 \sum_{\mu,\alpha\beta\gamma\delta} \epsilon_{\alpha\delta}\epsilon_{\beta\gamma} \left[\phi_x \phi_{x+\mu}^\dagger \tau_\gamma \phi_{x+\mu} \phi_x^\dagger, \tau_\delta\right] (M^T X)_{x-\mu,\alpha}^T X_{x\beta} ,
\end{aligned} \tag{5.139}
$$

$$
\begin{aligned}
F_{x-\mu}^{Ib} &= 2\sum_{\alpha} \left[\phi_{x-\mu} \phi_x^\dagger \tau_3 \phi_x \phi_{x-\mu}^\dagger, \tau_3\right] X_{x\alpha}^T (M^T X)_{x\alpha} , \\
\overline{F}_{x-\mu}^{IIb} &= -2 \sum_{\alpha\beta\gamma\delta} \epsilon_{\alpha\delta}\epsilon_{\beta\gamma} \left[\phi_{x-\mu} \phi_x^\dagger \tau_\delta \phi_x \phi_{x-\mu}^\dagger, \tau_\gamma\right] (M^T X)_{x\alpha}^T X_{x-\mu,\beta} , \\
F_{x-\mu}^{IIIb} &= -2 \sum_{\alpha\beta\gamma\delta} \epsilon_{\alpha\delta}\epsilon_{\beta\gamma} \left[\phi_{x-\mu} \phi_x^\dagger \tau_\delta \phi_x \phi_{x-\mu}^\dagger, \tau_\gamma\right] X_{x\alpha}^T (M^T X)_{x-\mu,\beta} ,
\end{aligned} \tag{5.140}
$$

$$
\begin{aligned}
F^{Ic}_{x+\mu} &= 2\sum_{\alpha}\left[\phi_{x+\mu}\phi^{\dagger}_{x}\tau_3\phi_x\phi^{\dagger}_{x+\mu},\tau_3\right]X^{T}_{x\alpha}(M^TX)_{x\alpha}\,,\\
F^{IIb}_{x+\mu} &= -2\sum_{\alpha\beta\gamma\delta}\epsilon_{\alpha\delta}\epsilon_{\beta\gamma}\left[\phi_{x+\mu}\phi^{\dagger}_{x}\tau_\delta\phi_x\phi^{\dagger}_{x+\mu},\tau_\gamma\right]X^{T}_{x-\mu,\alpha}(M^TX)_{x\beta}\,,\\
\overline{F}^{IIIb}_{x+\mu} &= -2\sum_{\alpha\beta\gamma\delta}\epsilon_{\alpha\delta}\epsilon_{\beta\gamma}\left[\phi_{x+\mu}\phi^{\dagger}_{x}\tau_\delta\phi_x\phi^{\dagger}_{x+\mu},\tau_\gamma\right](M^TX)^{T}_{x-\mu,\alpha}X_{x\beta}\,,
\end{aligned}
\tag{5.141}
$$

with B_x defined in Eq. 5.137, $X = \left(MM^T\right)^{-1}\phi$ and M is the reduced-model-ghost matrix M^{red} given in Eq. 5.83. The force terms in Eqs. 5.140 and 5.141 have been written in the shifted manner which is suitable for coding. Notice that, the second and third force terms in Eq. 5.141 require next-nearest-neighbor fields to be gathered during coding. This is non-trivially implemented in the code as an effective gather and scatter of the lattice fields.

The F_{mass} term corresponding to mass term in the action in Eq. 5.84 is given by

$$
(F_{\text{mass}})_x = 4\tilde{\kappa}m^2\left[B_x,\tau_3\right]. \tag{5.142}
$$

For studying symmetry breaking, the force corresponding to the symmetry breaking seed action $\mathcal{S}_{seed}$, given in Eq. 5.95, can be calculated to be

$$
(F_{seed})_x = h\left[B_x,\tau_3\right]\,, \tag{5.143}
$$

which is similar to the mass term.

Auxiliary field force

Since the auxiliary field terms are the same in the reduced model as in the full theory, the auxiliary field force term $\widetilde{F}$ is exactly the same as in the full theory, with just the full theory ghost matrix M being replaced by the reduced-model-ghost matrix M^{red}.

5.7 Results for the Reduced model

Before we confront the interesting possibility of SSB ($SU(2)_R \to U(1)_R$) in the reduced model, it is advisable to perform a few checks regarding the performance of the HMC algorithm on such a novel system with complicated terms in the action density, especially when no prior simulations have ever been done in such a theory. Obviously, the same novelty factor applies also to the HMC and the sTHMC simulations of the full eBRST theory, discussed next.

For the range of $\tilde{\kappa}$ between 1.0 and 10.0, the HMC on 8^4 lattices runs reasonably well for the reduced model (with no mass terms added), although to get acceptance rates around 50%, we needed to keep the MD step-size ~ 0.005 and the number of MD steps in a trajectory within 10. This already shows that the simulation in these systems is hard. Fortunately, despite the small step-size and the number of MD steps, the integrated autocorrelation time is within acceptable limits (< 200 in units of HMC trajectories of length $0.1 - 0.2$) and the system shows the desired fluctuation of the observables in its field configurations, as we shall show shortly. As we increase the lattice size to 12^4, the autocorrelation times increase quite rapidly, however, still within manageable limits of our resources. We have tried runs even on 16^4 lattices with smaller statistics (not presented in this thesis), just to validate our most important conclusions, but a full set of longer runs on 16^4 becomes too time-consuming on our resources.

Since the gauge-fixing coupling, $\tilde{g}$ (related to $\tilde{\kappa}$ as $\tilde{\kappa} = 1/(2\tilde{g}^2)$), is asymptotically free [19], the HMC algorithm faces critical slowing down as we make $\tilde{g}$ weaker, or equivalently $\tilde{\kappa}$ larger. As we increase the coupling $\tilde{\kappa}$, the acceptance rate of HMC decreases appreciably. One can tune the MD step size and number of steps to increase the acceptance, but that inevitably leads to generation of highly correlated configurations. Therefore, limited by

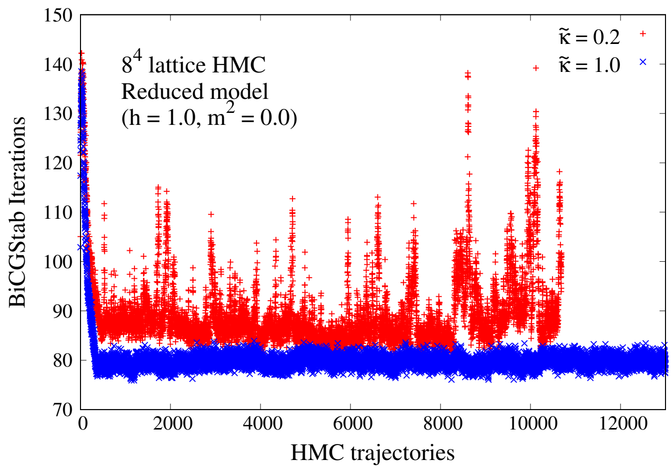

Figure 5.2: Average number of BiCGStab iterations required for ghost matrix (MM^T) inversions per HMC trajectory contrasted at $\tilde{\kappa} = 0.2$ and 1.0. Results obtained on 8^4 lattice with $m^2 = 0.0$ and $h = 1.0$.

our time frame and computational facilities, we could only explore the small $\tilde{g}$ or large $\tilde{\kappa}$ region of the gauge-fixing coupling upto a limit ($\tilde{\kappa} = 10.0$).

On the other hand, in the region where the gauge-fixing coupling $\tilde{g}$ is strong or $\tilde{\kappa}$ small (< 1.0), we face problems with ghost matrix inversion using our BiCGStab inverter[2]. A typical situation is demonstrated in Fig. 5.2, which contrasts the matrix inversion steps required at two different values of $\tilde{\kappa}$. The numerical run at $\tilde{\kappa} = 0.2$ struggles and eventually fails due to the inability of BiCGStab to invert the matrix anymore, while the run at $\tilde{\kappa} = 1.0$ keeps going uninterrupted. A point to note here is that, the ghost matrix inversion problems at small $\tilde{\kappa}$ in the eBRST reduced model is not associated with a sharp rise of the force term in the MD trajectory steps, as is usual for lattice Quantum Chromodynamics (LQCD) investigations when an eigenvalue of the fermion matrix approaches zero. A future investigation of the eigenvalue distributions in such situations may shed some light. As we shall see in the next section, the situation is different in the full eBRST theory (with the

[2]For a review of the BiCGStab algorithm, see Ref. [27]

transverse gauge degrees of freedom back in action). There the ghost matrix inversion problems are more severe except in the weak gauge coupling perturbative limit, and the force term in the MD trajectories rises sharply, resulting in non-acceptance.

The window of $\tilde{\kappa}$ between 1.0 and 10.0 is a relatively safe zone for the HMC simulations. However, the acceptance rates gradually decrease in this range as $\tilde{\kappa}$ is raised. If we assume that there are no sign changes needed to be tracked for $\tilde{\kappa} \geq 1.0$ since we face no problems with matrix inversion, our HMC implementation is quite adequate to compute faithfully the expectation values of operators in the reduced model, as long as we do not make $\tilde{\kappa}$ too large for low acceptance rates to affect the feasibility of the simulation.

In the following, we shall also present results (see Fig. 5.8) where we have pushed $\tilde{\kappa}$ lower than 1.0, actually to 0.5 or so. However, the simulations may not be completely faithful there since a few restarts of the runs were needed from a previous accepted configuration after the code faced problems with inversion of the ghost matrix during a MD trajectory. We have also tried HMC runs of the reduced model at these smaller values of $\tilde{\kappa}$ with an eBRST-invariant mass term (Eq. 5.84), and the problems with inversion reduced to a significant extent, confirming that the ghost matrix becomes better conditioned with the introduction of the eBRST-invariant mass term.

The unfixed τ_3 component of the $SU(2)$ gauge field maintains the $U(1)$ invariance in the reduced model as well. This symmetry is a local one and cannot be spontaneously broken (Elitzur's theorem). To check this point, we study the following expectation value

$$\overline{\phi} \equiv \langle \frac{1}{V} \sum_x \phi_x \rangle \,, \tag{5.144}$$

which has four components ($\phi = a_0 + i a_i \sigma_i$). This observable is not invariant under the $U(1)$ symmetry and hence should be zero everywhere in the reduced model. In Fig. 5.3,

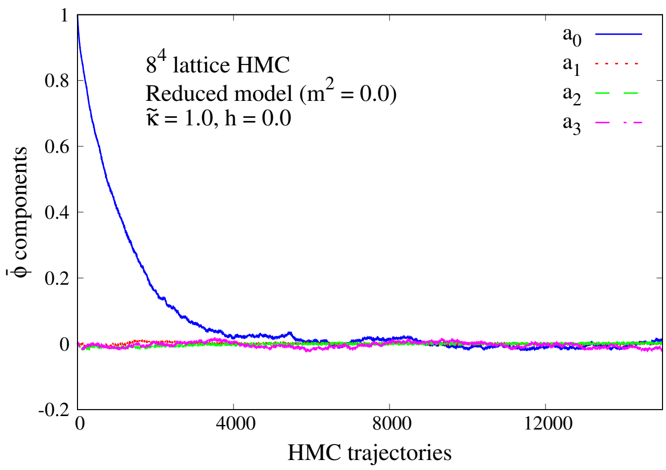

Figure 5.3: Evolution of components of $\overline{\phi}$ with HMC time. The run in a 8^4 lattice with $\tilde{\kappa} = 1.0, h = 0.0$ and $m^2 = 0.0$, was started with a "cold" configuration (components $a_0 = 1, a_i = 0$ for ϕ at all sites).

the evolution of the 4 components of $\overline{\phi}$ with HMC time, at $\tilde{\kappa} = 1.0$, is plotted. The figure shows that, after an initial equilibration period of around 4000 trajectories, all of the components of $\overline{\phi}$ fluctuate closely around zero. Similar results have been found at other $\tilde{\kappa}$ values as well. This verifies the fact that, the local $U(1)$ invariance is unbroken in the reduced model. One should note that, in Fig. 5.3, the initial starting configuration for the HMC run, is $a_0 = 1, a_i = 0$, for all sites. Therefore, as expected, the a_0 component starts from 1 and goes to fluctuations around zero as the system equilibrates, while the other components keep fluctuating around zero. Starting from any other configuration, the system always equilibrates to all the components being around zero, which shows the consistency of the algorithm. The evolution of $\overline{\phi}$ components with the HMC trajectories serves as a general check of equilibration and was used for this purpose in all our runs.

As discussed previously, the $\tilde{A}_x$ vector at each site x points in a direction in the 3 dimensional $SU(2)$ algebra space. In the phase where the global continuous $SU(2)_R$ symmetry is broken, the average $\tilde{A}$ vector in a given configuration is non-zero and points in

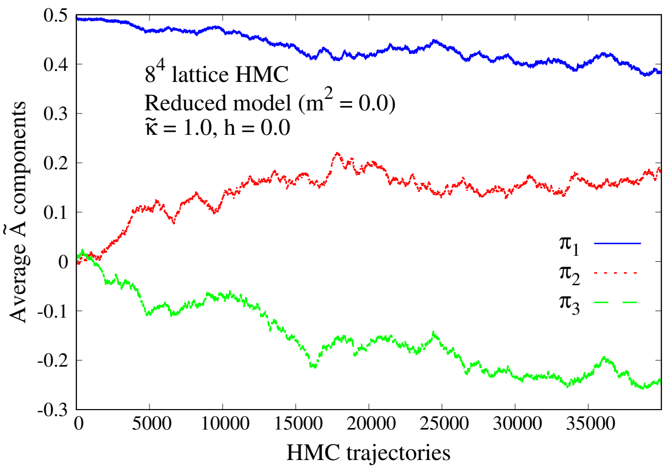

Figure 5.4: Components of average $\tilde{A}$ of each configuration with HMC time. Data given from a run with parameters, $\tilde{\kappa} = 1.0$, $h = 0.0$ and $m^2 = 0.0$, on a 8^4 lattice.

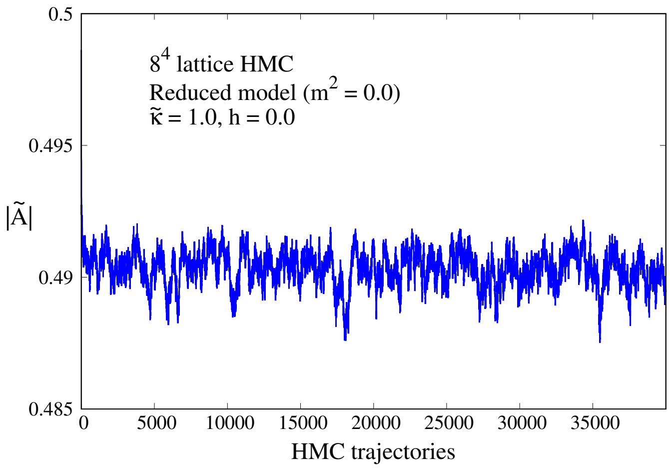

Figure 5.5: Length of average $\tilde{A}$ of each configuration with HMC time, corresponding to the run in Fig. 5.4.

a certain direction. However, the direction can be arbitrary from configuration to configuration. In Fig. 5.4, we demonstrate the movement of the average $\tilde{A}$ vector in the algebra space with HMC evolution time. But as one would expect, the length of the average $\tilde{A}$ vector remains the same within small fluctuations, as seen in Fig. 5.5. In Figs. 5.4 and 5.5, both of which have been computed from the same run, the initial starting configuration is

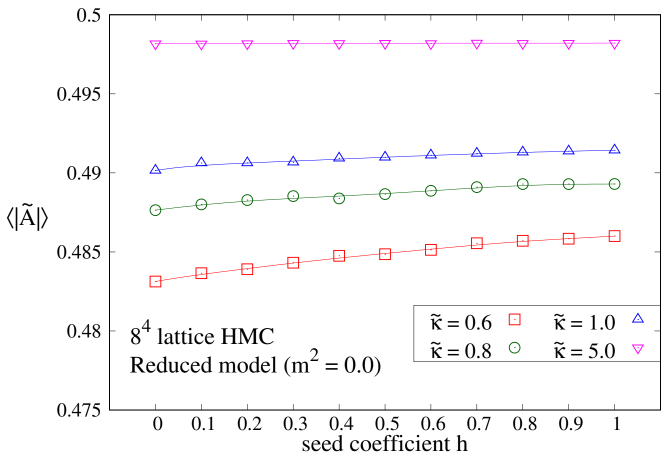

Figure 5.6: The order parameter $\langle|\tilde{A}|\rangle$ has been plotted versus h, at different $\tilde{\kappa} = 0.6, 0.8, 1.0$ and 5.0, with $m^2 = 0.0$. The results, obtained on a 8^4 lattice, clearly show that the order parameter is non-zero, i.e., the reduced model is in a broken phase for a range of $\tilde{\kappa}$.

$a_0 = a_i = 0.5$ (components of ϕ at each site). From Eq. 5.96, this corresponds to $\pi_1 = 0.5$ and $\pi_2 = \pi_3 = 0$ at the start, as can be clearly seen in Fig. 5.4.

With these initial checks regarding the faithfulness of the HMC runs, we now present our most significant result, i.e., evidence for spontaneous breaking of the global $SU(2)_R$ symmetry in the reduced model that is an eBRST theory on the trivial orbit and also a TFT. In Fig. 5.6, we have plotted the order parameter $\langle|\tilde{A}|\rangle$, as a function of the coefficient h of the symmetry-breaking seed term (see Eq. 5.95), for four different values of $\tilde{\kappa} = 0.6, 0.8, 1.0$ and 5.0, in 8^4 lattices. In the following, the statistical errors, wherever not indicated, are smaller than the symbol sizes. We observe that, for the range of $\tilde{\kappa}$ considered, the order parameter remains non-zero, at all values of h, indicating a phase with the global $SU(2)_R$ symmetry spontaneously broken to $U(1)_R$ (see Sec. 5.5.2). As we tune the coefficient h to zero, we see that the system still remains in the broken phase with a non-zero value of the order parameter. It should be mentioned here that in the presence of

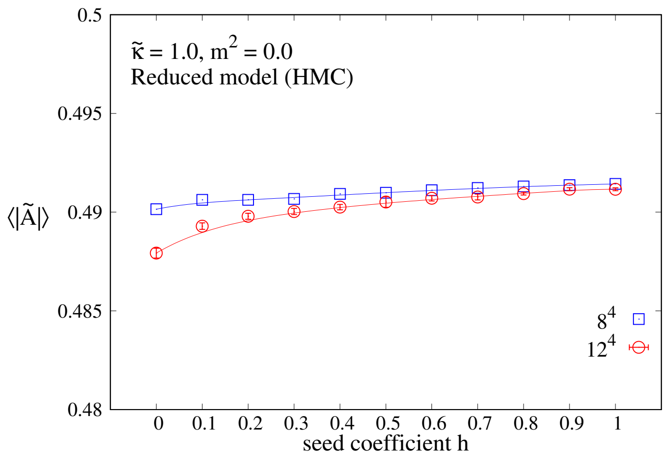

Figure 5.7: The order parameter, $\langle|\tilde{A}|\rangle$, plotted as a function of h, has been compared at different volumes, 8^4 and 12^4.

the seed, $\langle|\tilde{A}|\rangle$ and π_3 component of $\langle\tilde{A}\rangle$ become roughly equal on larger lattices (12^4).

In order to demonstrate that the above broken phase is not a finite lattice artefact, one needs to simulate in larger volumes. Fig. 5.7 compares the values of the order parameter, $\langle|\tilde{A}|\rangle$, at $\tilde{\kappa} = 1.0$, for two different lattice volumes, 8^4 and 12^4, as a function of h. The slightly sharper bend, as apparent in the figure as h approaches zero for the 12^4 data, is because of the blown-up scale used, otherwise this is insignificant. For absolute confirmation, we tried simulations on 16^4 lattices. The thermalization itself takes a long time and the code is rather slow on 16^4 lattices, as already remarked earlier in this section. Hence the generated statistics is low and the data is not shown here. The preliminary results on 16^4 lattices show the exact same qualitative trend.

Next, we study the order parameter $\langle|\tilde{A}|\rangle$ in dependence of the gauge-fixing coupling, $\tilde{\kappa}$, in the limit $h = 0$. Referring to Fig. 5.1 and remembering $\tilde{\kappa} = 1/(2\tilde{g}^2)$, this amounts to moving along the right vertical axis in the phase diagram. Fig. 5.8 explores a region of $\tilde{\kappa}$ on 8^4 lattices. There appears to be a significant downward trend of the order parameter in the small $\tilde{\kappa}$ region, consistent with the suggested transition from B to A in the strong $\tilde{g}$

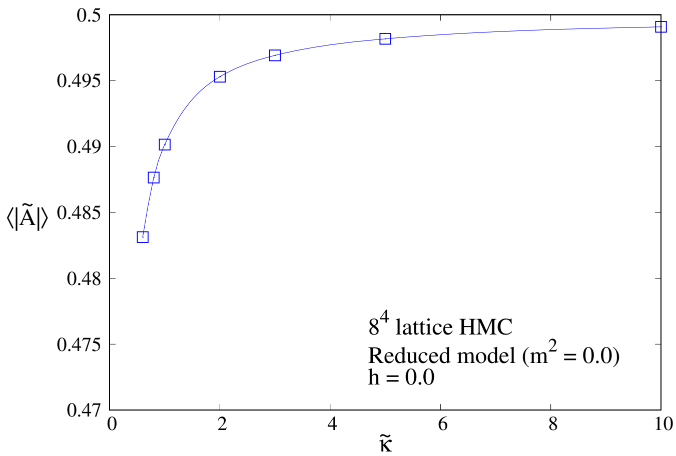

Figure 5.8: Variation of $\langle|\tilde{A}|\rangle$ with $\tilde{\kappa}$ on 8^4 lattices, with $m^2 = 0.0$ and $h = 1.0$.

(small $\tilde{\kappa}$) region in both the diagrams in Fig. 5.1. While there is no doubt about the general qualitative change of the order parameter at small $\tilde{\kappa}$ or strong $\tilde{g}$ region, we refrain from making a quantitative conclusion about the location and the order of what appears to be a symmetry restoring transition at small $\tilde{\kappa}$. This is because, the algorithm appears somewhat unstable in the small $\tilde{\kappa}$ region, as already pointed out earlier in the section, and the results are obtained only on 8^4 lattices. On the other hand, the broken phase appears to continue to exist all the way to arbitrarily large $\tilde{\kappa}$, i.e., the perturbative region of $\tilde{g}$.

A general study of the variation of the observable $\langle|\tilde{A}|\rangle$ with mass m, is shown in Fig. 5.9. The mass term (Eq. 5.84) is eBRST-invariant. One can see that, at $\tilde{\kappa} = 1.0$, the system remains in the broken phase even in the massive theory. Similar results are manifested at other values of $\tilde{\kappa}$ as well. Since the mass term (Eq. 5.84) also includes a diagonal ghost mass term, the inversions of the ghost matrix become easier in the massive theory. We point out that the $\langle|\tilde{A}|\rangle$ data goes over to its value at $m = 0$ smoothly.

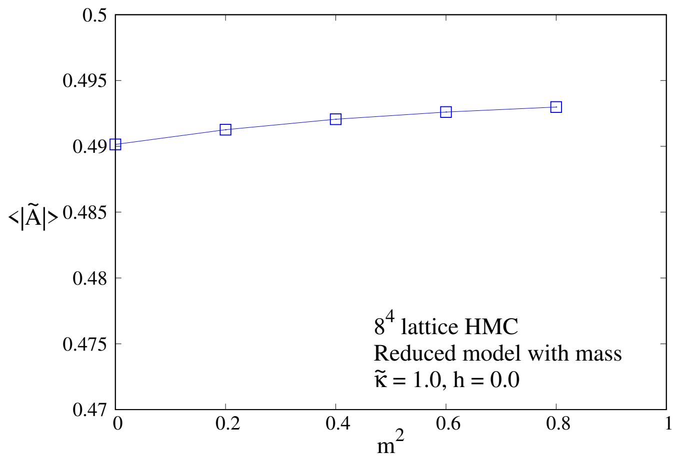

Figure 5.9: Plot of the order parameter, $\langle|\tilde{A}|\rangle$, versus the coefficient of the mass term, m^2, at a fixed $\tilde{\kappa} = 1.0$ in 8^4 lattice.

5.8 Results for the Full theory

In this section, we present our results for the full eBRST theory (with the transverse gauge degrees of freedom back in action) mostly on 8^4 lattices. We have comprehensively scanned the region $\beta = 3.0 - 8.0$ and $\tilde{\kappa} = 0.1 - 10$ for $m^2 = 0.0$ with the HMC algorithm. Unlike in the reduced model, there is no region found in the full theory in the scanned $\beta - \tilde{\kappa}$ parameter space where the ghost matrix inversions take place without issues. Generally, the number of iterations of the BiCGStab inverter blow up or the inversion fails at some point during the field updation. The severity of the inversion problem increases with decreasing β and/or decreasing $\tilde{\kappa}$, i.e., with stronger gauge and gauge-fixing couplings g and $\tilde{g}$ respectively. At the points of failure, spikes are observed in the change in action, ΔS, at the end of MD trajectories, which is due to large forces. All these symptoms generally indicate the presence of near-zero eigenvalues of the ghost matrix. On the other hand, critical slowing down, in the form of decreasing acceptance rate, is also found with increasing β and/or $\tilde{\kappa}$, as also seen in the reduced model for $\tilde{\kappa}$.

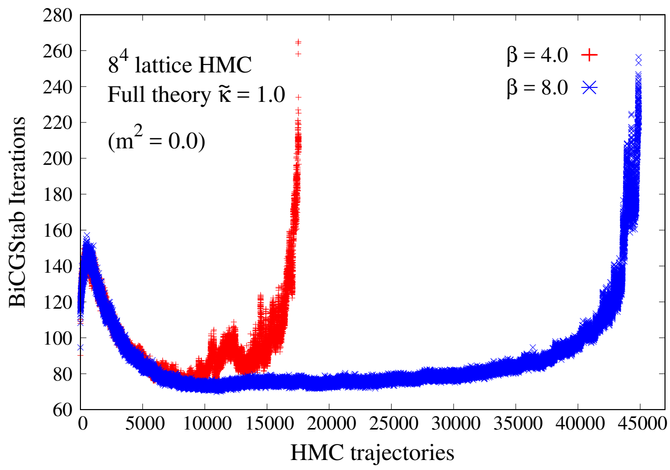

Figure 5.10: Evolution of the average number of BiCGStab iterations required for the ghost matrix iterations, per MD trajectory, with HMC time at $\beta = 4.0$ and 8.0, for a fixed $\tilde{\kappa} = 1.0$, on 8^4 lattice.

A typical behavior of the number of BiCGStab iterations for ghost matrix-inversion (MM^T inversion in the HMC MD trajectory, cf. Secs. 5.6, 5.6.3) in the full theory, evolving in HMC time, is shown in Fig. 5.10. In the figure, results are shown from two HMC runs at $\beta = 4.0$ and 8.0, both of which have been started from unit gauge-field configurations (cold start) and have similar acceptance rates after equilibration. We see that the number of BiCGStab iterations eventually blows up in each case, but with the larger β, the algorithm is able to run much longer without facing inversion-related problems. This trend, observed in runs at all β values, indicates that the system encounters fewer instances of near-zero eigenvalues with weaker gauge couplings g, i.e. larger β. This is consistent with the expectation that for perturbative gauge couplings, the ghost matrix determinant does not suffer from sign changes. We shall see in this section that the invariance theorem gets increasingly validated at larger β. This further confirms that at larger β, there are fewer or no sign changes of the ghost determinant, making calculation of the expectation values progressively more faithful with the HMC algorithm that ignores possible sign changes, .

The invariance theorem, a consequence of eBRST symmetry for the full theory and a rigorous result on a finite lattice, ensures the equality of the expectation value of any gauge-invariant operator between the unfixed gauge theory and the eBRST gauge-fixed theory at a given coupling β. We have calculated the expectation value of the gauge-invariant plaquette, the smallest Wilson loop, for both unfixed and gauge-fixed theories on the lattice to study the validity of the invariance theorem.

Without a symmetry breaking seed, the eBRST symmetry is exact, and on our finite lattices the invariance theorem is strictly applicable. Hence under these conditions, any violation of the invariance theorem appears to be an indicator of sign changes of the ghost determinant, something that our HMC algorithm ignores.

The expectation value of the average plaquette obtained with HMC at various β are compared in Fig. 5.11, for unfixed and gauge-fixed theories, in 8^4 and 12^4 lattices. The figure indicates that HMC gives increasingly matching results with increasing β, implying that sign changes become fewer with increasing β. This trend is corroborated by the BiCGStab inversion trends discussed earlier. These results are consistent with the expectation that in the perturbative regime of the gauge coupling, there are no sign changes of the ghost determinant. Approximate manifestation of the invariance theorem, at least at our larger β values, is also a validation for the eBRST gauge fixed theory, an alternate formulation of non-Abelian gauge theory on the lattice.

Next, we briefly consider the invariance theorem with an eBRST-invariant mass term (Eq. 5.79) in the action (the proof of the invariance theorem can be extended to this case). The massive eBRST gauge-fixed theory is compared to the unfixed theory with mass term for the coset gauge fields W_μ, the action of a such an unfixed gauge theory with massive

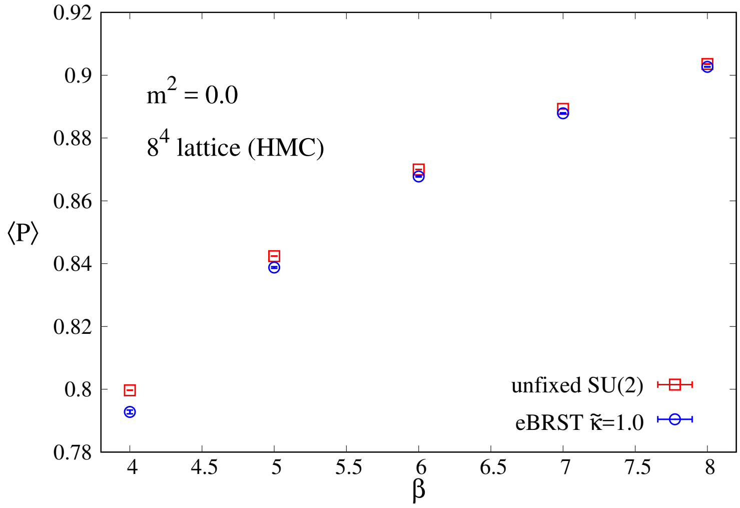

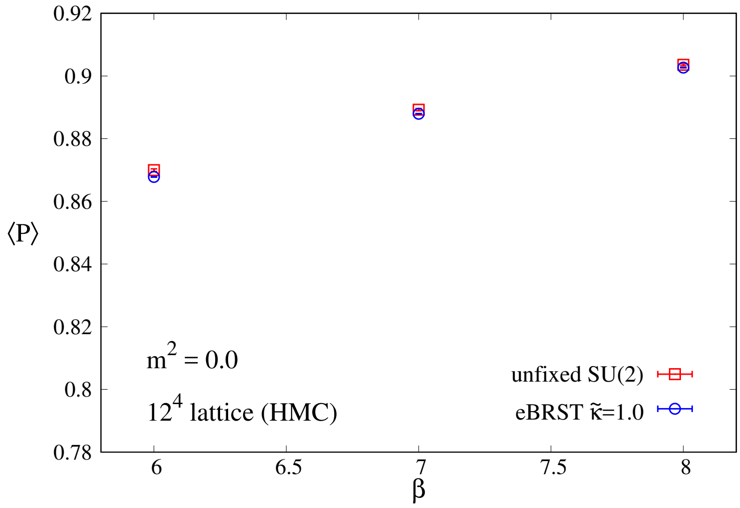

Figure 5.11: Comparison of plaquette expectation values $\langle P \rangle$ of unfixed and eBRST gauge-fixed theories at different β for a fixed $\tilde{\kappa} = 1.0$. Results obtained on 8^4 and 12^4 lattice.

W_μs, being given as (cf. Eq. 5.79),

$$S^{\text{unfixed}}_{\text{massive}} = S_W - 4\, m^2 \sum_x \operatorname{tr}(U_{x\mu} \tau_3 U^\dagger_{x\mu} \tau_3), \tag{5.145}$$

where S_W is the usual Wilson plaquette action. For the massive unfixed and eBRST gauge-fixed theories, the plaquette expectation values are plotted in Fig. 5.12. As is apparent from

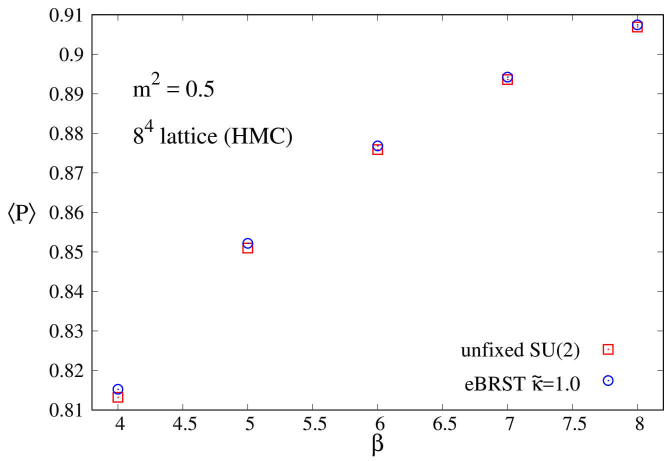

Figure 5.12: Comparison of plaquette expectation values $\langle P \rangle$ of unfixed and eBRST gauge-fixed theories at $m^2 = 0.5$. Results obtained on 8^4 lattice.

the figure, the degree of equality of the expectation values for the two theories, is better and extends more towards relatively smaller β values, indicating that fewer sign changes of the ghost determinant take place with the introduction of the eBRST-invariant mass term. The mass term in the eBRST action appears to make the ghost matrix better-conditioned, since its presence is clearly seen to help in the ghost matrix inversion during the MD trajectories of the HMC.

Fig. 5.13 shows the variation of the expectation value of the average plaquette as a function of the gauge-fixing coupling, $\tilde{\kappa}$, at $\beta = 8.0$. According to the invariance theorem, the expectation values of gauge-invariant operators of the eBRST gauge-fixed theory should be equal to those in the unfixed theory irrespective of the gauge-fixing coupling. In Fig. 5.13, we see the expected result, i.e., there is no significant variation of the expectation value of the average plaquette. On the left side of the figure, the value for the unfixed theory also appears at $\tilde{\kappa} = 0$. On a very very fine scale, deliberately chosen, there appears a slight but noticeable difference of the plaquette expectation values from the eBRST fixed and the unfixed theories. Statistical errors are within the symbols. However, we have not estimated

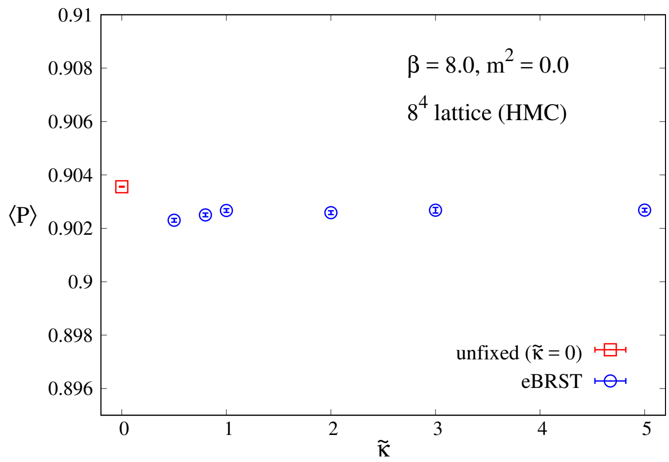

Figure 5.13: Variation of plaquette expectation values $\langle P \rangle$ of eBRST gauge-fixed theory with $\tilde{\kappa}$ at a fixed $\beta = 8.0$. The unfixed theory plaquette expectation value for $\beta = 8.0$ has been plotted at $\tilde{\kappa} = 0.0$ for comparison. Results obtained on 8^4 lattice.

the size of any systematic errors. We have noticed that, at our largest β $(= 8.0)$, the plaquette values from the eBRST theory with HMC and also sTHMC (shown next in this section) are very close, but systematically lie slightly below that from the unfixed theory with HMC algorithm. As we have already remarked, ignoring the occasional sign changes of the ghost determinant, however infrequent at this large β, may be a reason for the discrepancy, since the HMC code cannot take the possible sign changes of the ghost matrix determinant into account. Otherwise, a proper estimation of any possible systematic errors may also wipe out the tiny differences. It may also be pointed out that, three completely independent codes producing nearly the same value for the expectation value of the average plaquette is a good check of the correctness of the codes.

sTHMC results

We did a first-time implementation of the sTHMC algorithm and simulated the theory at regions of the $\beta - \tilde{\kappa}$ parameter space, to check whether we can track the sign changes of

β	α	k	No. of MD steps	MD step size	Average sTHMC Plaquette	No. of sign changes in matrix A	Auto correlation τ_{int}	Acc. rate %	Average Unfixed HMC Plaquette	Average eBRST HMC Plaquette
8	25	8	4	0.004	0.902600 +- 0.000064	0	285	69.7	0.903559 +- 0.000015	0.902667 +- 0.000068
8	25	10	4	0.0035	0.902624 +- 0.000091	0	315	76.2		
8	50	4	4	0.004	0.902471 +- 0.000070	0	293	68.1		
8	50	6	4	0.003	0.902574 +- 0.000072	0	406	77.1		
8	100	4	4	0.002	0.902814 Insufficient data	0	~1000	79.1		

Table 5.1: Comparison of sTHMC runs, for different algorithm parameters, with unfixed HMC and eBRST gauge-fixed HMC.

the ghost determinant for the calculation of observables.

The sTHMC algorithm employs a stochastic sampling method to deflate the ghost matrix. However, it does not guarantee that all the low-lying eigenvalues are raised. The two sTHMC parameters α and k provide a handle to study the effectiveness of the deflation.

We have so far not been able to optimize the values of the parameters α and k to the extent that the deflation matrix A is able to pick up all the sign changes, so that the MD trajectories are devoid of any ill-effects of small eigenvalues of the deflated ghost-matrix D (effective in the MD trajectories, cf. Sec. 5.6.2).

In Table 5.1, we present results of the sTHMC runs on 8^4 lattices at $\beta = 8.0$ with various combinations of the algorithm parameters α and k. The matrix A has not picked up any

	β	No. of MD steps	MD step size	Average Plaquette	Auto correlation τ_{int}	Acc. rate %
Unfixed HMC	8	13	0.04	0.903559 +- 0.000015	2	60.6
eBRST HMC ($\tilde{\kappa} = 1.0$, $m^2 = 0.0$)	8	4	0.006	0.902667 +- 0.000068	115	57.8

Table 5.2: Details of HMC runs at $\beta = 8.0$ in the unfixed $SU(2)$ theory and eBRST gauge-fixed one.

sign changes, and the plaquette expectation values are roughly equal to those obtained from the unfixed theory and those obtained from the eBRST theory with HMC algorithm. The integrated autocorrelation times appear to be on the higher side in comparison to those obtained from HMC in the eBRST theory. For comparison, we also provide in Table 5.2 some simulation details of the HMC algorithms both in the unfixed theory and in the eBRST theory. It is to be noted that we have tried running sTHMC at smaller β and have observed sign changes of the ghost determinant, but the inversion issues are still substantial and we have not shown any data due to lack of statistics.

5.9 Conclusion

The eBRST framework of gauge-fixing provides an alternate formulation of non-Abelian theories of compact gauge fields on the lattice. Moreover, the eBRST gauge-fixing technique provides a way to define a local anomaly-free non-Abelian chiral gauge theory on the lattice, provided the remaining Abelian gauge invariance is taken care of by a higher derivative gauge-fixing as described in Chaps. 3 and 4. However, it appears that the eBRST theory is itself an interesting theory to study for possible novel non-perturbative effects of the longitudinal gauge degrees of freedom onto the physical sector. Approximate analytic calculations have shown that the eBRST theory can accommodate non-trivial phase structure, where a novel Higgs phase, with no mass gap, may exist. In this chapter, we have initiated a first-time numerical investigation of the eBRST formalism in the $SU(2)$ case.

The lattice eBRST gauge-fixed theory with $SU(2)$ gauge fields, and ghost and auxiliary fields in the coset $SU(2)/U(1)$ was successfully implemented numerically in our work. The reduced model, the theory on the trivial orbit, with only the ghost fields and the longitudinal gauge degrees of freedom was also numerically investigated. Three field updation codes suitable for massively parallel computing architecture were written from scratch - HMC and sTHMC codes for the full eBRST theory and a HMC code for the reduced model. The coding was a non-trivial task with the complicated action, as it involved several effective gather and scatter operations of the lattice fields.

The global $SU(2)_R$ symmetry of the reduced model was found to be spontaneously broken for a wide range of the gauge-fixing coupling $\tilde{\kappa}$ - evidence of strong dynamics of the longitudinal degrees of freedom. At small values of $\tilde{\kappa}$ there was indication of symmetry restoration. Broken symmetry phase appears to persist for arbitrarily large values of $\tilde{\kappa}$, i.e., upto the perturbative region of $\tilde{g} = 1/\sqrt{2\tilde{\kappa}}$. Considering that the reduced model partition function is independent of $\tilde{\kappa}$, that is, it is a topological field theory, the spontaneous symmetry breaking in such a theory is a novel result, supporting claims in the literature from approximate analytic calculations.

We have investigated the full theory and produced evidence that this is a valid alternate formulation of an $SU(2)$ gauge theory, through verification of the invariance theorem at small gauge coupling (large β). We also have a good idea regarding where in the $\beta - \tilde{\kappa}$-plane the system is likely to encounter more sign-changes of the ghost matrix determinant.

Our results are also consistent with the expectation that in the perturbative region of this plane, there are no sign changes. However, we have not been able to track the sign changes and incorporate the sign changes into calculation of expectation values of gauge-invariant operators. To investigate the effect of the strong dynamics of the longitudinal gauge degrees of freedom on the full eBRST theory, and conclude about the possibility of a phase with no mass gap, we need to track the sign changes of the ghost determinant.

The eBRST theory is a very hard problem as it poses several algorithmic challenges. Due to the complicated actions in both the full theory and reduced model, to maintain a reasonable acceptance rate, the HMC trajectory had to be kept quite small and thus, the Monte Carlo simulation moved very slowly. The most important challenge was the sign changes of the ghost determinant. Since in principle, for small enough step sizes, HMC does not allow sign changes to occur, there is a possibility that the algorithm is non-ergodic in regions of the phase diagram where sign changes occur. The stochastic Tunneling HMC algorithm was implemented for the very first time in our work to study these sign changes. Through our exploration, we have been able to identify the numerical problems in the various regions of the theory and we hope that this will be beneficial in the future to implement a robust algorithm to solve these issues.

CHAPTER 6

SUMMARY

In this final chapter, we summarize briefly the main results of our work described in this thesis. Details are provided in the respective previous chapters.

We have studied two different approaches of non-perturbative gauge-fixing on the lattice, one for Abelian and another for non-Abelian gauge theories. The Wilson approach to lattice gauge theories, with compact gauge fields, is manifestly gauge-invariant and well-defined without any gauge-fixing. This works very successfully for vector-like gauge theories like Quantum Chromodynamics (QCD). However, for the construction of chiral gauge theories on lattice (ChLGT) with manifestly local lattice fermions, the need to tame the unphysical longitudinal gauge degrees of freedom (*lgdof*s) arises, since the *lgdof*s couple strongly with the physical degrees of freedom. The gauge-fixing technique offers a way to dynamically control the *lgdof*s, leading to a possible formulation of manifestly local ChLGTs. In addition, gauge-fixing provides an alternate way of non-perturbatively defining gauge theories on the lattice.

However, the standard perturbative Fadeev-Popov gauge-fixing procedure leading to the Becchi-Rouet-Stora-Tyutin (BRST) formalism faces an impasse in the form of a no-go theorem in the non-perturbative set-up with the compact gauge fields on the lattice. According to the no-go theorem [1], the partition function of a BRST-invariant gauge theory with compact gauge fields becomes zero and the vacuum expectation value of a gauge-invariant operator is rendered an indeterminate $0/0$ form. Obviously, gauge-fixing the compact gauge fields on the lattice leads to explicit breaking or modifying the BRST symmetry.

For the case of compact $U(1)$ gauge theory, a higher-derivative (HD) gauge-fixing scheme was proposed by Golterman and Shamir [9, 25], which evades the no-go theorem and the action has a unique absolute minimum around which weak-coupling perturbation theory can be done. In the classical continuum limit, the HD term goes to the renormalizable Lorentz gauge along with irrelevant terms. Counter-terms can be added through power counting and can be tuned to restore gauge symmetry in the continuum. It may be pointed out in this context that, the pure compact $U(1)$ theory, given by just the Wilson plaquette action on the lattice, displays a weak first-order transition and, therefore, has no quantum continuum limit. The HD gauge-fixing scheme provides an alternate way of defining $U(1)$ gauge theories.

The HD gauge-fixing compact $U(1)$ lattice gauge theory was investigated earlier [10] at weak gauge coupling in perturbation theory and with non-perturbative methods using numerical simulations. At relatively large values of the coefficient of the HD gauge-fixing term in the action, a novel continuous phase transition was obtained separating a regular ordered (FM) phase from a rotationally non-invariant spatially-modulated ordered (FMD) phase. The scaling region from within the FM phase was obtainable by tuning appropriate counter-terms. In the scaling region of the FM phase, the gauge symmetry was recovered with emergence of massless free photons with the *lgdof*s decoupled. Feasibility of $U(1)$

chiral gauge theories with Wilson fermions and lattice domain wall fermions was also demonstrated in Refs. [11–14] in the quenched approximation.

The question naturally arises about the nature of the theory at strong gauge couplings. This is interesting for several reasons. Firstly, for an alternate and gauge-fixed version of the compact lattice $U(1)$ gauge theory suitable for an Abelian chiral gauge theory on the lattice, it is important to know the behavior of the theory at a wide range of the coupling parameter space. Secondly, to probe the short distance behavior of the $U(1)$ gauge theory and any possible non-trivial properties, the theory at strong gauge coupling needs to be understood. Thirdly, even for the non-Abelian chiral gauge theory with the equivariant BRST (eBRST) formalism, the invariant Abelian part has to be eventually gauge-fixed through the HD mechanism, and as a result, a knowledge of the theory at strong gauge couplings cannot be overlooked.

In our work in Refs. [15, 16], we have extensively studied the HD gauge-fixing scheme in the strong coupling region. The main result we have established is that the novel continuous FM-FMD transition is also present at strong gauge couplings for suitably large gauge-fixing coupling $\tilde{\kappa}$. The gauge symmetry is recovered at the continuous FM-FMD transition and the same physics as in the weak coupling region, is obtained. Massless free photons have been obtained in the scaling region of the FM phase near the FM-FMD transition and the *lgdofs* are decoupled. Careful studies at various lattice volumes have generated a clear picture of the entire phase diagram and its features as we go from the weak to strong coupling region. Investigation at finely separated parameter values reveal the scaling of the gauge boson mass near the phase transition and the expected approach of the field renormalization constant to unity with increasing $\tilde{\kappa}$. The nature of the phase transitions has been established through analysis at different lattice volumes and standard methods. The physics at the strong gauge coupling seems to be governed by the same universality class as in the weak gauge coupling region, except for a tricritical line that appears to be the only place for any possible non-perturbative and non-trivial behavior. However, probing the universality class at the tricritical line is a separate study by itself and is outside the scope of the present work.

An important conclusion from our $U(1)$ study was regarding the use of Multihit Metropolis (MM) algorithm, a local algorithm, for numerical simulations. The MM algorithm was extensively used in the previous non-perturbative studies of this theory at weak couplings. However, it has been found to be inadequate at strong gauge and gauge-fixing couplings. The HD action density is spread over sites further than the nearest neighbors. Hence it is not surprising that, a local algorithm like MM fails to produce correct results, especially at strong gauge couplings where larger values of the coefficient $\tilde{\kappa}$ of the HD gauge-fixing term is required to access the continuous FM-FMD transition. We have implemented the Hybrid Monte Carlo (HMC), a global algorithm, to study the strong gauge coupling region with good results. A comparative study of the two algorithms has been presented in this thesis to make our point explicit.

The eBRST scheme of gauge-fixing for non-Abelian theories was first proposed by Schaden [17] for the $SU(2)$ gauge theories and later extended by Golterman and Shamir [18] for $SU(N)$ case. Basically, in the eBRST scheme, the total gauge group is not gauge-fixed, instead a coset is fixed leaving a subgroup unfixed (which contains at least a Cartan subgroup). This method evades the no-go theorem associated with exact BRST symmetry. An extended eBRST algebra can be constructed with eBRST and anti-eBRST symmetry for general $SU(N)$ theories and there can be in general several ways to gauge-fix the gauge group down upto the Cartan subgroup. However, for $SU(2)$, the extended eBRST algebra reduces to the usual eBRST, where the only way to gauge-fix is by fixing the coset $SU(2)/U(1)$. In Ref. [18], the authors provided a prescription of constructing ChLGTs using the eBRST scheme, where the remaining Abelian subgroup is fixed by the HD gauge-fixing method described above. We have done a first-time numerical investigation of the eBRST $SU(2)$ theory where the coset $SU(2)/U(1)$ is gauge-fixed leaving the subgroup $U(1)$ unfixed.

The pure gauge eBRST theory involves gauge fields and Grassmann-valued ghosts and the numerical implementation is similar to a gauge theory with fermions, except that the ghost fields are in the coset and are replaced in the simulation by real scalar pseudo-ghost fields. The ghost determinant obtained after integrating out the ghost fields is real but can have both positive and negative values. Thus, an important challenge of the numerical code is the sign-tracking of the ghost determinant, which requires tracking the near-zero eigenvalues of the ghost matrix. Considering the absolute value of the determinant, we have developed two separate parallelized numerical codes using HMC in the full theory and the reduced model (the theory of *lgdof*s and ghosts on the trivial orbit). The coding was non-trivial as it involved many more effective gathers and scatters of the field values than usual, required during communication among the parallel nodes. To track the sign, we have done a first-time implementation of the stochastic Tunneling HMC algorithm (sTHMC).

Through a perturbative calculation [19], it was shown that the eBRST gauge-fixing coupling is also asymptotically free like the non-Abelian gauge coupling and therefore, becomes strong at an infrared scale [21]. It was argued that the gauge-fixing coupling can become strong when the gauge coupling is still weak and the strong dynamics of the longitudinal sector can affect the physics of the transverse sector. This raises an unusual question seldom asked, that whether the dynamics of the unphysical longitudinal sector can affect the physical sector. The reduced model of the eBRST gauge-fixed theory, obtained by setting the gauge coupling to zero and containing just the *lgdof*s and ghost fields, offers us a system to investigate the strong dynamics of the unphysical sector. It was found out through a combination of strong coupling and mean field techniques [20] that the eBRST $SU(2)$ reduced model can have a spontaneous symmetry breaking (SSB) of a global $SU(2)_R$ symmetry down to $U(1)_R$. The SSB in the reduced model is interesting in its own right since the reduced model is a topological field theory, the partition function being independent of the gauge-fixing coupling. With the gauge coupling turned on, interesting possibilities were discussed as effect of this SSB of the reduced model on the eBRST gauge theory: the coset gauge fields could become massive through a Higgs mechanism with a remaining massless photon, thereby, giving a new phase with no mass gap in the pure $SU(2)$ theory different from the usual confining phase. Massive coset gauge fields do not necessarily mean a breaking of the eBRST symmetry, since the eBRST can be maintained with addition of an appropriate ghost mass.

Through our numerical simulations in the reduced model, we have obtained strong evidence of the existence of the above-mentioned SSB, $SU(2)_R \to U(1)_R$, for a range of the bare gauge-fixing coupling. Our simulations with HMC do not take into account the sign change of the ghost determinant. However, for the gauge fixing coupling above a certain small value, the ghost matrix inversion is well behaved in the reduced model, even with very small step size of the molecular dynamics part of the HMC, suggesting against presence of small eigenvalues and therefore, a sign change.

The eBRST gauge-fixed theory obeys an invariance theorem which ensures that the expectation value of gauge-invariant operators obtained in the gauge-fixed theory is exactly equal to the one obtained in the unfixed theory. This serves as a check for our simulations with HMC, where we ignore the sign of the ghost determinant. Deviations of the results obtained from the eBRST HMC code with that obtained from the unfixed theory would mean that sign changes are relevant. Our numerical simulations with HMC have revealed that the invariance theorem gets increasingly validated as we make the gauge coupling weaker.

This is consistent with the expectation that sign changes do not occur in the perturbative regime. The above also validates the eBRST gauge-fixed theory as an alternate formulation of non-Abelian gauge theories on the lattice. The interesting issue of how a Higgs phase with massive coset gauge fields can appear despite the invariance theorem, that is a rigorous result from eBRST on a finite system, has not been pursued in this thesis. This is an issue that can be handled only after finding a proper method of tracking the sign changes of the ghost matrix determinant.

In order to track the sign of the ghost determinant for accurate calculation of expectation values, we employed the sTHMC algorithm. It involves a type of stochastic deflation which aims to ease the numerical difficulties faced due to the presence of near-zero eigenvalues. However, being a stochastic method, it does not guarantee the successful deflation of the ghost matrix and also the sign-tracking of the determinant. In our simulations at the weakest gauge coupling of our study ($\beta = 8.0$) with several values of the tunable parameters of sTHMC, we have found no sign changes and the results are very similar to the ones obtained from the eBRST theory with HMC. At higher values of the gauge coupling, sTHMC trajectories also suffered from presence of near-zero eigenvalues, indicating that the driving Hamiltonian in the trajectory was not deflated properly.

Our first-time study of the eBRST gauge-fixed $SU(2)$ theory has produced enough interesting results. It also leaves us with several issues, both physics related and algorithm oriented, to be pursued in the future. The first and foremost, would be the faithful tracking of the sign of the ghost determinant. The eigenvalue distribution of the ghost matrix needs to be investigated to determine efficient methods for the deflation. The effect of the SSB in the reduced model on the full eBRST theory is still unclear, and it is to be studied with the introduction of a symmetry-breaking seed, as discussed in Sec. 5.5.3.

BIBLIOGRAPHY

[1] H. Neuberger, *Nonperturbative BRS invariance and the Gribov problem*, *Physics Letters B* **183** (1987) 337 – 340.

[2] H. Nielsen and M. Ninomiya, *Absence of neutrinos on a lattice: (I). Proof by homotopy theory*, *Nuclear Physics B* **185** (1981) 20 – 40.

[3] H. Nielsen and M. Ninomiya, *A no-go theorem for regularizing chiral fermions*, *Physics Letters B* **105** (1981) 219 – 223.

[4] L. H. Karsten and J. Smit, *Lattice fermions: Species doubling, chiral invariance and the triangle anomaly*, *Nuclear Physics B* **183** (1981) 103 – 140.

[5] W. Bock, A. K. De and J. Smit, *Fermion masses at strong Wilson-Yukawa coupling in the symmetric phase*, *Nuclear Physics B* **388** (1992) 243 – 274.

[6] M. F. Golterman, D. N. Petcher and J. Smit, *Fermion interactions in models with strong Wilson-Yukawa couplings*, *Nuclear Physics B* **370** (1992) 51 – 68.

[7] P. H. Ginsparg and K. G. Wilson, *A remnant of chiral symmetry on the lattice*, *Phys. Rev. D* **25** (May, 1982) 2649–2657.

[8] M. Luescher, *Abelian chiral gauge theories on the lattice with exact gauge invariance*, *Nuclear Physics B* **549** (1999) 295 – 334.

[9] M. F. Golterman and Y. Shamir, *A gauge-fixing action for lattice gauge theories*, *Physics Letters B* **399** (1997) 148 – 155.

[10] W. Bock, K. C. Leung, M. F. L. Golterman and Y. Shamir, *Phase diagram and spectrum of gauge-fixed Abelian lattice gauge theory*, *Phys. Rev. D* **62** (Jul, 2000) 034507.

[11] W. Bock, M. F. L. Golterman and Y. Shamir, *Lattice Chiral Fermions Through Gauge Fixing*, *Phys. Rev. Lett.* **80** (Apr, 1998) 3444–3447.

[12] W. Bock, M. F. L. Golterman and Y. Shamir, *Chiral fermions on the lattice through gauge fixing: Perturbation theory*, *Phys. Rev. D* **58** (Jun, 1998) 034501.

[13] S. Basak and A. K. De, *Chiral gauge theory on the lattice with domain wall fermions*, *Phys. Rev. D* **64** (May, 2001) 014504.

[14] S. Basak and A. K. De, *Gauge fixed domain wall fermions on lattice at small Yukawa coupling*, *Physics Letters B* **522** (2001) 350 – 357.

[15] A. K. De and M. Sarkar, *Tricritical points in a compact $U(1)$ lattice gauge theory at strong coupling*, *Phys. Rev. D* **93** (Jun, 2016) 114504.

[16] A. K. De and M. Sarkar, *Non-perturbatively gauge-fixed compact $U(1)$ lattice gauge theory*, *Journal of High Energy Physics* **2017** (Oct, 2017) 125.

[17] M. Schaden, *Equivariant gauge fixing of $SU(2)$ lattice gauge theory*, *Phys. Rev. D* **59** (Dec, 1998) 014508.

[18] M. Golterman and Y. Shamir, *$SU(N)$ chiral gauge theories on the lattice*, *Phys. Rev. D* **70** (Nov, 2004) 094506.

[19] M. Golterman and Y. Shamir, *Running couplings in equivariantly gauge-fixed $SU(N)$ Yang-Mills theories*, *Phys. Rev. D* **73** (Jan, 2006) 014510.

[20] M. Golterman and Y. Shamir, *Phase with no mass gap in nonperturbatively gauge-fixed Yang-Mills theory*, *Phys. Rev. D* **87** (Mar, 2013) 054501.

[21] M. Golterman and Y. Shamir, *Dimensional transmutation in the longitudinal sector of equivariantly gauge-fixed Yang-Mills theory*, *Phys. Rev. D* **90** (Aug, 2014) 034504.

[22] M. Golterman and Y. Shamir, *Tunneling hybrid Monte-Carlo algorithm*, *Phys. Rev. D* **76** (Nov, 2007) 094512.

[23] `http://physics.utah.edu/~detar/milc.html`.

[24] K. G. Wilson, *Confinement of quarks*, *Phys. Rev. D* **10** (Oct, 1974) 2445–2459.

[25] Y. Shamir, *The standard model from a new phase transition on the lattice*, *Phys. Rev. D* **57** (Jan, 1998) 132–146.

[26] K. Osterwalder and R. Schrader, *Axioms for Euclidean Green's functions*, *Communications in Mathematical Physics* **31** (Jun, 1973) 83–112.

[27] Gattringer, Christof and Lang, Christian B., *Quantum chromodynamics on the lattice*, *Lect. Notes Phys.* **788** (2010) 1–343.

[28] A. Pelissetto, *LATTICE NONLOCAL CHIRAL FERMIONS*, *Annals Phys.* **182** (1988) 177.

[29] L. H. Karsten, *Lattice fermions in euclidean space-time*, *Physics Letters B* **104** (1981) 315 – 319.

[30] V. Gribov, *Quantization of non-abelian gauge theories*, *Nuclear Physics B* **139** (1978) 1 – 19.

[31] C. Becchi, A. Rouet and R. Stora, *Renormalization of gauge theories*, *Annals of Physics* **98** (1976) 287 – 321.

[32] I. V. Tyutin, *Gauge Invariance in Field Theory and Statistical Physics in Operator Formalism*, 0812.0580.

[33] Giusti, Leonardo and Paciello, M. L. and Parrinello, C. and Petrarca, S. and Taglienti, B., *Problems on lattice gauge fixing*, *Int. J. Mod. Phys.* **A16** (2001) 3487–3534, [hep-lat/0104012].

[34] J. Smit, *Fermions on a Lattice*, *Acta Phys. Polon.* **B17** (1986) 531.

[35] P. Swift, *The electroweak theory on the lattice*, *Physics Letters B* **145** (1984) 256 – 260.

[36] E. Eichten and J. Preskill, *Chiral gauge theories on the lattice*, *Nuclear Physics B* **268** (1986) 179 – 208.

[37] D. B. Kaplan, *Chiral fermions on the lattice*, *Nuclear Physics B - Proceedings Supplements* **30** (1993) 597 – 600.

[38] M. F. L. Golterman, K. Jansen, D. N. Petcher and J. C. Vink, *Investigation of the domain wall fermion approach to chiral gauge theories on the lattice*, *Phys. Rev. D* **49** (Feb, 1994) 1606–1620.

[39] M. F. L. Golterman and Y. Shamir, *Domain wall fermions in a waveguide: The phase diagram at large yukawa coupling*, *Phys. Rev. D* **51** (Mar, 1995) 3026–3033.

[40] A. Borrelli, L. Maiani, G. Rossi, R. Sisto and M. Testa, *Neutrinos on the lattice. The regularization of a chiral gauge theory*, *Nuclear Physics B* **333** (1990) 335 – 356.

[41] M. Golterman and Y. Shamir, *SU(N) chiral gauge theories on the lattice: A Quick overview*, *Nucl. Phys. Proc. Suppl.* **140** (2005) 671–673, [hep-lat/0409052].

[42] M. Golterman and Y. Shamir, *Lattice chiral gauge theories through gauge fixing*, in *Strong coupling gauge theories and effective field theories. Proceedings, International Workshop, SCGT'02, Nagoya, Japan, December 10-13, 2002*, pp. 206–212, 2002. hep-lat/0205001. DOI.

[43] M. Luscher, *Lattice regularization of chiral gauge theories to all orders of perturbation theory*, *JHEP* **06** (2000) 028, [hep-lat/0006014].

[44] M. Golterman, *Lattice chiral gauge theories*, *Nuclear Physics B - Proceedings Supplements* **94** (2001) 189 – 203.

[45] S. Duane, A. Kennedy, B. J. Pendleton and D. Roweth, *Hybrid monte carlo*, *Physics Letters B* **195** (1987) 216 – 222.

[46] D. J. E. Callaway and A. Rahman, *The Microcanonical Ensemble: A New Formulation of Lattice Gauge Theory*, *Phys. Rev. Lett.* **49** (1982) 613.

[47] D. J. E. Callaway and A. Rahman, *Lattice Gauge Theory in Microcanonical Ensemble*, *Phys. Rev.* **D28** (1983) 1506.

[48] Gottlieb, Steven and Liu, W. and Toussaint, D. and Renken, R. L. and Sugar, R. L., *Hybrid-molecular-dynamics algorithms for the numerical simulation of quantum chromodynamics*, *Phys. Rev. D* **35** (Apr, 1987) 2531–2542.

[49] S. Basak, A. K. De and T. Sinha, *On the continuum limit of gauge-fixed compact U(1) lattice gauge theory*, *Physics Letters B* **580** (2004) 209 – 215.

[50] W. Bock, M. F. L. Golterman and Y. Shamir, *Phase diagram of a lattice U(1) gauge theory with gauge fixing*, *Phys. Rev. D* **58** (Aug, 1998) 054506.

[51] A. K. De and T. Sinha, *More on the continuum limit of gauge-fixed compact U(1) lattice gauge theory*, `hep-lat/0506033`.

[52] H. Evertz, K. Jansen, J. Jersk, C. Lang and T. Neuhaus, *Photon and bosonium masses in scalar lattice QED*, *Nuclear Physics B* **285** (1987) 590 – 605.

[53] K. Bitar, A. Kennedy, R. Horsley, S. Meyer and P. Rossi, *The QCD finite temperature transition and hybrid Monte Carlo*, *Nuclear Physics B* **313** (1989) 348 – 376.

[54] R. Kapri and S. M. Bhattacharjee, *Manipulating a single adsorbed DNA for a critical endpoint*, *EPL (Europhysics Letters)* **83** (2008) 68002.

[55] G. Arnold, B. Bunk, T. Lippert and K. Schilling, *Compact QED under scrutiny: it's first order*, *Nuclear Physics B - Proceedings Supplements* **119** (2003) 864 – 866.

[56] M. Vettorazzo and P. de Forcrand, *Electromagnetic fluxes, monopoles, and the order of 4d compact U(1) phase transition*, *Nuclear Physics B* **686** (2004) 85 – 118.

[57] M. Panero, *A Numerical study of confinement in compact QED*, *JHEP* **05** (2005) 066.

[58] G. Curci and R. Ferrari, *On a Class of Lagrangian Models for Massive and Massless Yang-Mills Fields*, Nuovo Cim. **A32** (1976) 151–168.

[59] I. Ojima, *Another BRS Transformation*, Prog. Theor. Phys. **64** (1980) 625.

[60] L. Baulieu and J. Thierry-Mieg, *The principle of BRS symmetry: An alternative approach to Yang-Mills theories*, Nuclear Physics B **197** (1982) 477 – 508.

[61] M. Schaden, *Mass generation in continuum $SU(2)$ gauge theory in covariant Abelian gauges*, `hep-th/9909011`.